PNWD-3361

In Situ Redox Manipulation Permeable Reactive Barrier Emplacement: Final Report

Frontier Hard Chrome Superfund Site, Vancouver, WA

January 2004

V. R. Vermeul
B. N. Bjornstad
C. J. Murray
D. R. Newcomer
M. L. Rockhold
J. E. Szecsody
M. D. Williams
Y. Xie

Battelle – Pacific Northwest Division
Richland, WA 99352

LEGAL NOTICE

This report was prepared by Battelle Memorial Institute (Battelle) as an account of sponsored research activities. Neither Client nor Battelle nor any person acting on behalf of either:

MAKES ANY WARRANTY OR REPRESENTATION, EXPRESS OR IMPLIED, with respect to the accuracy, completeness, or usefulness of the information contained in this report, or that the use of any information, apparatus, process, or composition disclosed in this report may not infringe privately owned rights; or

Assumes any liabilities with respect to the use of, or for damages resulting from the use of, any information, apparatus, process, or composition disclosed in this report.

Reference herein to any specific commercial product, process, or service by trade name, trademark, manufacturer, or otherwise, does not necessarily constitute or imply its endorsement, recommendation, or favoring by Battelle. The views and opinions of authors expressed herein do not necessarily state or reflect those of Battelle.

PNWD-3361

In Situ Redox Manipulation Permeable Reactive Barrier Emplacement: Final Report

Frontier Hard Chrome Superfund Site, Vancouver, WA

V. R. Vermeul
B. N. Bjornstad
C. J. Murray
D. R. Newcomer
M. L. Rockhold
J. E. Szecsody
M. D. Williams
Y. Xie

January 2004

Battelle – Pacific Northwest Division
Richland, WA 99352

Executive Summary

This report documents results from the in situ redox manipulation (ISRM) permeable reactive barrier emplacement for the treatment of hexavalent chromium in the groundwater at the Frontier Hard Chrome (FHC) site in Vancouver, Washington. The ISRM technology creates a permeable treatment zone downstream of a contaminant plume or contaminant source through injection of a chemical reducing agent to alter the redox potential of aquifer fluids and sediments. Injected reagents create the zone through reactions that reduce iron naturally present in aquifer sediments from Fe(III) to Fe(II). Following the creation of the ISRM treatment zone, hexavalent chromium-contaminated groundwater will flow into and through the treatment zone under natural groundwater flow conditions. As the dissolved hexavalent chromium (in the form of highly soluble and mobile chromate anion CrO_4^{2-}) enters the reducing environment, it reacts with the ferrous iron in the treatment zone and is reduced to the trivalent form, which readily hydrolyzes and precipitates as $Cr(OH)_3(s)$.

The primary objective of the ISRM permeable reactive barrier, which is one of two technologies composing the selected remedy for the FHC site, is to provide long-term protection of groundwater in addition that provided by the source area treatment (direct reductive treatment) as well as to protect downgradient groundwater during augering/injection of reductant into source area soils and the plume "hot spot" area. Bench-scale studies using sediment from the site and a pilot-scale field test were conducted prior to full-scale deployment of the permeable reactive barrier technology; these studies/tests demonstrated the field-scale feasibility of using ISRM for treating hexavalent chromium contamination in the groundwater at the FHC site.

Results from the ISRM pilot field test showed that the site hydrogeology was relatively complex and characterized by a large degree of variability in the hydraulic properties that control the direction and extent of reagent transport and reductive capacity distribution realized during the treatment process. These data demonstrated the need for detailed characterization of hydrogeologic conditions and contaminant distribution along the full length of the proposed barrier alignment. To meet this data requirement, seven temporary characterization wells were installed and tested. Data collected at each location included a detailed investigation of the hydrostratigraphy, vertical contaminant distribution, and hydraulic conductivity distribution. The hydraulic conductivity distribution was investigated with electromagnetic borehole flow meter (EBF) tests designed to characterize the vertical distribution of horizontal hydraulic conductivity at each location and to quantify the magnitude and spatial distribution of formation heterogeneity along the barrier alignment. These data, which were analyzed using geostatistical techniques, were used to refine the site conceptual model and were incorporated into a reactive transport model that was the basis for the injection design analysis.

Based on the detailed characterization data collected at the site, it was determined that two injection wells, each targeting a separate depth interval, would be required at each injection location. The full-scale ISRM permeable reactive barrier was installed by coalescing the

individually emplaced treatment zones at each of these locations to form a continuous linear barrier. Over a two-month period, from late May through early August 2003, eight injection operations were conducted that resulted in the successful installation of a 250-ft ISRM permeable reactive barrier at the FHC site. During these operations, a total of 168,000 lb of dithionite and pH buffer, which placed in solution produced 560,000 gallons of reagent, were injected along the full barrier alignment. Detailed operational and performance monitoring was conducted throughout all phases of the barrier emplacement operations.

Data from emplacement operations along the barrier alignment provide a good qualitative measure of the spatial distribution of treatment. In general, these data indicate that a finite amount of treatment was achieved along the full barrier alignment, although in two separate instances the iron distribution in the overlap zones between two injection well pairs may have been less than that predicted in the design simulations. The observed responses were indicative of the formation heterogeneities present at the FHC site and provide an example of the challenges associated with deploying an effective remedial technology at hydrogeologically complex sites. However, in both cases, the monitoring well pair in question did receive substantial treatment during the injection operation on the opposing side of the monitoring well. In addition, even under these non-ideal iron distribution conditions, it is likely that, given the relatively small hydraulic gradient at the site and the effectiveness of the source area treatment, even the lowest-capacity regions of the barrier contained sufficient quantities of reduced iron to meet remedial objectives.

In addition to the observed dithionite arrivals at the various monitoring wells, results from a two-dimensional (2D) radial reactive transport model were used to help quantify the amount and distribution of iron reduction. A relatively good fit between the predicted and observed arrival responses indicated that the 2D radial reactive transport model constructed during this effort provided a reasonable representation of actual site conditions and was a useful tool for estimating the distribution of reductive capacity generated during emplacement operations at the site. These simulated iron distributions were used to develop bounding estimates of barrier longevity.

Preliminary post-emplacement performance assessment monitoring results are consistent with results from the pilot test and the expected response for an ISRM treatment zone. Observed responses within the reduced iron treatment zone, relative to baseline conditions, included 1) a decrease in the dissolved oxygen concentration associated with the creation of a reducing environment, 2) a decrease in the oxidation-reduction potential, 3) a small increase in the pH associated with the pH buffered reagent, 4) an increase in the electrical conductivity associated with treatment residuals, and 5) a decrease in hexavalent chromium concentration within the treatment zone to below detection limits.

Contents

Figures

Tables

1.0 Introduction

This report documents results from the in situ redox manipulation (ISRM) permeable reactive barrier emplacement for the treatment of hexavalent chromium in the groundwater at the Frontier Hard Chrome (FHC) site in Vancouver, Washington. Vancouver is situated in the southwestern part of Washington State; the site is approximately one-half mile north of the Columbia River and covers about one-half acre. Chrome plating operations were performed at the FHC site for approximately 25 years, between 1958 and 1982. FHC, which operated at the site between 1970 and 1982, discharged process wastewaters containing hexavalent chromium directly to an onsite dry well.

In 1982, Washington State Department of Ecology (Ecology) determined that FHC was violating Washington State Dangerous Waste Regulations for disposal of hazardous waste. At that time, chromium concentrations greater than twice the state groundwater cleanup standard of 50 µg/L (Amended Model Toxics Control Act [WAC 173-340]) were detected in groundwater samples from an industrial well approximately 0.5 mile southwest of the site. FHC went out of business shortly after Ecology identified the violation. In December 1982, the site was proposed for inclusion on the National Priorities List (NPL) under CERCLA. The site was added to the NPL in September 1983.

Releases from FHC operations contaminated groundwater with reported chromium concentrations as high as 300,000 µg/L. At the time the contaminated groundwater was first detected, a plume exceeding Washington State groundwater cleanup standards (50 µg/L) extended approximately 1600 ft southwest from the facility. The July 1988 record of decision (ROD) for the groundwater operable unit called for extraction of groundwater from the area of greatest contamination (chromium levels exceeding 50,000 µg/L) via extraction wells and treatment of the extracted water. Groundwater monitoring since the initial discovery has shown that the plume has receded. Monitoring in 2000 indicated that the plume exceeding state groundwater cleanup standards extends approximately 1000 ft south of the site. The change in overall plume size and the shift in groundwater flow from the site in a southwesterly direction to a more southerly direction are largely due to the discontinued pumping of three large industrial supply wells to the southwest. With the influence of these wells eliminated, the plume is conforming to natural groundwater flow. While monitoring indicates that the plume has receded, it also shows that concentrations beneath the FHC site, or the plume "hot-spot" area, remain consistently high. This plume hot-spot area is defined in the proposed plan for cleanup of soils and groundwater at FHC contaminated by chromium in concentrations exceeding 5,000 µg/L.

Concentrations of total chromium found in surface soil samples collected for the remedial investigation were as high as 5,200 mg/kg, while recent samples revealed concentrations of hexavalent chromium near the FHC building as high as 42 mg/kg. Subsurface concentrations for total and hexavalent chromium have been noted as high as 31,800 and 7,506 mg/kg, respectively. Contaminated subsurface soils extend beneath the neighboring Richardson Metal Works

building. The December 1987 ROD for the soils/source control operable unit called for removal, stabilization, and replacement of 7400 cubic yards of soil—or all soils with concentrations greater than 550 mg/kg total chromium (this number was based on a site-specific leachate test for protection of groundwater).

The Environmental Protection Agency (EPA) issued separate RODs for the soils/source control operable unit in December 1987 and for the groundwater operable unit in July 1988. Evaluation of these proposed remedies by EPA after the RODs were issued revealed that the soils remedy was ineffective. Groundwater monitoring conducted after the ROD was issued indicated that the contaminated groundwater plume was decreasing in size as downgradient industrial supply wells at FMC were taken off line. Because the immediate threat of further downgradient migration of the plume appeared to be in decline, and local government controls prevented installing new wells in the aquifer, EPA also began to reevaluate the need for pump and treat as the most appropriate solution for groundwater cleanup. Since then, EPA has continued to monitor groundwater and soils and to evaluate new, innovative cleanup technologies to address the persistently high concentrations in soils and groundwater at the FHC site.

In October 1994, Ecology conducted an interim removal action of chromium-contaminated soil on the property adjacent to and east of the FHC site. Approximately 160 cubic yards of soil were removed and disposed of, allowing for redevelopment of the property. With the exception of this interim removal action, no active cleanup had been undertaken. While monitoring was ongoing, no active steps had been taken to control or remediate contaminated groundwater, and no actions had been taken to deal with contaminated soils on the FHC and adjacent Richardson Metal Works properties, which continue to act as a source of contamination to the groundwater resource. In May 2000, EPA finalized a Focused Feasibility Study that identified and evaluated several new and innovative technologies for addressing the problems at the site.

In June 2001, EPA released a proposed plan for ROD amendment addressing both the groundwater and soils at the site. The preferred remedy calls for the reduction of hexavalent chromium to trivalent chromium in soils and groundwater. The preferred alternative in the proposed plan includes in situ treatment of source area soils and groundwater, in conjunction with an in situ downgradient treatment barrier (In Situ Redox Manipulation, or ISRM). The preferred methodology for delivering reductant to both soils and groundwater for in situ treatment in the soils source area and the plume hot spot was augering/injection. The ISRM permeable reactive barrier was selected to provide additional treatment on the downgradient edge of the groundwater hot spot (Figure 1.1). For this remedial approach, groundwater downgradient of the ISRM treatment barrier, which is contaminated above state cleanup standards, would be left to disperse and dilute. The combination of these alternatives would treat groundwater and soils in the soils source area (soils exceeding 19 mg/kg hexavalent chromium) and the groundwater plume hot spot at the same time (groundwater exceeding 5,000 μg/L) using the same reductant and the same methodology (augering).

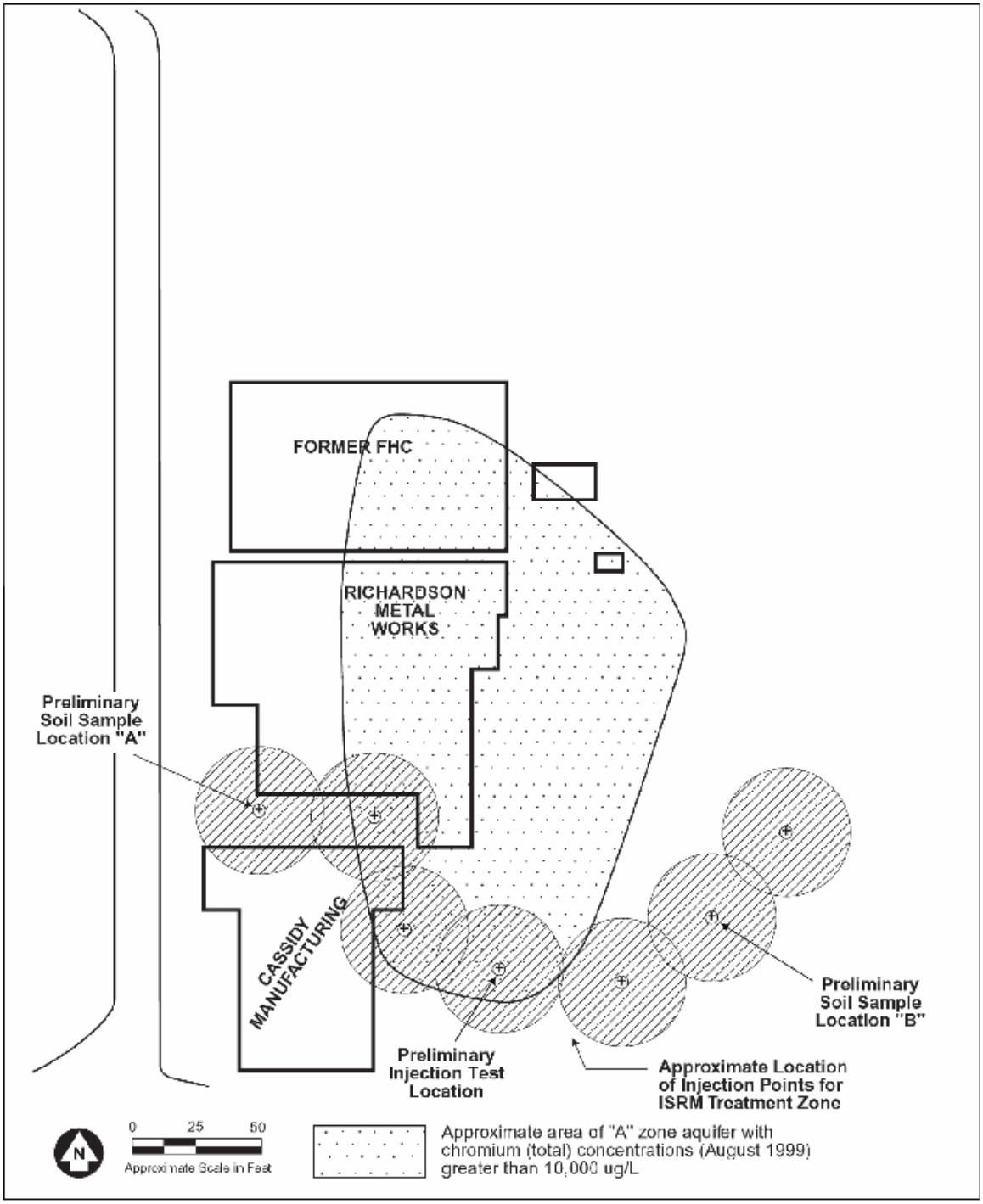

Figure 1.1. Site Map Showing Initial Planned Locations of Source Area Shallow Soil Mixing Area and ISRM Barrier Location (actual barrier alignment was modified based on site-specific characterization data)

Installing an ISRM barrier provides additional long-term protection of groundwater as well as protection of downgradient groundwater during augering/injection of reductant into source area soils and the plume hot-spot area. This alternative provides effective treatment of all soils and groundwater in source areas and a long-term treatment barrier for any residual contaminant leaching should it occur.

Shallow groundwater in the FHC area occurs within a complex, heterogeneous alluvial aquifer system that is hydraulically connected to the Columbia River. In general, the alluvial aquifer system exhibits both quasi-confined and confined characteristics. This semiconfined condition is due in part to a low-permeability clayey silt unit that directly overlies the alluvial aquifer and to permeability contrasts within the alluvial aquifer.

The site hydrogeology consists of 15 to 20 feet of random fill and silty sand that is largely unsaturated, a 5- to 10-ft-thick upper confining bed of clayey silt, and a heterogeneous anisotropic alluvial aquifer system that may be as thick as 70 ft beneath the site. Localized zones of perched groundwater are present above the top of the clayey silt within the fill materials. Figure 1.2 is a conceptual diagram of the general hydrostratigraphy inferred to be locally present in the FHC area.

The uppermost hydrogeologic unit consists of perched groundwater in the fill unit. The fill unit is generally unsaturated, but locally perched water is present. Groundwater in the perched aquifer is generally recharged from precipitation by direct infiltration, stormwater dry wells, and roof drains. Separating the fill unit from the alluvial unit is a 1- to 10-ft-thick confining unit.

Underlying the clayey silt unit is the alluvial aquifer, which is a sand and gravel layer beginning 15 to 20 ft below ground surface. The upper portion of the alluvial unit has been subdivided into two water-bearing zones based on the apparent presence of a discontinuous silty sand or sandy silt zone present at depth of 25 to 35 ft below ground surface. The upper zone has been referred to as the "A" zone, or "A" aquifer, and the lower zone has been designated as the "B" zone, or "B" aquifer. The silt zone, when present, is generally from 1 to 3 ft thick. The silt appears to be discontinuous. Although this silt layer may act locally as a confining unit, most evidence suggests that it does not act as an areally extensive hydraulic barrier within the alluvial aquifer. Variations from this site-scale hydrogeologic conceptual model for the ISRM permeable reactive barrier location, based on site-specific characterization data collected during pilot test and barrier emplacement field activities, are discussed in Section 2.2.

The potentiometric surface is relatively flat across the inactive floodplain on which the FHC site is located. In an effort to quantify the hydraulic gradient controlling groundwater flow through the ISRM barrier location, EPA Region 10 personnel collected depth to groundwater measurements from monitoring wells throughout the site from March through September 2003. Gradient calculations incorporated data from wells located up to 2,760 ft apart, the approximate distance between the farthest upgradient and downgradient wells used.

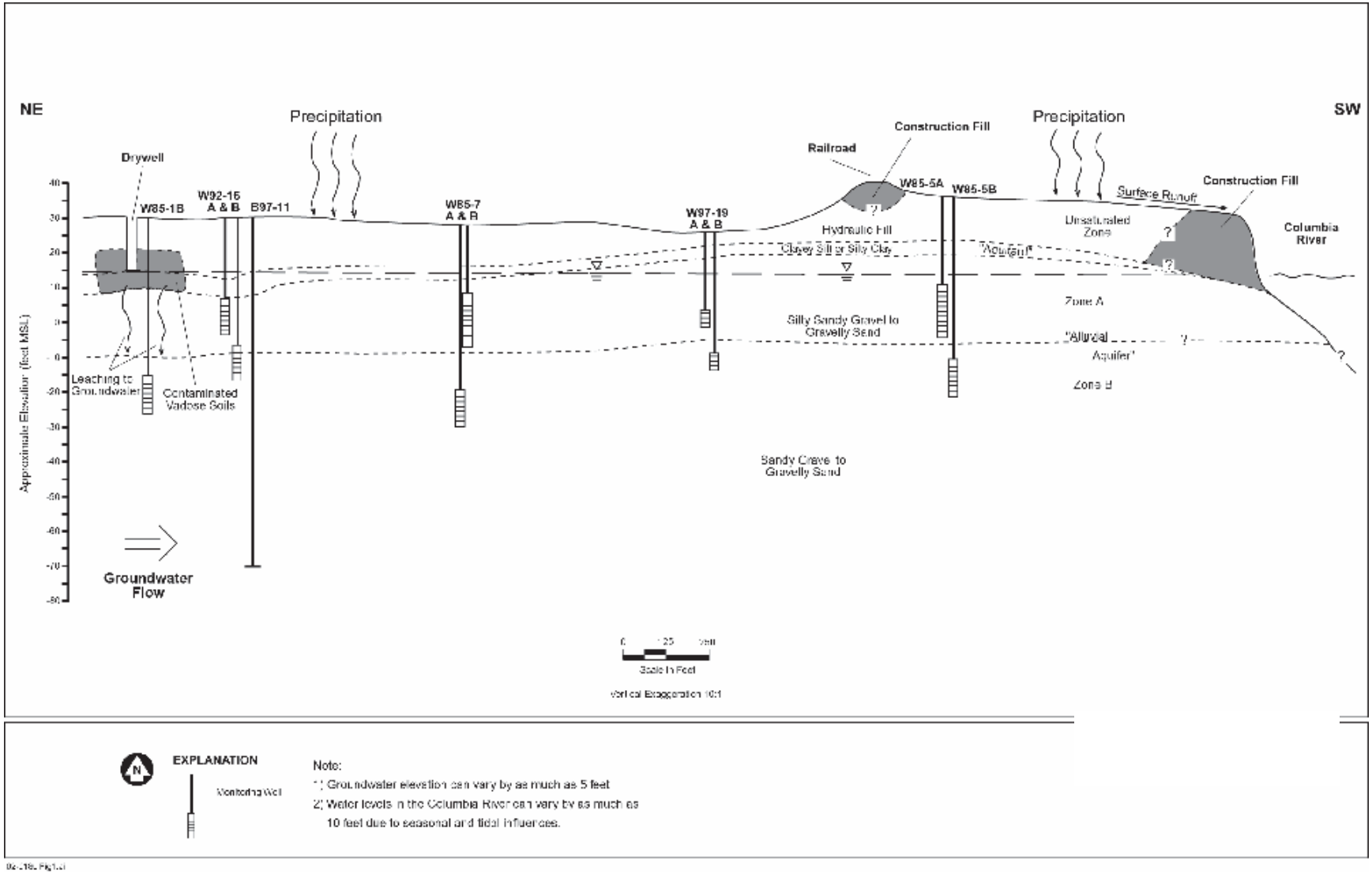

Figure 1.2. Original Site Hydrogeologic Conceptual Model

Evaluation of these data showed that, although the water table drops several feet over the course of the year, only small differences could be observed in water table elevations in the upgradient and downgradient wells. The Columbia River stage during most of this time was lower than the measured groundwater level, indicating that the predominant flow direction was to the south where groundwater discharges to the Columbia River. The average horizontal hydraulic gradient during this time was 2.8E-05 ft/ft. Based on this average gradient and hydraulic property data collected during installation of the ISRM barrier, groundwater velocity in the "A" zone is estimated to range from 0.02 to 2 ft/d.

1.1 Technology Description

The ISRM approach involves creating a permeable treatment zone downstream of a contaminant plume or contaminant source by injecting a chemical reducing agent to alter the redox potential of aquifer fluids and sediments (Fruchter et al. 1994, 2000; Vermeul et al. 2002a). Redox-sensitive contaminants migrating through this treatment zone are immobilized (metals) or destroyed (organic solvents). Injected reagents create the zone through reactions that reduce iron naturally present in aquifer sediments from Fe(III) to Fe(II). Using standard wells to create the treatment zone enables treatment of contaminants too deep for conventional trench-and-fill technologies. Figure 1.3 is a conceptual diagram of the ISRM technology.

This technology has been demonstrated successfully in two field tests at the Hanford Site in Washington State, where it was installed to remediate hexavalent chromium in the groundwater (Fruchter et. al. 1996, 2000; Williams et al. 2000). The reducing agent used in these field and laboratory tests is sodium dithionite ($Na_2S_2O_4$), which is a strong reducing agent that possesses a number of desirable characteristics for this type of application, including instability in the natural environment (~days) with reaction and degradation products that ultimately oxidize to sulfate. A potassium carbonate pH buffer is also added to the injection solution to enhance the stability of dithionite during the reduction of available iron.

Following the creation of the ISRM treatment zone, hexavalent chromium-contaminated groundwater flows into and through the treatment zone at natural groundwater velocity. As the dissolved hexavalent chromium (in the form of highly soluble and mobile chromate anion, CrO_4^{2-}) enters the reducing environment, it reacts with the ferrous iron and is reduced to the trivalent form. Trivalent chromium is much less toxic and mobile in the environment. Trivalent chromium in solution readily hydrolyzes and precipitates as $Cr(OH)_3(s)$ (Rai et al. 1989). When trivalent chromium is precipitated in soils containing ferric iron, solid solutions with ferric iron also form $(Cr,Fe)(OH)_3(s)$. A more detailed review and discussion of these processes are contained in Fruchter et al. (2000).

Potential secondary effects associated with the ISRM technology include metals mobilization, treatment residuals, hydraulic performance (i.e., aquifer plugging), and dissolved oxygen depletion. In previous bench- and field-scale demonstrations of the ISRM technology at

other locations, none of these effects were shown to exceed technical or regulatory limits. Of primary concern is the potential for releasing unwanted constituents as the chemical treatment zone is formed. For example, as the reductive environment is formed, otherwise stable minerals or hydroxides can be broken down to release metals such as arsenic and manganese. The ISRM technology has been field-tested at several sites, including a proof-of-principle test at the Hanford 100-H Area for removing chromium from groundwater (Fruchter et al. 2000), a treatability test at the Hanford 100-D Area (Williams et al. 2000), and a 2,300-ft-long ISRM barrier installed at the same 100-D Area location.

For each of these sites, batch and column tests were conducted to investigate the release of trace metals and to gain regulatory approval for the field-scale injection. Results from these field- and laboratory-scale tests indicate that, although trace metals are mobilized (constituents of primary concern include iron, manganese, and arsenic) and exceed regulatory limits during the injection and withdrawal phases of the barrier emplacement, most are removed during the

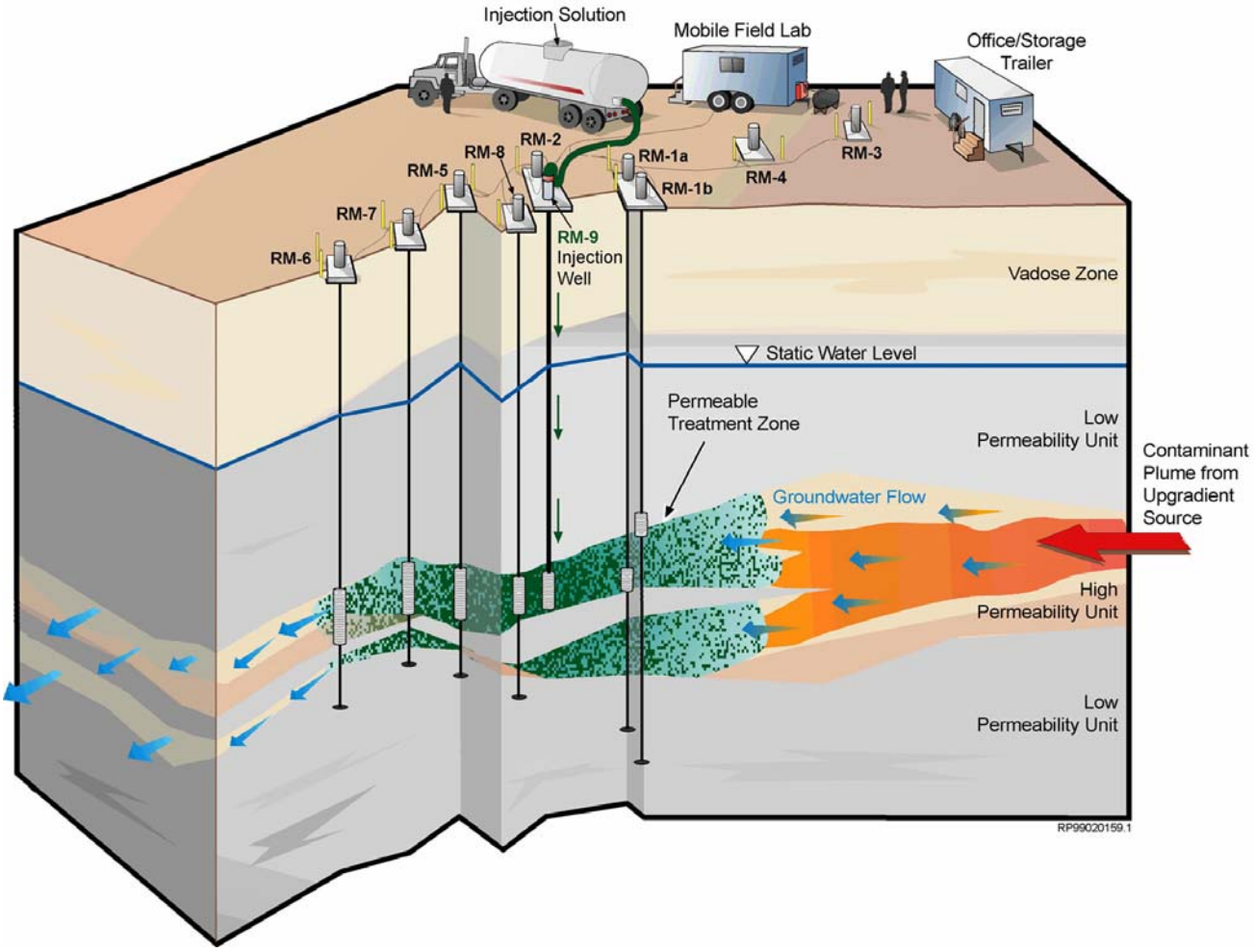

Figure 1.3. ISRM Conceptual Diagram. Schematic hydrology is based on the ISRM proof-of-principle test site at the Fort Lewis Logistics Center.

withdrawal and following the emplacement do not migrate outside the reduced zone in quantities significant enough to create a regulatory concern. In addition to the mobilization of trace metals, poor recovery during the withdrawal phase of the treatment zone emplacement can result in a significant mass of reaction products (i.e., residual chemicals) remaining in the aquifer. The primary reaction product of the dithionite injection is sulfate, which is regulated under a secondary drinking water standard. All constituents of concern were included in the operational and performance monitoring programs for the ISRM pilot test.

Analysis of hydraulic performance data from ISRM field demonstrations to date (Fruchter et al. 2000; Williams et al. 1999) has not indicated a significant reduction in formation permeability from deployment of the ISRM technology. The hydraulic test analysis did indicate a near-well decrease in permeability at the injection/withdrawal well following the injection. This small zone of reduced permeability (i.e., skin effect) is attributed to entrapment of suspended or colloidal material or mineralization associated with the carbonate buffer in the sandpack zone and well screen during the withdrawal phase. This near-well reduction in permeability caused no adverse effects during the injection or withdrawal phases of the demonstrations and did not result in any significant degradation in the overall hydraulic performance of the treatment zone.

Another secondary effect associated with the ISRM technology that may be of concern at some sites is oxygen depletion. At the ISRM treatability test site at the Hanford 100-D Area, proximity to the Columbia River (~500 ft) and potential salmon-spawning habitat resulted in regulatory and stakeholder sensitivity. To address regulatory concerns, a modeling study simulated this near-river system and investigated mechanisms important to attenuation of the anoxic plume. The model predicted how far downgradient from the ISRM barrier acceptable dissolved oxygen concentrations were achieved (Williams et al. 1999; Williams and Oostrom 2000). At the 100-D site, the numerical model predicted 75 to 95% oxygen saturation at the river and determined that air entrapment caused by water table fluctuations (associated with diurnal fluctuations in river stage) had the greatest impact on attenuation of the anoxic plume. Oxygen depletion is not expected to be a secondary effect of regulatory concern at FHC.

1.2 ISRM Barrier Objective

The objective of the ISRM permeable reactive barrier, which is one of two technologies that make up the selected remedy for the FHC site, is to provide long-term protection of groundwater in addition to that provided by the source area treatment as well as protection of downgradient groundwater during augering/injection of reductant into source area soils and the plume hot-spot area. Bench-scale studies using sediment from the site[(a)] and a pilot-scale field test (Vermeul et al. 2002b) were conducted prior to full scale deployment of the permeable reactive barrier and

(a) Szecsody JE, BJ DeVary, VR Vermeul, MD Williams, and JS Fruchter. October, 2002. *In Situ Redox Manipulation Bench-Scale Tests: Remedial Design Support for ISRM Barrier Deployment, Frontier Hard Chrome Site, Vancouver, Washington*. Letter Report to EPA from Pacific Northwest National Laboratory, Richland, WA.

demonstrated the field-scale feasibility of using the ISRM technology for the treatment of hexavalent chromium contamination in groundwater at the FHC site.

1.3 Report Organization

This report describes the site characterization, design, and emplacement of a full-scale ISRM barrier at the FHC site. A discussion of the ISRM pilot test site characterization activities, conceptual model development, and treatment zone emplacement is provided in Section 2. Subsequent detailed characterization of the full ISRM barrier alignment and incorporation of this information into the barrier design analysis are presented in Sections 3 and 4, respectively. Field site and operational/monitoring equipment setup are discussed in Section 5 and activities associated with barrier emplacement in Section 6. Section 7 assesses the preliminary performance of the ISRM permeable reactive barrier. Conclusions are provided in Section 8, and Section 9 contains cited references. Supporting documentation, including well logs and as-built diagrams, electromagnetic borehole flow meter testing results, geostatistical analysis results, barrier design analysis results, pressure response data during barrier emplacement, and dithionite injection breakthrough curves at each injection well pair along the barrier alignment, can be found in the appendixes.

2.0 Pilot Test Results

This section presents a brief description of the characterization and treatment zone emplacement activities conducted during the ISRM pilot test at the FHC site. A detailed description of these activities is provided in a letter report to EPA.[(a)]

2.1 Well Installation

In support of characterization and injection testing activities at the FHC ISRM pilot test site, two injection wells and 11 monitoring wells were installed (Figure 2.1). Three different drilling methods were used to install wells at the site, including sonic, hollow-stem auger, and direct push (Geoprobe) methods. This approach, although not ideal due to differences in sediment core sample quality and well installation/completion methodologies for the various drilling methods, was adopted due to budgetary limitations.

Wells at the site were installed in two separate campaigns. During the initial drilling campaign (May 2002), which was designed to provide site-specific characterization information and the initial well network needed to monitor the ISRM injection tests, one injection well (INJ-1) and 11 monitoring wells were installed. Based on results from a tracer injection test, it was determined that a second injection well (INJ-2) targeting the uppermost portion of the A aquifer would be required. INJ-2 was installed by hollow-stem auger in August 2002.

For the five monitoring wells installed using hollow-stem auger and the one installed using the sonic drill, a 6-in. borehole was advanced to total depth and completed with 2-in. PVC casing and screen. Screen material consisted of a 10-slot continuous wire wrap (v-wire) screen and was set in a 20/40 Colorado silica sand filter pack. For the five monitoring wells installed using the direct push method, a 3.25-in. drill rod was advanced to total depth and completed with a 2-in. PVC casing and screen. Screen material consisted of slotted pipe (10-slot) with native formation as the filter pack (i.e., drill rods were back-pulled, allowing native formation to collapse around the screen). During site-specific characterization of the full barrier alignment, it was determined that the direct push wells did not provide an adequate annular seal throughout the upper, more fine-grained portion of the aquifer (see discussion in Section 3.3), and these wells were subsequently abandoned. Abandonment consisted of over-drilling each well installation using hollow-stem auger, removing the PVC casing and screen material, and sealing the borehole with bentonite.

(a) Vermeul VR, MD Williams, JE Szecsody, and JS Fruchter. December 2002. *In Situ Redox Manipulation Pilot Field Test: Remedial Design Support for ISRM Barrier Deployment, Frontier Hard Chrome Site, Vancouver, Washington*. Letter Report to EPA from Pacific Northwest National Laboratory, Richland, WA.

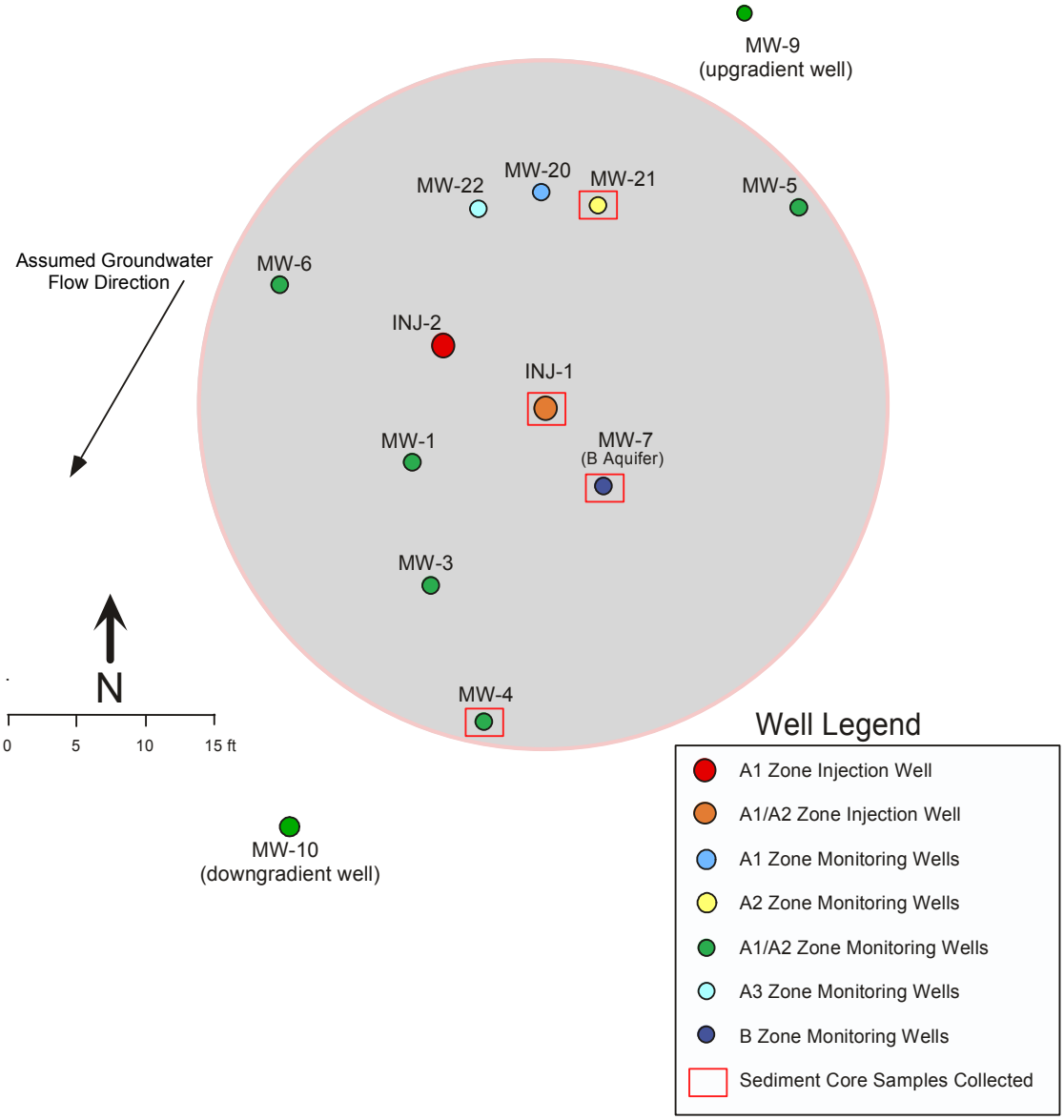

Figure 2.1. Well Layout at the ISRM Pilot Test Site

For the two injection wells installed at the site, one by the sonic method and the other by hollow-stem auger, a 10-in. borehole was advanced to total depth and completed with 6-in. PVC casing and screen. Screen material consisted of a 20-slot continuous wire wrap (v-wire) screen set in a 10/20 Colorado silica sand filter pack. Installation and completion of all wells was conducted in accordance with Washington Administrative Code Standards ("Minimum Standards for Construction and Maintenance of Wells," WAC 173-160). Appendix A contains a complete set of geologic logs and well installation reports.

Samples were collected from four of the 13 boreholes (the two sonic boreholes and two hollow-stem auger boreholes indicated in Figure 2.1) for lithologic description, physical property analysis, and geochemical analysis (i.e., reducible iron content). Differences in sediment core sample quality were observed between the 4-in. cores collected by the sonic method and the smaller-diameter core (2.5-in.) collected using the hollow-stem auger method. Comparison of particle size distribution data in the two sampling methods indicates that the smaller sampler was not appropriately sized for the gravel fraction at the site and thus skewed the particle size distributions toward the smaller size fraction. Due to the nature of the drilling methods used to install the rest of the wells, limited additional lithologic information was obtained.

2.2 Hydrogeologic Characterization

As discussed above, a limited set of sediment core samples was collected for lithologic description and physical property analysis. As a result, precise contact depths for the various hydrostratigraphic units identified at the site were available only at a few select locations. Although additional information would have improved the overall conceptual understanding of the site prior to conducting the pilot test, sufficient information was collected to develop a generalized site-specific hydrogeologic conceptual model (Figure 2.2). As indicated, the hydrogeology encountered beneath the ISRM pilot test site was much more heterogeneous than the original idealized hydrogeologic conceptual model of the site. The refined conceptual model for the pilot test site consisted of, in descending order, hydraulic or construction fill to a depth of ~ 10 ft, a clayey silt layer ~10 ft thick, a silty sandy gravel layer ~5 ft thick (referred to here as the A1 zone), another silty sandy gravel layer ~8 ft thick (referred to here as the A2 zone) that has an estimated hydraulic conductivity value an order of magnitude higher than that of the A1 zone, and a sandy gravel layer ~ 5 ft thick that was estimated to be approximately another order of magnitude higher in hydraulic conductivity (A3 zone).

Summary results from particle size distribution analysis of collected sediment core samples along with best estimates of other physical and hydraulic properties for each zone are shown in Figure 2.2. A detailed discussion of sediment physical property analyses and results are contained in a letter report to the U.S. Environmental Protection Agency (EPA).[(a)] The average hydraulic conductivity values were derived from analytical methods that, although valid for a layered system, are based on a homogeneous porous media concept and do not account for heterogeneities within each layer. As discussed in subsequent sections of this report, the hydraulic and transport responses observed in site monitoring wells during subsequent characterization activities provided substantial evidence of formation heterogeneities that were not represented by this three-layer model. However, the indicated values do provide a qualitative estimate of average hydraulic properties for the layered system. In addition, vertical Cr(VI)

(a) Szecsody JE, BJ DeVary, VR Vermeul, MD Williams, and JS Fruchter. October 2002. *In Situ Redox Manipulation Bench-Scale Tests: Remedial Design Support for ISRM Barrier Deployment, Frontier Hard Chrome Site, Vancouver, Washington*. Letter Report to EPA. Pacific Northwest National Laboratory, Richland, WA.

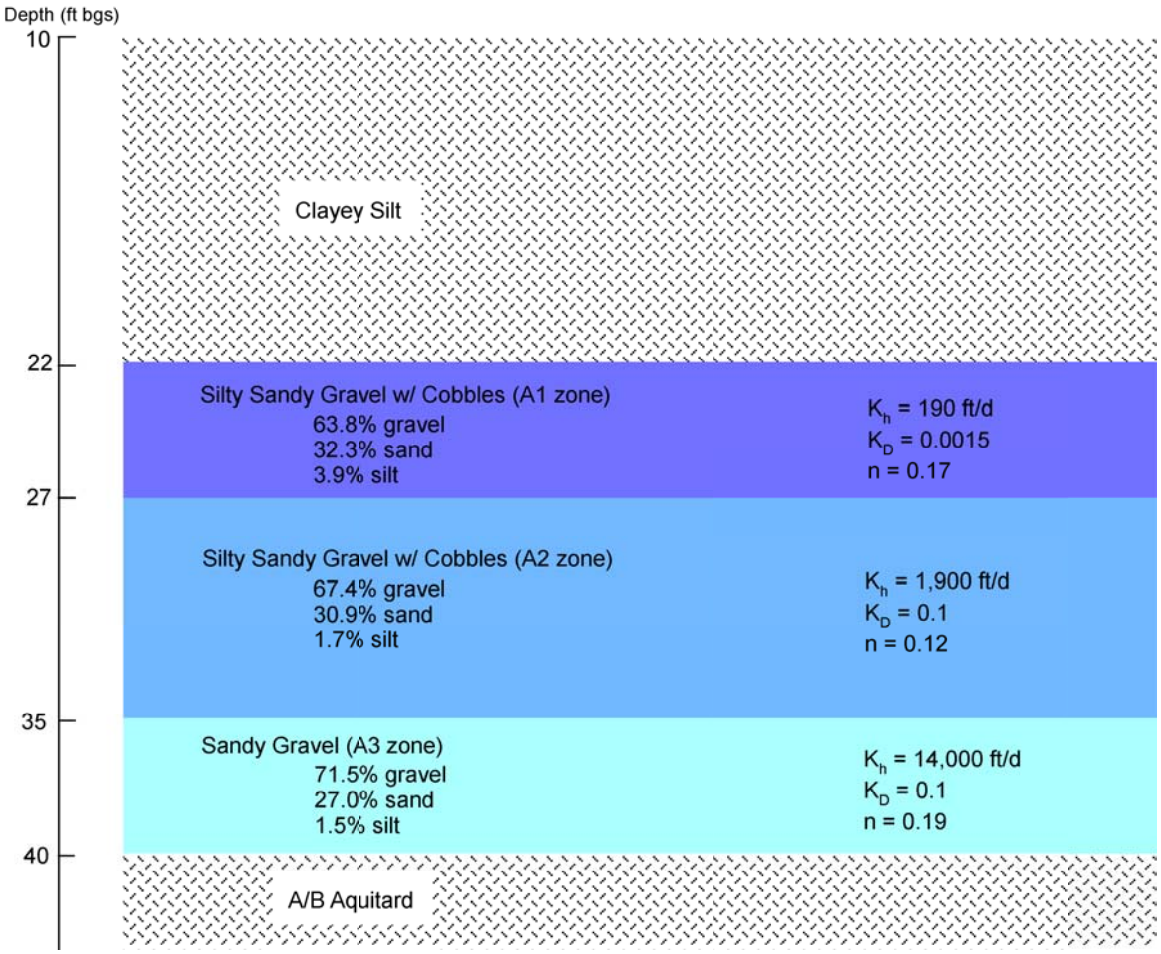

Figure 2.2. Generalized Hydrogeologic Conceptual Model of the ISRM Pilot Test Site

profile data collected by the EPA showed that the highest concentrations of Cr(VI) measured at the site were within the A1 zone (Figure 2.3). These characterization results demonstrated the importance of fully characterizing the hydrogeologic complexities present within the extent of the proposed treatment zone and the need to incorporate these complexities into the ISRM treatment zone emplacement design.

Figure 2.4 shows a cross section of the screened interval of all wells installed at the pilot test site. Due to the requirement that all planned monitoring wells be installed in a single drilling campaign, most of the wells installed at the pilot test site were completed based on the original hydrogeologic conceptual model (i.e., no discernable layering within the A zone, Figure 1.2) and the Cr(VI) profile data collected by EPA (Figure 2.3). As indicated in Figure 2.4, the majority of monitoring wells intercept multiple aquifer units, which limits their usefulness for interpreting tracer and reagent arrivals. Interpretation of the ISRM pilot test treatment zone emplacement data was limited by this lack of suitable wells (wells capable of providing depth discrete data from each of the hydrostratigraphic units identified at the site) and the well construction deficiencies in wells installed by the direct-push method.

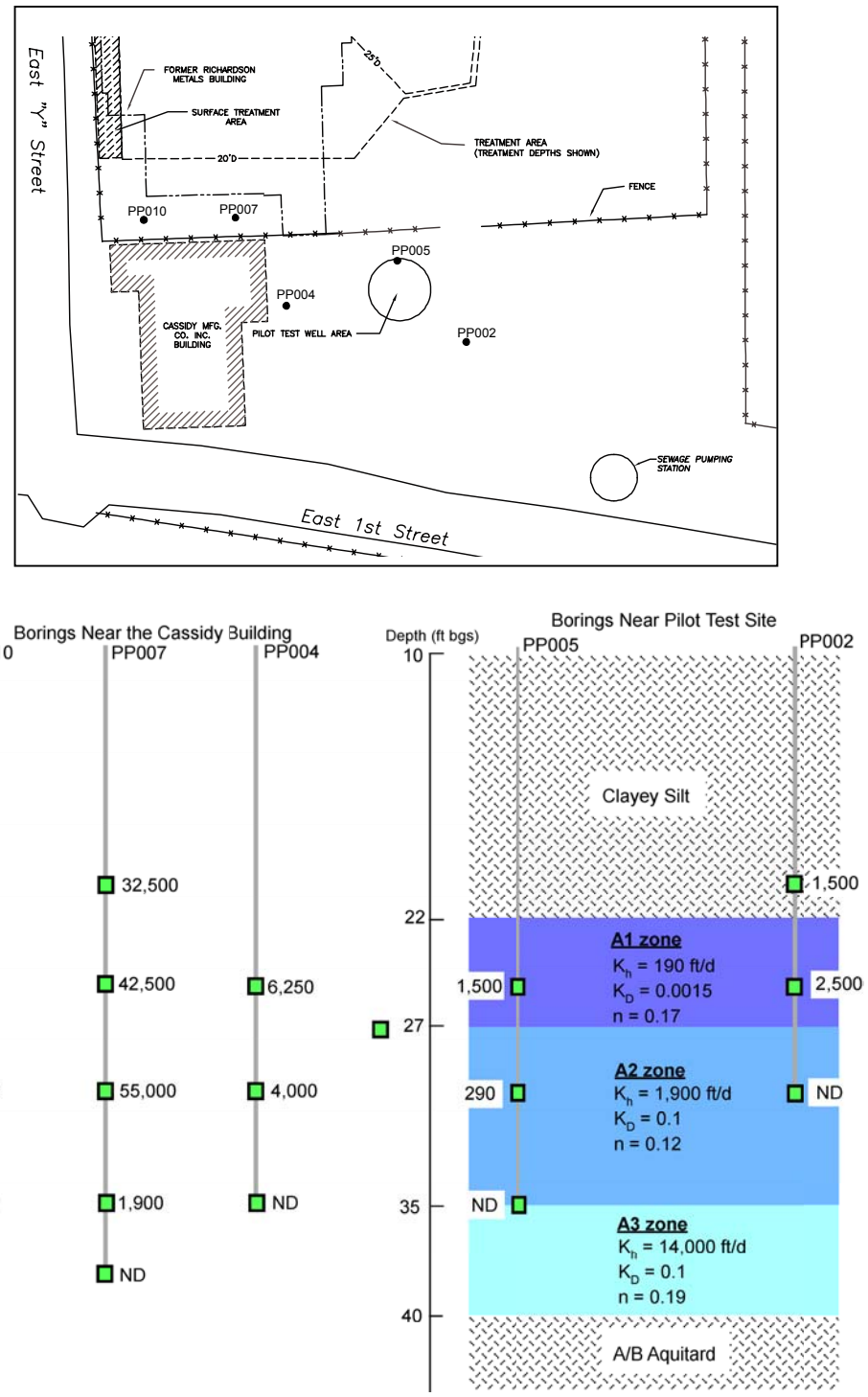

Figure 2.3. Geoprobe Sampling Locations and Aqueous Cr(VI) Concentrations (µg/L) Measured During the Initial Vertical Profile Sampling at the Site (EPA)

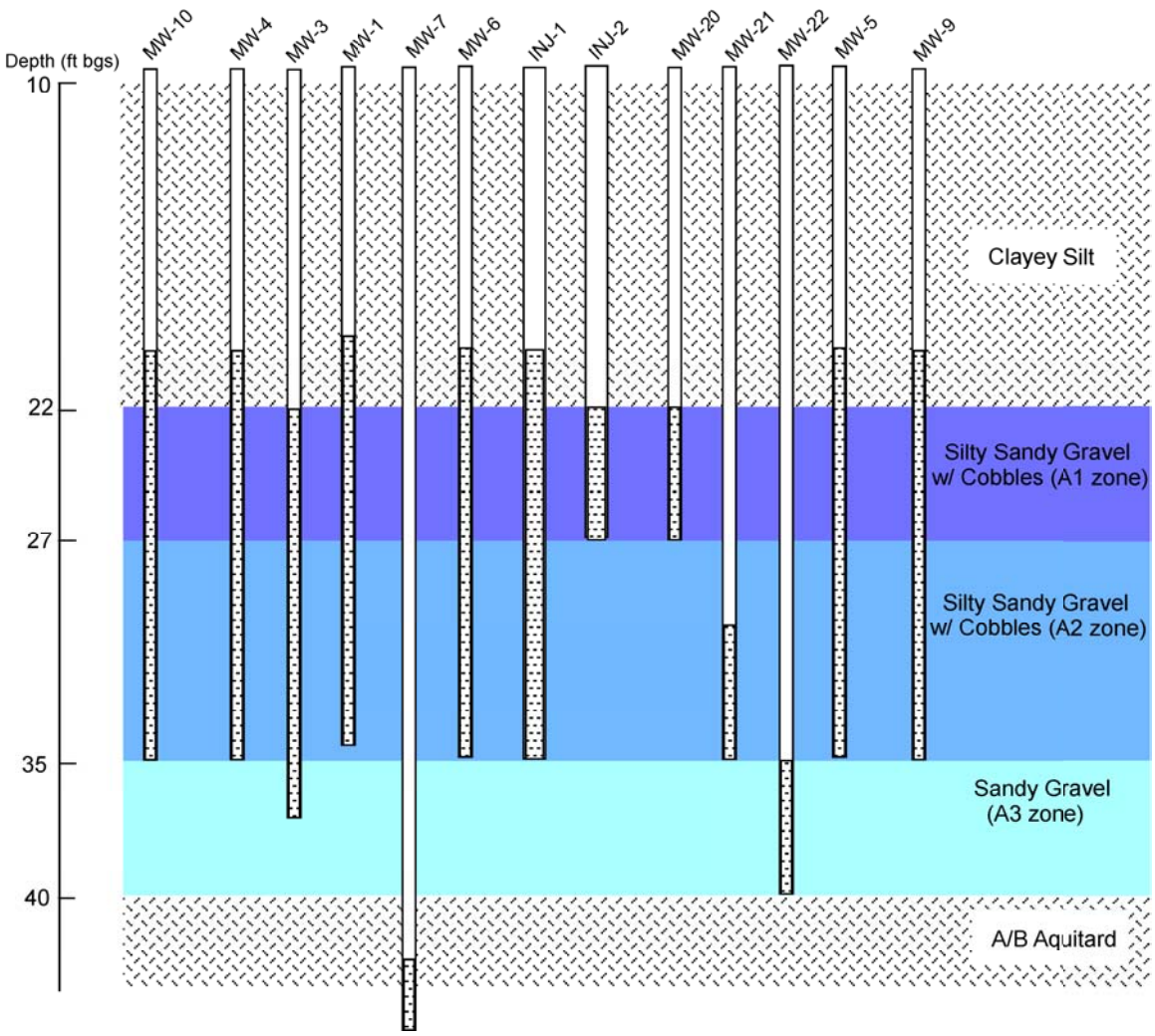

Figure 2.4. Monitoring Well Screened Intervals at the ISRM Pilot Test Site

2.3 Geochemical Characterization

Laboratory tests were conducted on 16 sediment core samples collected from four boreholes (across multiple depth intervals) to determine the reducible iron content and spatial distribution of iron for the targeted treatment zone. Laboratory experiments showed that chemical reduction yielded a redox capacity [0.26% Fe(II)] that falls within the range of values observed in sediments analyzed from sites where field-scale deployment of the ISRM technology is in progress or being considered (0.1% Hanford WA 100D area, 0.24% Ft Lewis WA, 0.4% Moffett Federal Airfield CA, 0.3% in preliminary FHC samples). A detailed discussion of sediment geochemical analyses and results are provided in a letter report to EPA.[(a)]

(a) Szecsody JE, BJ DeVary, VR Vermeul, MD Williams, and JS Fruchter. October 2002. *In Situ Redox Manipulation Bench-Scale Tests: Remedial Design Support for ISRM Barrier Deployment, Frontier Hard Chrome Site, Vancouver, Washington*. Letter Report to EPA from Pacific Northwest National Laboratory, Richland, WA.

2.4 Hydrologic Characterization

Two short constant-rate injection tests were conducted at the ISRM pilot test site to provide the site-specific hydraulic property estimates needed to develop a treatment zone emplacement design. In addition, a series of electromagnetic borehole flow meter tests were conducted to characterize the vertical distribution of horizontal hydraulic conductivity and formation heterogeneities encountered at the site.

Hydraulic tests conducted at the site were limited (both in injection rate and duration) due to schedule, budget, and waste disposal constraints and were designed to provide a semiquantitative estimate of areal hydraulic properties within the region affected by the treatment zone. The first constant-rate injection test, conducted on June 13, 2002, was run at a constant rate of 50 gpm for approximately six hours. The test was run by injecting clean water from a local fire hydrant into a centrally located injection well (INJ-1) and monitoring pressure response in all site monitoring wells. Pressure response data were monitored using pressure transducers (10 and 20 psi, 0.1% of full-scale accuracy) and continuously recorded with a Campbell Scientific data logger.

As discussed in Section 2.2, the hydrogeology encountered beneath the ISRM pilot test site was inconsistent with the original hydrogeologic conceptual model. Subsequently, the initial constant-rate injection test conducted in INJ-1, which was screened across both the A1 and A2 aquifer zones (Figure 2.4), provided test conditions that were not suited to obtaining hydraulic property estimates for the A1 zone and thus resulted in a large degree of error in that estimate. With additional information from a tracer injection test, it was determined that well INJ-1 would not be an effective treatment zone emplacement well, so a new injection well targeting the A1 zone was drilled (INJ-2, Figure 2.4). To improve hydraulic property estimates prior to finalizing the design for the dithionite injection test, a second constant-rate injection test was conducted in INJ-2 using the same approach. The test was conducted on September 12, 2002 at a constant rate of 20 gpm for approximately 90 minutes. Due to the relatively low permeability of this zone and the relatively shallow static depth to water (~20 ft), an inflatable packer was required to pack off the screened interval and prevent injection fluid from overflowing the casing.

Using the response data from each of these tests, an iterative approach was used to obtain a solution that best approximated both sets of data. The resulting best estimates of hydraulic properties for the layered system are shown in Table 2.1 and Figures 2.2 and 2.3.

Table 2.1. Hydraulic Property Estimates

Hydrostratigraphic Unit	Hydraulic Conductivity (K_h)	Anisotropy Ratio (K_D)
A1	190 ft/d	0.0015
A2	1,900 ft/d	0.1
A3	14,000 ft/d	0.1

To better characterize formation heterogeneities that were observed during a tracer injection test conducted at the site and to provide additional information for designing the dithionite injection test, a series of electromagnetic borehole flow meter (EBF) tests were conducted in pilot test site monitoring wells. These data were useful in interpreting tracer and reagent arrival curves and provided valuable guidance for placing the alternate injection well (INJ-2) screen interval. Due to this demonstrated usefulness of the EBF testing approach at the pilot test site, additional testing was conducted along the full length of the barrier alignment to better characterize formation heterogeneities (see Section 3.3). A detailed discussion of the test methods and plots of results along the full ISRM barrier alignment are presented in Appendix B.

2.5 Baseline Groundwater Chemistry

Two rounds of groundwater samples were collected from all test site injection and monitoring wells (with the exception of well INJ-2, which had not been installed yet) before beginning any injection testing at the ISRM pilot test site. Samples were collected by EPA during the weeks of June 3 and June 10, 2002. Field parameters that were measured during the sampling events included electrical conductivity (EC), temperature, oxidation-reduction potential (ORP), pH, dissolved oxygen (DO), and hexavalent chromium. Laboratory analyses were also performed to measure common anions (ion chromatography, EPA-300.0) and trace metals (ICP-OES, EPA-SW-846 6010) concentrations.

Average baseline aqueous chemistry results for the two baseline sampling events are listed in Tables 2.2 and 2.3. Baseline Cr(VI) data, the most critical performance measure, are also shown in Figure 2.5. These data, which represent the mean value for the two baseline sampling events, are also included in the discussion of ISRM treatment zone performance in Section 2.6 and Section 7.

Table 2.2. Field Parameters, Hexavalent Chromium, and Major Anions Monitoring Results Representing Baseline Conditions at the ISRM Pilot Test Site

Well Number	Chloride (mg/L)	Fluoride (mg/L)	Nitrate+Nitrate as N (mg/L)	Total Phosphorus (mg/L)	Sulfate (mg/L)	Hexavalent Cr (mg/L)	EC (µS/cm)	DO (mg/L)	pH	ORP (mV)
MW-1	5.48	0.135	1.30	0.064	19.5	0.58	381	1.5	6.63	261
MW-3	3.77	0.103	1.99	0.073	28.2	3.55	538	5.1	6.40	230
MW-4	5.59	0.098	1.60	0.067	15.2	0.65	522	3.4	6.60	218
MW-5	5.24	0.102	1.49	0.071	11.5	0.04	264	2.8	6.74	255
MW-6	5.44	0.094	1.32	0.067	14.8	1.50	316	3.0	6.74	283
MW-7	5.80	0.097	2.07	0.038	18.5	<0.05	312	3.2	7.23	28
MW-9	4.96	0.102	1.59	0.074	11.9	0.06	254	3.0	6.58	176
MW-10	4.78	0.093	1.60	0.063	24.4	1.90	411	1.7	6.50	231
MW-20	3.96	0.102	1.34	0.059	22.3	4.50	466	2.6	6.52	247
MW-21	5.47	0.102	1.49	0.063	10.6	0.05	260	3.2	6.80	291
MW-22	5.62	0.081	1.48	0.074	11.3	0.36	276	3.3	6.72	266
INJ-1	5.49	0.097	1.45	0.088	14.5	1.45	324	4.8	6.78	214

Table 2.3. Trace Metals Monitoring Results Representing Baseline Conditions at the ISRM Pilot Test Site

Well Number	Dissolved Metals (µg/L)										
	Ag	**Al**	**As**	**Ba**	**Be**	**Ca**	**Cd**	**Cr**	**Co**	**Cu**	**Fe**
INJ-1	0.50 U	20.1	2.0 U	31.2	0.20 U	46050	0.40 U	1630	0.70 U	1.4	9.5 J
MW-1	0.50 U	19.6 U	2.0 U	38.9	0.20 U	52400	0.40 U	621	1.3	1.0 U	9.5 U
MW-3	0.50 U	19.7	2.0 U	75.1	0.20 U	88070	0.40 U	3783	0.73	2.1 J	9.5 U
MW-4	0.50 U	24.7 U	2.0 U	20.2	0.20 U	42500	0.40 U	742	0.70 U	1.0 U	9.5 U
MW-5	0.60 U	16.8 U	3.1 U	18.4	0.20 U	32500	0.35 U	56.3	0.65 U	1.3 U	10.5 U
MW-6	0.60 U	18.9 U	3.1 U	16.4	0.20 U	40650	0.35 U	1400	0.65 U	1.3 U	10.5 U
MW-7	0.60 U	17.7 U	3.1 U	17.8	0.20 U	34575	0.35 U	2.2	2.5	1.1 U	33.6 U
MW-9	0.60 U	16.8 U	3.1 U	13.9	0.20 U	31650	0.35 U	54.7	0.65 U	1.1 U	10.5 U
MW-10	0.50 U	19.6 U	2.0 U	32.9	0.20 U	55800	0.40 U	1805	0.70 U	1.1	9.5 U
MW-20	0.60 U	16.8 U	3.1 U	59.5	0.20 U	65200	0.35 U	4770	0.65 U	2.6	10.5 U
MW-21	0.60 U	16.8 U	3.1 U	14.7	0.20 U	31100	0.35 U	55.1	0.65 U	1.5 U	10.5 U
MW-22	0.57 U	17.7 U	2.7 U	11.3	0.20 U	33600	0.37 U	370	0.67 U	1.4 U	10.1 U

Well Number	Dissolved Metals (µg/L)											
	Hg	**K**	**Mg**	**Mn**	**Na**	**Ni**	**Pb**	**Sb**	**Se**	**Tl**	**V**	**Zn**
INJ-1	0.12 U	2860	10095	92.9	7065	1.7 U	1.1 U	5.3	2.1 U	2.2 U	3.9	3.8 U
MW-1	0.61 U	3720	10900	507	14550	2.4 U	1.1 U	2.2 U	2.1 U	2.2 U	3.3	6.7 U
MW-3	0.43 U	3743	13730	207	10480	3.6 U	1.1 U	9.2	2.1 U	2.2 U	2.2	4.7 U
MW-4	0.61 U	2915	10125	96.7	6795	1.6 U	1.1 U	2.5	2.3	2.2 U	4.3	3.0 U
MW-5	0.6 U	2485	8320	80.8	7190	1.7	1.2 U	1.9 U	2.2 U	2.8 U	5.0	2.5 U
MW-6	0.6 U	2660	10550	48.4	8275	1.04 U	1.2 U	3.1	2.2 U	2.8 U	5.1	2.2 U
MW-7	0.6 U	3703	10145	805	11206	2.0 U	1.2 U	1.9 U	2.2 U	2.8 U	2.2	2.0 U
MW-9	0.10 U	2360	8225	33.6	7305	0.98 U	1.2 U	1.9 U	2.2 U	2.8 U	5.2	2.1 U
MW-10	0.6 U	3265	12350	88.5	7950	1.7 U	1.1 U	4.5	2.2	2.2 U	3.8	4.2 U
MW-20	0.6 U	3575	10300	205	19450	3.4	1.2 U	11.5	2.2 U	2.8 U	1.8	2.6 U
MW-21	0.6 U	2495	8465	95.2	7435	1.2	1.2 U	1.9 U	2.2 U	2.8 U	4.5	1.8 U
MW-22	0.43 U	3067	9337	44.6	6727	1.5 U	0.8 U	2.1	2.1 U	2.6 U	5.4	1.9 U

U = Not detected (<MDL)
J = Reported value is an estimate. Analyte was detected, but has a large associated error.

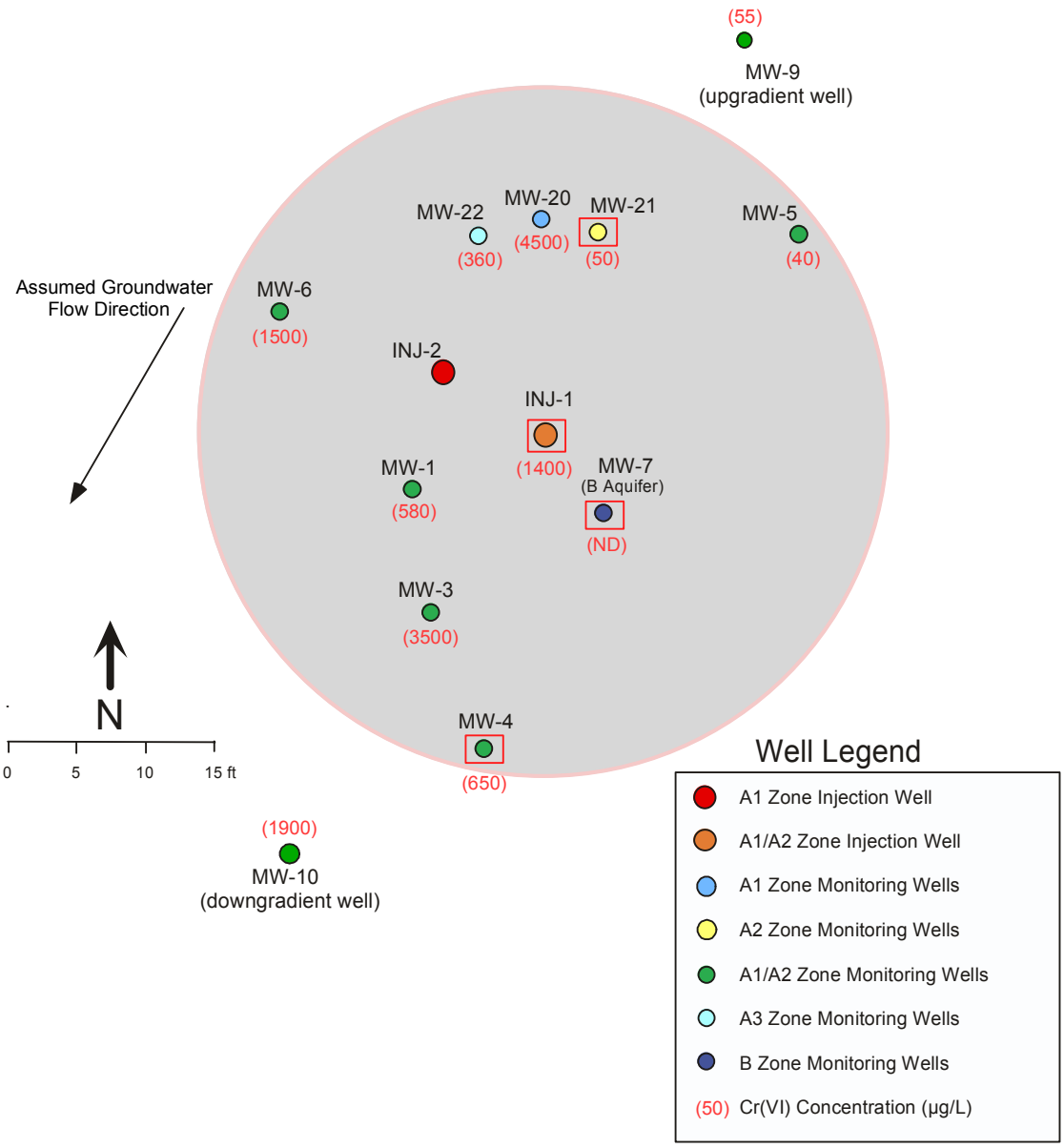

Figure 2.5. Baseline Cr(VI) Concentrations at the ISRM Pilot Test Site

2.6 Treatment Zone Emplacement

The pilot-scale ISRM treatment zone was created by injecting and withdrawing a sodium dithionite solution with a potassium carbonate pH buffer to reduce the naturally occurring Fe(III) to Fe(II)in the aquifer sediments. During this test, which was conducted from October 17 to 20, 2002, reagent injection and withdrawal was performed in well INJ-2 (Figures 2.1 and 2.4) using

an injection/withdrawal (or push-pull) approach that consisted of three phases: injection, residence, and withdrawal. During the injection phase, the solution is injected into a central injection/withdrawal well. The residence phase provides additional time for the reagent solution to react with the aquifer sediments. During the withdrawal phase, the solution is extracted from the aquifer by pumping it from the same well used for injection. Well INJ-1 was also used for extraction during the withdrawal phase to help remove reaction products from the lower A aquifer zone. Process/monitoring equipment and operational procedures that were used during all phases of the pilot test are discussed in Section 5.

The objective of the ISRM pilot test was to create a reduced zone in the targeted portion of the aquifer (unit A1 and the upper portion of unit A2, as shown in Figure 2.2) that would significantly lower hexavalent chromium concentrations in groundwater migrating through the treatment zone. This field test was needed to gather information for the design of a full-scale ISRM barrier at the site (see Section 4). While the bench-scale studies demonstrated the feasibility of the ISRM concept at a small scale, the field test incorporated all additional complexities of full-scale remediation (formation heterogeneities and their effect on reagent distribution, iron oxide spatial heterogeneity, etc.). Operational parameters from the ISRM pilot test are summarized in Table 2.4. Figure 2.6 provides the dithionite and EC measurements for the injection and withdrawal streams during the test.

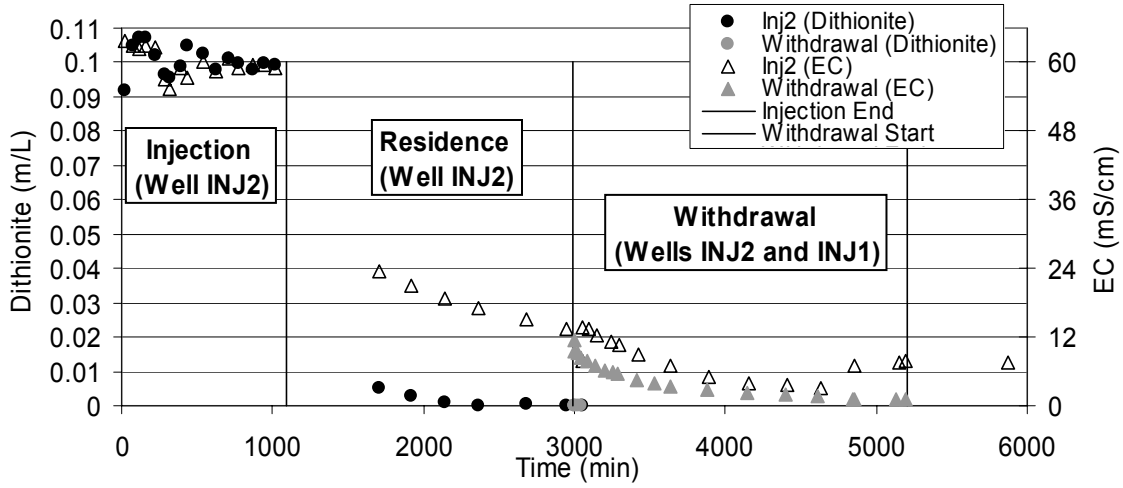

Figure 2.6. Dithionite and EC Measurements of During Injection, Residence, and Withdrawal Phases of FHC Pilot-Scale Dithionite Injection/Withdrawal Test

Table 2.4. Summary of ISRM Pilot-Scale Dithionite Injection/Withdrawal Test

Test Parameter	Value
Injection Phase	
Reagent Mass	5,300 lb 90% purity sodium dithionite ($Na_2S_2O_4$) 15,000 lb potassium carbonate (K_2CO_3)
Tanker Truck Volume	5,736 gal
Total Injection Rate	40.3 gal per min
Tanker Truck Injection Rate	5.2 gal per min
Fire Hydrant Injection Rate	34.9 gal per min
Injection Concentration	0.1 moles/L $Na_2S_2O_4$
Injection Duration	1097 min (18.3 hr)
Injection Volume	44,000 gal
Residence Phase	
Duration	1,893 min (31.5 hr)
Withdrawal Phase	
Total Withdrawal Volume	44,400 gal
Total Withdrawal Mass	5% of injection sulfur (based on EC/sulfur trend analysis)
INJ-1 – Withdrawal Rate	15–20 gal per min
INJ-1 – Volume	36,200 gal
INJ-1 – Duration	2,215 min (36.9 hr)
INJ-2 – Withdrawal Rate	~5 gal per min
INJ-2 – Volume	~8,200 gal
INJ-2 – Duration	1,662 min (27.7 hr)

During emplacement of the pilot-scale treatment zone, approximately 5,700 gallons of concentrated sodium dithionite solution with a potassium carbonate pH buffer was delivered to the site in a tanker truck. Before shipment to the ISRM site, the solution was chilled (during the dissolving process), and the headspace of the tank was blanketed with nitrogen gas to prevent oxidation with atmospheric oxygen. The molar concentration of potassium carbonate was four times that of the sodium dithionite to maintain a high pH (i.e., an injection solution pH of 11) for enhanced stability of dithionite.

The concentrated reagent was pumped directly from the tanker truck and diluted inline using a local water supply from a nearby fire hydrant. The volume of concentrated reagent in the tanker truck was estimated based on tank level measurements and was used to determine the injection rate of the concentrated reagent that would provide the specified concentration, injection rate, and total injection volume. The dithionite injection concentration was monitored closely at the beginning of the test and at regular intervals throughout the test to verify that the delivered tanker volume, reagent mass, and purity met design specifications. Dithionite was measured at the field site in an onsite mobile laboratory using two automated high-performance liquid chromatography (HPLC) systems. Because of its instability, dithionite must be measured at the site shortly after sample collection. In addition, a blanket of argon gas was maintained in

the headspace of the tanker throughout the injection to minimize reagent degradation from contact with atmospheric oxygen.

The average reagent concentration for the pilot dithionite injection test was 0.1 M sodium dithionite with a 0.4 M potassium carbonate pH buffer. A total volume of 44,000 gallons of reagent was injected into well INJ-2 at a rate of 40 gpm for 18.3 hours. Aqueous samples were collected at roughly five-minute intervals with samples collected from the injection stream and all the monitoring wells every 1.25 hours on average. Breakthrough curves (BTCs) for dithionite and EC were generated and are provided in Vermeul et al. (2002a). During this test, most monitoring wells did not indicate high dithionite and EC concentrations during the injection phase; this was not unexpected because the injection was focused on the A1 zone, and only one monitoring well (MW-20) was discretely screened in this lower-permeability zone. The one exception to this was well MW-6, which had a very rapid arrival early in the injection phase. However, during site-specific characterization of the full barrier alignment, it was determined that the direct-push wells (e.g., MW-6) did not provide an adequate annular seal throughout the upper, more fine-grained portion of the aquifer and that data from this well should be considered suspect.

EC and dithionite measurements in the wells discretely screened in the A2 and A3 zones during the injection phase were very low (1% and less of injection dithionite concentrations). Data from these wells show that there was not much vertical spreading of the reagent at these locations during the injection phase. The monitoring results from the one well screened below the A aquifer (MW-7) showed no significant change in EC or dithionite concentration.

Following the injection phase, the residence phase provided additional time for the dithionite to react with the aquifer sediments. Aqueous samples were collected during the residence phase and measured for dithionite and field parameters. The duration of the residence phase was determined by the estimated field-scale dithionite reaction and degradation rates and from dithionite concentrations measured at the site. The duration of the residence phase for the pilot dithionite injection test was 31.5 hours. Sampling frequencies for the wells during this phase of the test started at 2-hr intervals and was decreased to a 4-hr frequency by the end of this phase. Very low levels of dithionite (<0.2% of the injection concentration) were measured in site monitoring wells at the end of the residence phase. This decrease in dithionite concentration was due to reaction with ferric iron, disproportionation, and density effects.

During the withdrawal phase, 44,400 gallons was pumped from wells INJ-2 and INJ-1 and disposed of to the City of Vancouver's sanitary sewer southeast of the test site; this volume was approximately the same as the injection volume. Extraction rates and volumes are shown in Table 2.4. EC and dithionite concentrations in the withdrawal stream and well INJ-2 are shown in Figure 2.6. The majority of the withdrawn water was pumped from well INJ-1 at 15 to 20 gpm for 36.9 hr for a total extraction volume of 36,200 gallons. An additional 8,200 gallons was extracted from well INJ-2 at a rate of ~5 gpm for 27.7 hours. Extraction from well INJ-2

was limited due to the lower hydraulic conductivity materials composing the A1 zone and its ability to sustain a higher yield. Extraction from well INJ-2 was stopped prior to completion of the withdrawal phase due to a pump failure.

The sampling frequency of the withdrawal stream was high (~1/2 hr) at the beginning of the withdrawal phase and then decreased gradually to a 4-hr interval during the second half of this phase. Dithionite concentrations were very low in the withdrawal stream. Measurements quickly dropped below detection limits within a few hours of the start of withdrawal. Overall withdrawal concentrations (reaction products) were very low relative to the injection concentrations based on EC data. Peak concentrations in the withdrawal phase were less than 20% of the injection concentration in the beginning of the phase and rapidly dropped to below 10% in the first few hours. Concentrations in well INJ-2 slightly rebounded once extraction from that well was stopped, as shown in Figure 2.6.

Aqueous samples from the withdrawal stream were collected and analyzed to determine mass recovery from the withdrawal phase by total sulfur (as sulfate) and EC (Figure 2.7). Based on these analyses, an estimated 5% of the total injected reagent mass was recovered during the withdrawal phase. This relatively poor recovery is most likely associated with the heterogeneous nature of the formation materials at FHC and density sinking of the reagent. Table 2.5 summarizes the results for EC, total sulfur, and total sulfur (as SO_4) immediately after the pilot-scale test. These results indicate how much spent reagent remained in the aquifer after completing the test. As expected, EC increased following treatment from an average baseline value of 360 µS/cm to an average post-emplacement value of 2355 µS/cm. Post-emplacement total sulfur (as SO_4) averaged 569 mg/L, as indicated by both the EC and total sulfur data. Residuals were significantly more elevated in the A1 zone (INJ-2, MW-20) than in the lower portion of the aquifer. These elevated residual concentrations are associated with the difficulty of withdrawing spent reagent from this relatively low-permeability material.

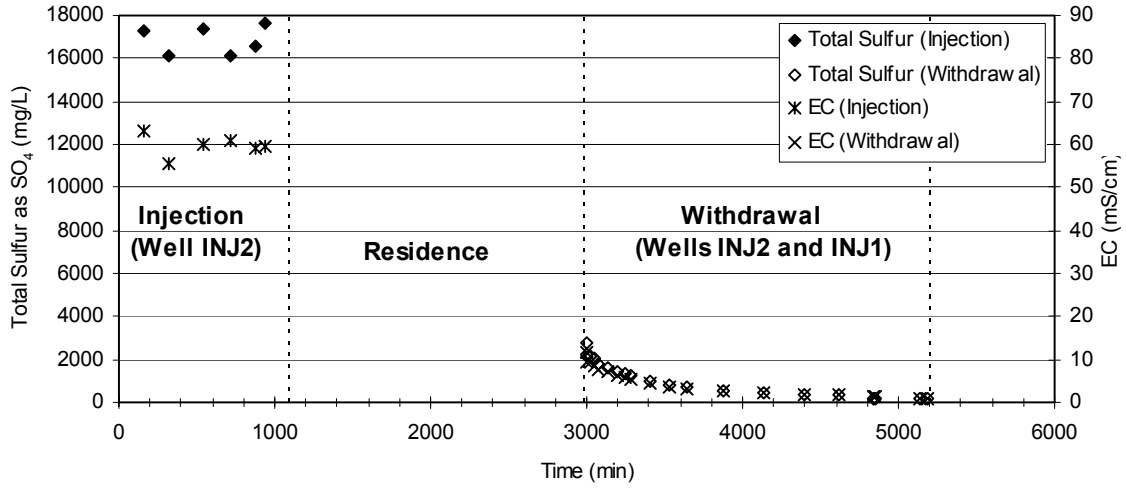

Figure 2.7. Total Sulfur and EC Measurements of the Injection and Withdrawal Streams During the FHC Pilot-Scale Dithionite Injection/Withdrawal Test

Table 2.5. Results for Conductivity, Total Sulfur, and Total Sulfur as Sulfate Following Treatment at the ISRM Pilot Test Site in October 2002

Well Number	EC (µS/cm)	Total S (mg/L)	Total S as SO_4 (mg/L)
INJ-1	1861	144	433
INJ-2	7490	659	1977
MW-4	1970	137	410
MW-5	428	24	72
MW-6	2450	210	629
MW-9	429	21	62
MW-10	2190	165	494
MW-20	5450	437	1311
MW-21	494	38	115
MW-22	792	63	189

Because the injected reagent is a high pH, high ionic-strength reducing agent, it has the potential to mobilize some trace metals through several processes, including reduction, amorphic dissolution, and cation exchange. Table 2.6 summarizes the trace metals analysis results for filtered samples collected after emplacement of the pilot-scale treatment zone and for comparison with baseline conditions. Average post-treatment concentrations within the treatment zone, which is represented by monitoring wells INJ-1, INJ-2, MW-4, MW-6, MW-20, MW-21, and MW-22, are shown for comparison with average baseline concentrations and with the primary and/or secondary maximum contaminant levels (MCL). Well MW-5 was excluded from the average post-treatment concentration because, due to formation heterogeneities and the resulting asymmetry in the radial extent of reagent transport, very little treatment was realized in the region monitored by this well. Average post-treatment concentrations within the treatment zone can also be compared with concentrations outside the targeted treatment zone, represented by upgradient well MW-9 and downgradient well MW-10. Average baseline concentrations represent the mean result for all site monitoring wells, as provided in Table 2.3.

Table 2.6 shows that iron and manganese exceeded the secondary MCL. Iron increased from a baseline level below the detection level in all but one well (well INJ-1 in Table 2.3) to levels that exceeded the secondary MCL in 6 of the 10 wells sampled following treatment. The highest levels were associated with the A1 and A2 monitoring zones within the targeted treatment zone (shaded area in Figure 2.1). Baseline levels for manganese exceeded the secondary MCL in most of the wells (Table 2.3). Following treatment zone emplacement, manganese increased by a factor of about 10, or approximately 40 times the secondary MCL, and exceeded the secondary MCL in all zones monitored, including the upgradient and downgradient wells. These increases indicate that, as expected, iron and manganese were mobilized by the reductive treatment.

Although the average post-test concentration for arsenic within the treatment zone did not exceed the primary MCL, arsenic did exceed the MCL in two wells (INJ-2 and MW-20)

completed solely within the A1 monitoring zone. Arsenic concentrations increased from levels below detection to 12.1 and 11.5 µg/L, respectively. The increases suggest that some arsenic was also mobilized by reduction. These elevated metal concentrations are not expected to migrate a significant distance downgradient of the reduced zone. This anticipated response will be assessed through long-term performance monitoring of the ISRM barrier emplacement (preliminary results contained in Section 7.1).

All major cations (Ba, Ca, K, Mg, and Na) increased between baseline and post-test monitoring due to injection of the high ionic strength reagent. The relatively large increase in potassium and sodium was due to the added potassium carbonate buffer (K_2CO_3) and sodium based reagent ($Na_2S_2O_4$), respectively. Other trace metal constituents showing discernable average increases between baseline and post-test monitoring include cobalt, copper, nickel, lead, and zinc; the increases were not significant and levels were well below MCL for lead and zinc.

Tables 2.7 through 2.9 summarize the results for hexavalent chromium and field parameters (conductivity, dissolved oxygen, pH, and oxidation reduction potential) during the two months following the pilot-scale test. These post-emplacement performance assessment monitoring results are consistent with the expected response for an ISRM treatment zone. Observed responses within the reduced iron treatment zone, relative to baseline conditions, included: 1) a decrease in the dissolved oxygen concentration associated with the creation of a reducing environment, 2) a decrease in the ORP, 3) a small increase in the pH associated with the pH buffered reagent, and 4) a decrease in hexavalent chromium concentration within the treatment zone to below detection limits. Also worth noting is the EC and sulfite data that indicate continued drainage of the higher-concentration spent reagent (i.e., residuals) in the A1 zone into the deeper, higher-permeability A2 zone. At the two locations where depth discrete information is available (INJ-1/INJ-2 and MW-20/MW-21 well pairs), a decreasing trend was observed in the A1 zone while a corresponding increasing trend was observed in the deeper wells.

The primary measure of performance for the ISRM pilot-scale treatment zone was based on comparing Cr(VI) concentrations within the treatment zone after emplacement of the reduced zone with pretreatment baseline conditions. These Cr(VI) performance data, collected approximately two, four, and eight weeks after treatment zone emplacement, are shown in Figures 2.8, 2.9, and 2.10, respectively. As indicated, the preliminary results were promising. Hexavalent chromium concentrations were reduced from as high as 4,500 µg/L to below detection limits (spectrophotometric method, 20 µg/L reported by EPA, 10 µg/L cited in manufacturer specifications) in all monitoring wells within the established treatment zone. MW-5 (along with the up- and downgradient monitoring wells) is not considered within the treatment zone due to the limited (or absence of) treatment at these wells. Based on these preliminary results, a decision was made to proceed with full-scale deployment of an ISRM permeable reactive barrier at the FHC site.

Table 2.6. Trace Metals Monitoring Results Following Treatment at the ISRM Pilot Test Site, October 2002

Well Number	Dissolved Metals (µg/L)										
	Ag	**Al**	**As**	**Ba**	**Be**	**Ca**	**Cd**	**Cr**	**Co**	**Cu**	**Fe**
INJ-1	0.80 U	28.3 U	2.6 U	256	0.40 U	69200	0.50 U	4.2 B	32.0 B	2.1 U	3420
INJ-2	0.80 U	28.3 U	12.1	775	0.40 U	108000	0.50 U	22.1	96.9	2.9 B	16400
MW-4	0.80 U	28.3 U	2.6 U	432	0.49 B	76200	0.50 U	16.3	54.3	2.9 B	2980
MW-5	0.80 U	28.3 U	2.6 U	64.3 B	0.40 U	49400	0.50 U	119	14.8 B	2.3 B	366
MW-6	0.80 U	28.3 U	2.0 U	72.9 B	0.42 B	46200	0.50 U	3.2 B	95.8	2.1 U	756
MW-9	0.80 U	28.3 U	2.6 U	80.8 B	0.40 U	47300	0.50 U	785	9.8 B	6.9 B	36.2 B
MW-10	0.80 U	28.3 U	2.6 U	506	0.40 U	71900	0.50 U	28.0	93.2	9.7 B	2.8 B
MW-20	0.80 U	43.4 B	11.5	1140	0.40 U	118000	0.50 U	26.8	108	5.5 B	29600
MW-21	0.80 U	28.3 U	2.6 U	54.9 B	0.40 U	42500	0.50 U	12.1	16.4 B	4.1 B	294
MW-22	0.80 U	28.3 U	2.0 U	61.2 B	0.40 U	40700	0.50 U	19.7	34.5 B	2.2 B	243
Baseline											
Average for All Wells	0.56 U	18.8	2.6 U	29.2	0.20 U	46175	0.37 U	1274	0.88	1.4	12.0
Post Treatment											
Average for Treatment Zone Wells	0.80 U	30.4	5.1	398.9	0.42	71543	0.50 U	14.9	62.6	3.1	7670
Upgradient Well	0.80 U	28.3 U	2.6 U	80.8 B	0.40 U	47300	0.50 U	785	9.8 B	6.9 B	36.2 B
Downgradient Well	0.80 U	28.3 U	2.6 U	506	0.40 U	71900	0.50 U	28.0	93.2	9.7 B	2.8 B
Primary MCL			10		4		5	100		1300	
Secondary MCL	100	50 to 200								1000	300

Well Number	Dissolved Metals (µg/L)											
	Hg	**K**	**Mg**	**Mn**	**Na**	**Ni**	**Pb**	**Sb**	**Se**	**Tl**	**V**	**Zn**
INJ-1	0.20 U	255000	24500	2060	141000	64.8	1.9 B	2.0 U	2.5 U	7.0 U	1.5 B	13.6 B
INJ-2	0.54	1470000	51300	3180	962000	13.5 B	3.2	6.6 B	4.7 B	7.0 U	6.1 B	34.5
MW-4	0.20 U	247000	24600	2370	161000	6.6 B	3.7	2.0 U	2.5 U	7.0 U	2.7 B	11.2 B
MW-5	0.20 U	31500	11200	1840	18200	2.9 U	2.3 B	2.0 U	2.5 U	7.0 U	1.5 U	13.4 B
MW-6	0.20 U	423000	25700	626	210000	4.6 B	1.8 B	2.0 U	2.5 U	7.0 U	1.5 U	17.1 B
MW-9	0.62	13500	11900	1140	17600	2.9 U	2.5 B	2.0 U	2.5 U	7.0 U	2.2 B	15.7 B
MW-10	0.20 U	310000	21700	2980	218000	7.4 B	2.8 B	2.0 U	2.5 U	7.1 B	2.1 B	21.0
MW-20	1.3	970000	49900	5480	784000	16.2 B	4.3	5.0 B	2.5 U	7.0 U	10.1 B	27.0
MW-21	0.20 U	37300	10400	822	20300	2.9 U	2.9 U	2.0 U	2.5 U	7.0 U	1.8 B	14.8 B
MW-22	0.20 U	120000	13500	1750	50500	10.7 B	3.9	2.0 U	2.5 U	7.0 U	2.2 B	11.4 B
Baseline												
Average for All Wells	0.49 U	3071	10212	192	9536	1.9	1.1 U	4.0	2.2	2.5 U	3.9	3.1 U
Post Treatment												
Average for Treatment Zone Wells	0.41	503000	28600	2330	333000	17.0	3.1	3.1	2.8	7.0 U	3.8	18.5
Upgradient Well	0.62	13500	11900	1140	17600	2.9 U	2.5 B	2.0 U	2.5 U	7.0 U	2.2 B	15.7 B
Downgradient Well	0.20 U	310000	21700	2980	218000	7.4 B	2.8 B	2.0 U	2.5 U	7.1 B	2.1 B	21.0
Primary MCL	2						15	6	50	2		
Secondary MCL				50								5000

U = Not detected (<MDL) B = Detected at >MDL, but less than the contract required detection limit.

Table 2.7. Results of Hexavalent Chromium, Sulfite, and Field Parameters Following the Pilot-Scale Test, November 4-6, 2002

Well Number	Hexavalent Cr (mg/L)	Sulfite (as Na_2SO_3) (mg/L)	EC (µS/cm)	DO (mg/L)	pH	ORP (mV)
INJ-1	<0.02	110	1433	0.05	7.41	-24
INJ-2	<0.02	500	6130	0.10	7.59	-202
MW-1	<0.02	300	2770	0.07	7.74	-190
MW-3	<0.02	200	2700	0.10	7.42	-152
MW-4	<0.02	70	1408	0.38	7.20	86
MW-5	0.03	<1	545	2.90	6.83	181
MW-6	0.02[(a)]	320	2160	0.07	8.40	-110
MW-7	<0.02	6	1004	2.70	6.93	95
MW-9	0.15	8	448	0.10	6.52	140
MW-10	< 0.02	90	1487	0.07	6.88	113
MW-20	< 0.02	310	4310	0.17	7.05	-120
MW-21	0.02[(a)]	70	908	0.11	7.12	95
MW-22	0.02[(a)]	50	706	0.04	7.31	97
(a) Instrument reading probably due to a matrix effect.						

Table 2.8. Results of Hexavalent Chromium, Sulfite, and Field Parameters Following the Pilot-Scale Test, November 18-20, 2002

Well Number	Hexavalent Cr (mg/L)	Sulfite (as Na_2SO_3) (mg/L)	EC (µS/cm)	DO (mg/L)	pH	ORP (mV)
INJ-1	<0.02	140	2130	0.00	7.71	-135
INJ-2	<0.02	300	5220	0.00	7.37	-203
MW-1	<0.02	230	2990	0.00	7.59	-157
MW-3	<0.02	90	2700	0.00	7.66	-138
MW-4	<0.02	16	801	1.08	7.19	104
MW-5	0.32	< 1	609	1.30	6.91	177
MW-6	<0.02	18	1885	0.25	8.34	-55
MW-7	<0.02	7	1491	2.38	7.06	85
MW-9	1.65	1	448	2.03	6.63	189
MW-10	0.02	60	1226	1.21	7.08	125
MW-20	<0.02	200	3770	0.00	6.92	-101
MW-21	<0.02	< 1	863	0.00	7.48	63
MW-22	<0.02	10	644	2.10	6.99	121

Table 2.9. Results of Hexavalent Chromium, Sulfite, and Field Parameters Following the Pilot-Scale Test, December 16-18, 2002

Well Number	Hexavalent Cr (mg/L)	Sulfite (as Na_2SO_3) (mg/L)	EC (µS/cm)	DO (mg/L)	pH	ORP (mV)
INJ-1	<0.02	170	3530	0.29	6.99	-78
INJ-2	<0.02	330	4870	0.00	7.29	-97
MW-1	<0.02	410	5400	0.00	9.33	-135
MW-3	<0.02	300	4920	0.00	9.3	-98
MW-4	0.04[(a)]	100	2400	0.00	8.57	46
MW-5	<0.02	40	1233	5.05	6.89	111
MW-6	<0.02	270	4690	0.00	7.43	-131
MW-7	<0.02	6	1442	2.58	9.13	-43
MW-9	0.03	30	1488	6.67	6.79	107
MW-10	0.03	70	2030	0.78	8.19	109
MW-20	<0.02	170	3490	0.00	6.87	-39
MW-21	<0.02	90	1816	4.95	7.11	20
MW-22	<0.02	120	2030	0.00	7.1	39

(a) Instrument reading probably due to a matrix effect.

2.7 Emplacement Results and Discussion

The results of the pilot dithionite injection test indicated that two injection wells, one targeting the A1 zone and another the A2 zone, would be required to adequately treat the targeted interval of the A aquifer. The pilot test was conducted using only the INJ-2 injection well (A1 zone) for emplacing the treatment zone. The three depth-discrete monitoring wells available at the site (MW-20, MW-21, and MW-22) indicated that, under these injection conditions, formation properties in the A1 zone prevented sufficient reagent from contacting the A2 and A3 aquifer zone sediments. These conditions resulted in most of the reagent contacting only sediments within the A1 zone, with hydrogeologic and hydraulic properties of this zone limiting the amount of reagent contacting deeper sediments through density sinking during the residence phase.

Results from the pilot dithionite injection test, in conjunction with results from a tracer injection test conducted at the site, showed that the site has a very high degree of variability in hydraulic properties controlling the direction and extent of reagent transport and treatment capacity distribution during the emplacement process. Treatment of the A1 zone and the upper portion of the A2 zone is the primary objective of the remedial action injection design given the much greater hexavalent chromium concentrations in upper portion of the aquifer relative to concentrations observed deeper in the profile. Pilot-scale testing activities demonstrated the need for detailed characterization of hydrogeologic conditions and contaminant distribution

Figure 2.8. Comparison of Baseline Cr(VI) Concentrations with Measurements from the First Post-Emplacement Performance Assessment Sampling Event (two weeks after treatment)

along the full length of the barrier. This information was needed to determine the level of variability across the proposed barrier alignment relative to that observed at the pilot test site so that this variability could be incorporated into the injection design for full-scale deployment.

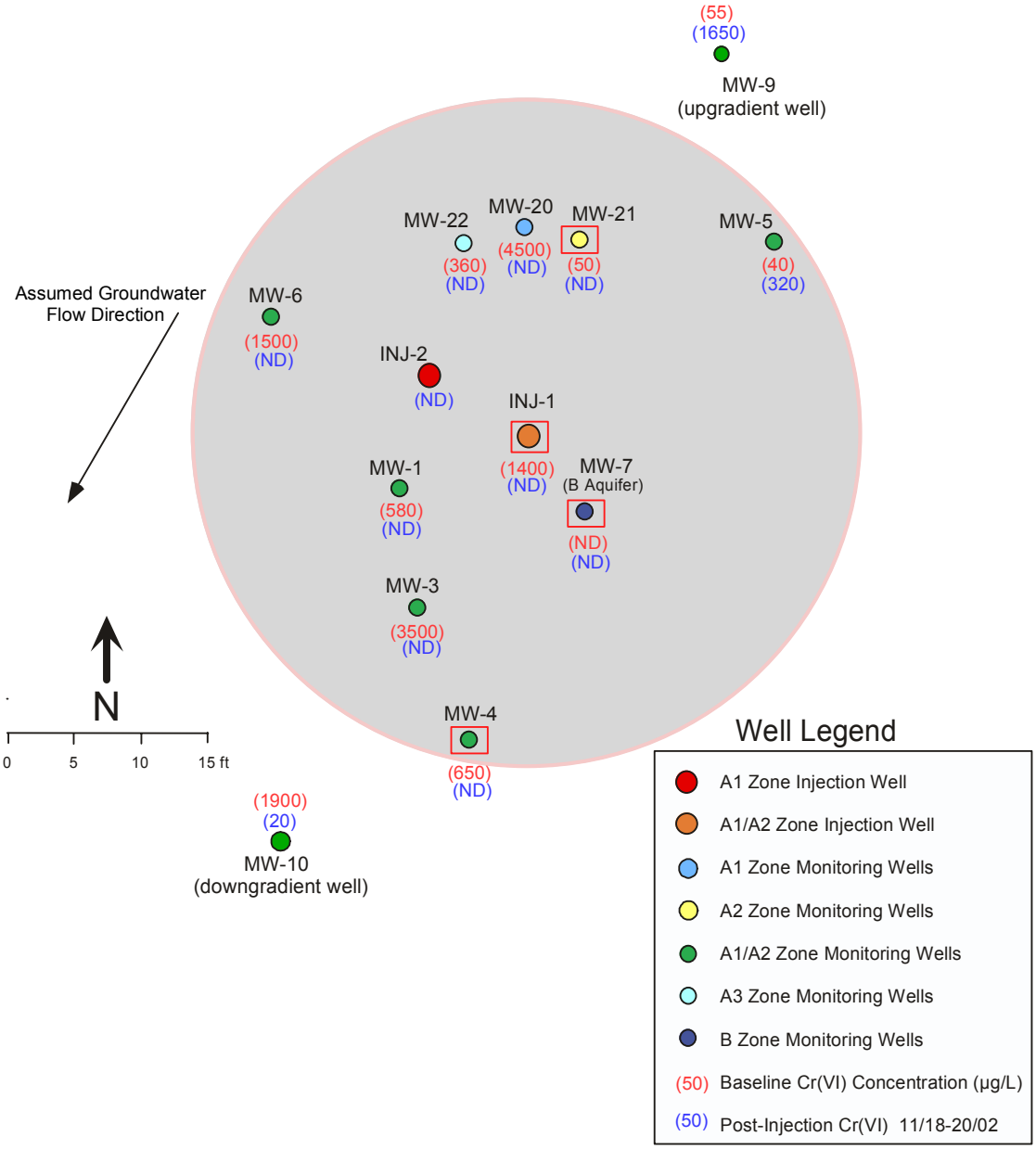

Figure 2.9. Comparison of Baseline Cr(VI) Concentrations with Measurements from the Second Post-Emplacement Performance Assessment Sampling Event (four weeks after treatment)

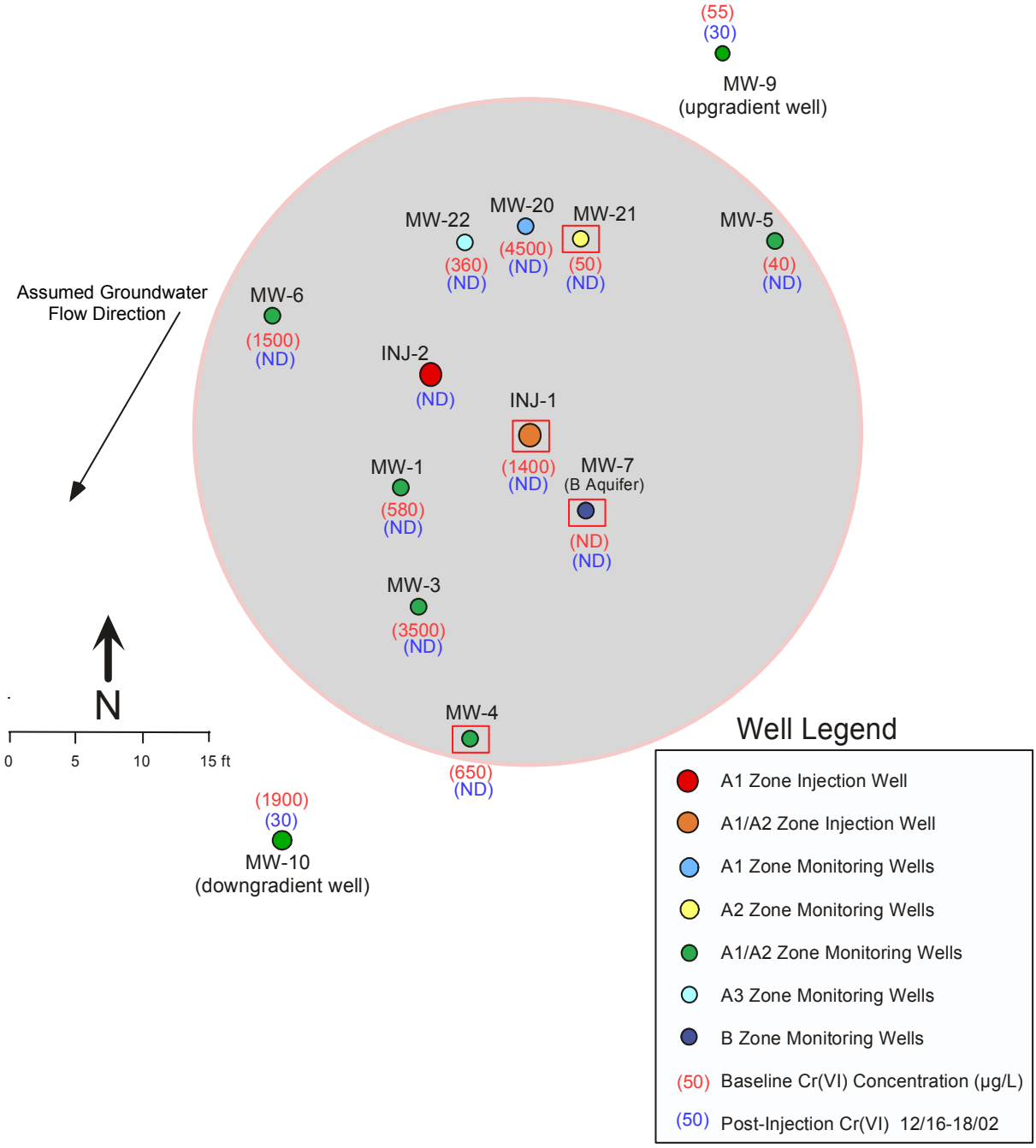

Figure 2.10. Comparison of Baseline Cr(VI) Concentrations with Measurements from the Third Post-Emplacement Performance Assessment Sampling Event (eight weeks after treatment)

3.0 Characterization of the Barrier Alignment

This section contains a description of characterization activities that were conducted along the full length of the barrier alignment and the resulting injection and monitoring wells that were installed to emplace and monitor the performance of the ISRM permeable reactive barrier.

3.1 Characterization Well Installation

As discussed in the previous section, pilot test results showed that hydraulic properties at the ISRM test site are highly variable and demonstrated the need for detailed characterization of hydrogeologic conditions and contaminant distribution along the full length of the barrier. These site-specific characterization data were needed to design the injection well network and develop an injection design for full-scale deployment of the ISRM technology. This section describes the field activities associated with installation and sampling of the seven temporary wells used to collect this information (Figure 3.1). These temporary characterization wells were installed in March of 2003 using the direct push (Geoprobe) method.

Sediment samples were collected as the push probes were advanced using a nominal 2-in.-diameter split-spoon sampler. Once collected, sample liners were split open to expose the sediments, and a detailed geologic log of each boring was prepared. Grab samples of the cuttings were collected at regular intervals and archived in chip trays for an integrated visual inspection of the entire sediment column thickness. These geologic logs and cuttings were used to identify formation contacts along the barrier alignment and develop a refined hydrogeologic conceptual model of the site (Section 3.2). In addition to sediment samples, groundwater samples were collected at regular intervals and analyzed for hexavalent chromium as the push probes were advanced. These depth-discrete Cr(VI) data are shown in Figure 3.2. As indicated by the chromium distribution data along the barrier alignment, at the time these data were collected, the highest concentrations were observed in the upper portion of the A aquifer and were primarily confined to the central portion of the plume.

Once these characterization probes were pushed to total depth, monitoring wells were installed using a modified approach developed to work with the direct-push drilling method. The approach involved advancing a 3.25-in. drill rod to total depth and completing the well with 2-in. PVC casing and screen. Screen material consisted of slotted pipe (10-slot) with native formation as the filter pack (i.e., drill rods were back-pulled, allowing native formation to collapse around the screen). Although this modified approach is a non-ideal well-completion methodology with inherent risks associated with the potential for a compromised annular seal, it was the only option available for installing 2-in.-diameter monitoring wells using the direct-push method. Following completion of these temporary well installations, each well was developed by surging and pumping to improve their hydraulic performance and groundwater sample quality. Once the well was sufficiently developed, a groundwater sample was collected from the completed well

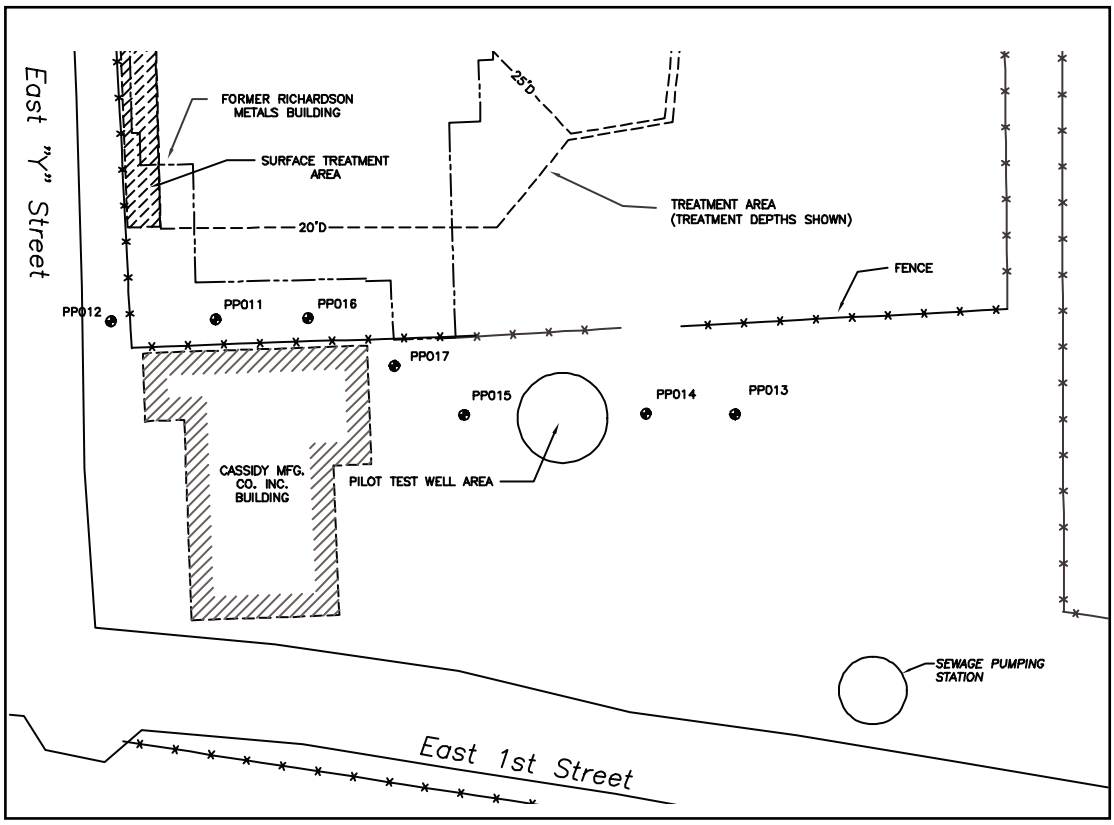

Figure 3.1. Location of Direct Push (Geoprobe) Well Installations used for Hydrogeologic Characterization Along the Barrier Alignment

and analyzed for hexavalent chromium (see Figure 3.2, boxed value above well ID). A comparison of results from the completed well with depth discrete data is instructive and provides a good example of the limitations associated with screened intervals that intersect multiple zones with different hydraulic properties. In the case of PP016, the maximum concentration observed during the depth-discrete sampling was 73 mg/L. However, because the highest concentrations exist within the lower-permeability materials and the completed screen draws the majority of the sample from the more permeable materials deeper in the formation (where concentrations are significantly lower), this well installation is ineffective for monitoring the highest concentration portion of the profile. This example illustrates the importance of using multilevel monitoring well networks to adequately monitor chromium distributions at the FHC site.

Once the temporary well installations had been sampled and EBF tests conducted at each location, the wells were over-drilled using the sonic method, removed, and the locations completed again as the deep injection well at each injection well pair (Section 3.4).

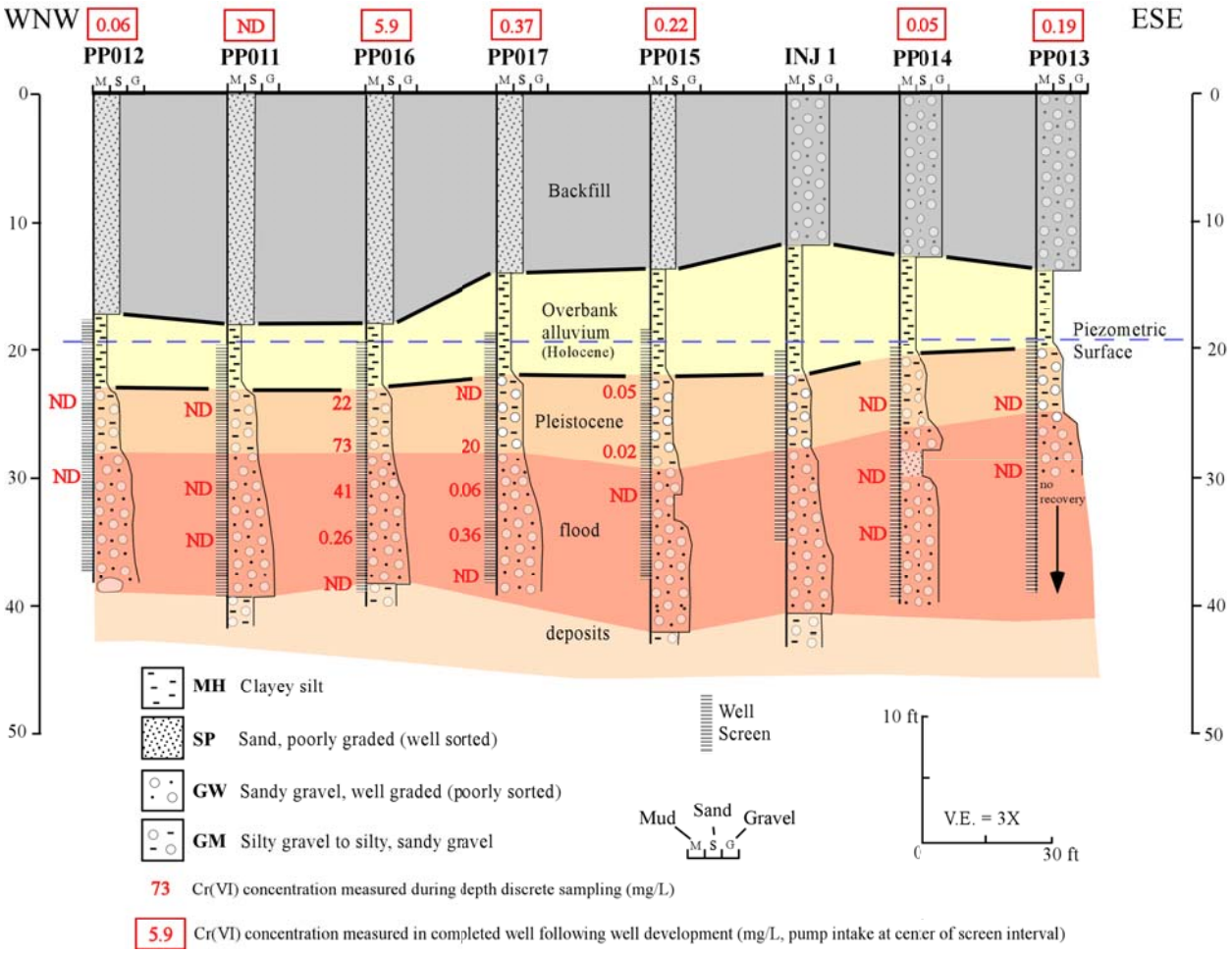

Figure 3.2. Hexavalent Chromium Concentrations Measured Along the Proposed ISRM Barrier Alignment

3.2 Hydrogeologic Characterization

Geologic logs and drill cuttings from the seven direct-push (Geoprobe) installed characterization wells were examined and used to refine the hydrogeologic conceptual model for the ISRM barrier alignment location. The previous conceptual model of the site (Figure 2.2) was a simple layered model based on limited characterization data collected from the pilot test site. The geologist's log from one well at this location (INJ-1), drilled using the resonant-sonic method, was also used in this conceptual model refinement. Based on this information, three distinct stratigraphic units can be identified within 40 ft of the present ground surface. From youngest to oldest, these units are 1) manmade backfill materials, 2) Holocene overbank deposits of the Columbia River, and 3) Pleistocene cataclysmic flood deposits. A hydrogeologic cross section showing the thickness and distribution of the different strata and descriptions based on the unified soil classification system is presented in Figure 3.3.

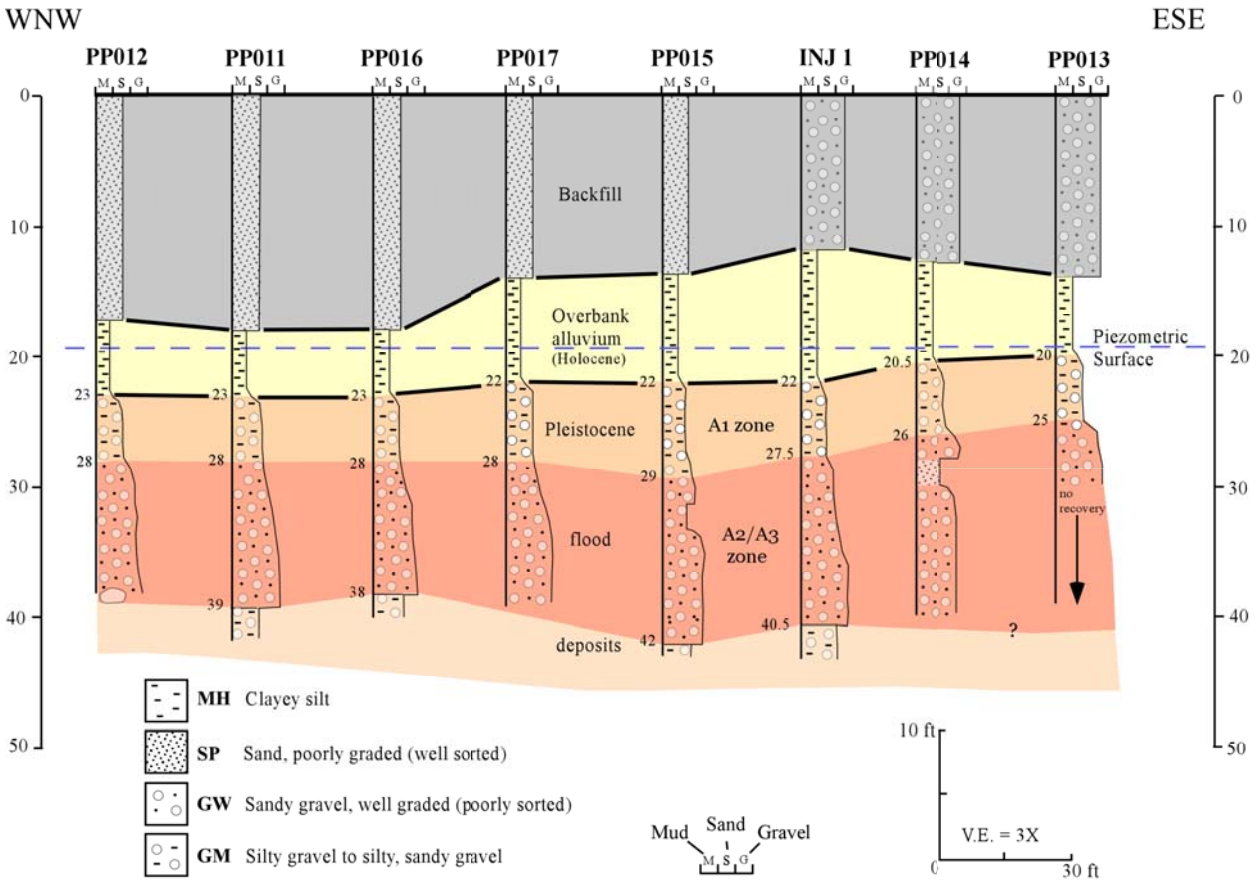

Figure 3.3. Hydrogeologic Conceptual Model for the ISRM Barrier Alignment Location

Comparison of the previous generalized conceptual model with this refined conceptual model that was based on data collected along the full length of the barrier alignment, shows that the models are similar in nature but include some notable differences. In addition to incorporating the differences in various contact elevations along the barrier, the revised model no longer considers the A2 and A3 zones separate. Instead, the revised model treats the A2/A3 as a single unit comprising a heterogeneous distribution of the higher- and lower-conductivity materials. Efforts to quantify the observed heterogeneity using geostatistical techniques are discussed in Section 4.1. To provide a visual representation of the types of sediments that were encountered at the site, a composite photograph of the drill cuttings for borehole PP016 is shown in Figure 3.4 and for the remaining boreholes in Appendix A. Also included in Appendix A is a complete set of geologic logs and well installation reports for both the pilot test well network and the remedial action injection and operational monitoring well network.

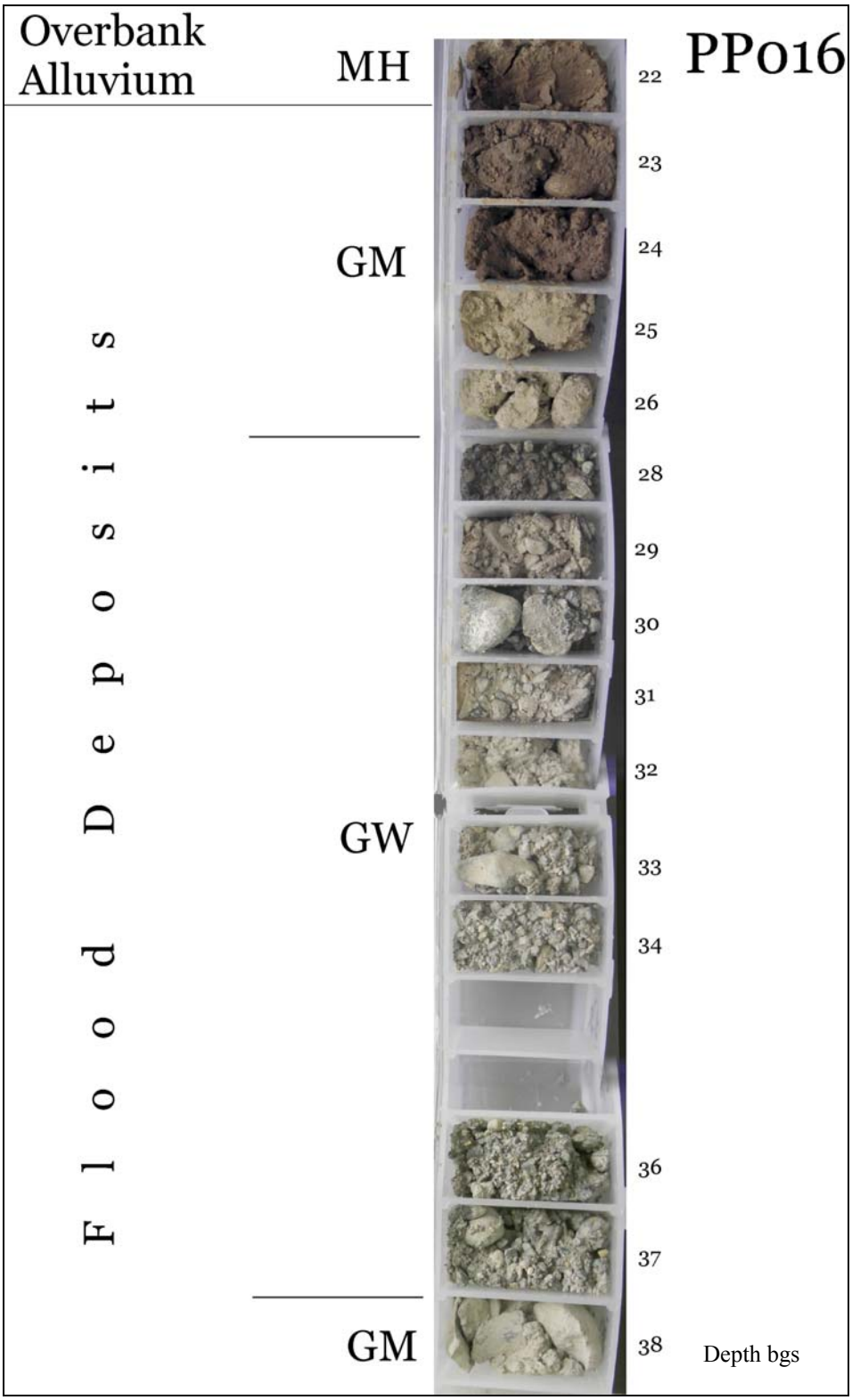

Figure 3.4. Composite Photograph of the Drill Cuttings for Borehole PP016

Two types of backfill material underlie the FHC site. One type, referred to as "hydraulic fill," consists of a gray, poorly graded (i.e., well-sorted) sand. This material, denoted as SP using the standard Unified Soil Classification System, was dredged or pumped from the bottom of the nearby Columbia River and redeposited upland. Another type of backfill material, gray, well-graded (i.e., poorly sorted) silty sandy gravel (GW) called "construction fill," includes brick and asphalt debris and was derived from an agglomeration of multiple on-land sources and dumped dry into its present location. During drilling, large unfilled voids were occasionally encountered in this material. Hydraulic fill was used in the area west of well INJ-1 while coarser construction fill was used to the east (Figure 3.3).

These backfill materials were used to raise the level of the land for industrialization and commercial purposes in this area. The base of the backfill represents the prehistoric, natural land surface; prior to development the land surface was within about 5 ft of normal river level (approximated by the potentiometric surface in Figure 3.3). This area would be flooded during high runoff events, and overbank alluvium would accumulate along the floodplain.

Up to 10 ft of fine-grained, compact, gray to brown clayey silt (MH) underlie the backfill materials. These sediments, which lie near the present river level, represent deposition that occurred on the floodplain of the Columbia River during normal, seasonal-type Holocene flooding. Holocene floods were much smaller and less vigorous than the Ice-Age floods that swept through this area from glacial outbursts during the Pleistocene. Holocene alluvium is easily distinguished from strata above and below by its fine-grained texture and brown color (see drill cutting photographs in Figure 3.4 and Appendix A). The distinctive red- to yellowish brown color of this unit is the result of thousands of years of weathering and oxidation of iron-rich soils under constantly alternating wet and dry conditions.

Beneath Holocene alluvial deposits lies a sequence of coarse-grained, glacial-outburst flood deposits. Considerable quantities of flood deposits accumulated in the Portland-Vancouver basin when multiple cataclysmic Ice-Age floods expanded beyond the confines of the Columbia River Gorge to the east. These deposits start about 20–30 ft below the present land surface and extend to the bottom of the borings in Figure 3.3. Cataclysmic flood deposits consist of mostly loose, well-graded (poorly sorted), clast-supported sandy pebble-cobble gravel. The gravel fraction consists predominantly of subangular to subrounded basalt clasts. Occasional layers and lenses of flood-deposited, poorly graded sand (SP) may also exist locally within the flood sequence.

The uppermost 5 ft of the flood sequence (A1 zone in Figure 3.3) consists of gravels mixed with significant amounts (20–30%) of brown clayey silt (GM), rendering it much less permeable than the underlying well-graded gravel (GW, A2/A3 zone), which generally contains <10% silt. The texture and color of the silt at the top of the flood sequence is the same as the overlying overbank alluvium (MH), suggesting the fine-grained material percolated downward during deposition of the Holocene alluvium, infiltrating and filling the pores of underlying gravels along

the contact between these two units. Hydraulic test data indicate the GM layer is much less permeable than the underlying GW deposits.

A second silty gravel (GM) layer was encountered in some of the deeper borings (lower light-brown layer in Figure 3.3). It acts as an aquitard and defines a locally confining boundary for the A aquifer. This lower GM layer may represent the eroded and weathered upper surface of an older Pleistocene flood deposit.

Basalt boulders, similar to the one shown in Figure 3.5, are occasionally present within flood deposits. One of these erratics may have been encountered in borehole PP012, where the direct push drilling method met refusal prior to reaching total depth. In another case (PP017), refusal was met at a depth of 24 ft at two locations before the third boring successfully reached total depth; each time the drill location was moved approximately 1 ft. The photos in Figures 3.5 and 3.6 were taken in February 2000 at Fisher Quarry. This borrow pit is adjacent to the Columbia River about 8 miles ESE of the FHC site; the sediments here are roughly equivalent to the Pleistocene deposits at FHC. Large-scale, planar-tabular, foreset bedding is characteristic of coarse-grained, cataclysmic flood deposits. This type of bedding developed as the sediment was transported downstream in giant waves along the bottom. Because the floods traveled from east to west down the Columbia Gorge, all foreset bedding in these deposits should dip to the west, as shown in Figures 3.5 and 3.6. Slight gradations in grain size within these foreset bedded gravels likely create some degree of hydraulic anisotropy and preferential flow within the formation.

Figure 3.5. Giant Basalt Boulder in Pleistocene Flood Deposits (Fisher Quarry, 8 mi E of FHC). Note large-scale foreset bedding dipping to the right in the downstream direction of the floods. View looking south.

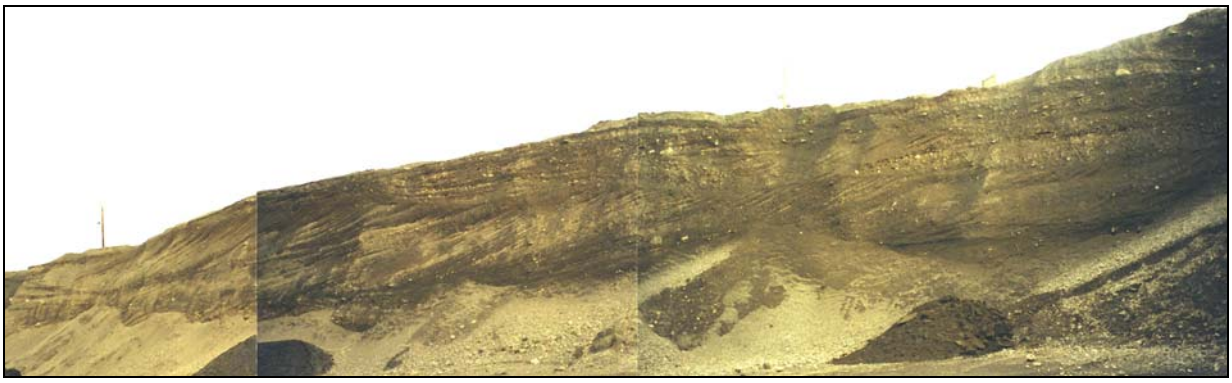

Figure 3.6. Large-Scale, Foreset Bedding in Pleistocene Flood Deposits Exposed at Fisher Quarry. Foreset bedding dips in the downstream direction. View looking north.

3.3 Electromagnetic Borehole Flow Meter Testing

Following temporary completion of the barrier alignment characterization wells over the entire depth interval of interest (see well screen intervals in Figure 3.2), a suite of electromagnetic borehole flow meter (EBF) tests were conducted to characterize the vertical distribution of horizontal hydraulic conductivity and to quantify the magnitude and spatial distribution of formation heterogeneity along the barrier alignment. These tests were conducted to supplement data obtained from an initial EBF testing campaign at the pilot test well network. This section provides a brief discussion of the methodology and results obtained from these tests. A detailed discussion of the EBF testing, including theoretical background, testing approach, and testing results (with plots showing the flow profile and estimated hydraulic conductivity distribution at each well tested), is provided in Appendix B.

The primary objective of the EBF testing was to determine the profile of relative hydraulic conductivity at locations along the ISRM barrier alignment. These data, along with other hydrogeologic information, were then analyzed using geostatistical techniques and were incorporated into the injection design analysis. The EBF technique involves measuring flow velocity within the well at regular intervals as water is transmitted through a well under induced pumping (or injection) conditions. These data can serve as the basis for computing the relative hydraulic conductivity at each interval.

Ten wells from the pilot test network and six of the seven temporary characterization well installations were tested. Tests were not conducted at pilot test well MW-9 and temporary characterization well PP011 due to an obstruction that prevented passage of the flow meter. As discussed previously, tested monitoring wells were completed with 2in.-diameter PVC casing and screen. The down-hole probe was designed to provide a snug fit in PVC casing of this diameter; therefore, a collar or inflatable packer was not required to prevent bypass flow around the recording interior of the flow meter. For the one test conducted in INJ-1, which is a

6-in.-diameter injection well, a set of rubber disk packers was used to minimize the amount of bypass flow around the sensor.

Most flow rate profiles recorded during testing in the temporary characterization well installations reveal a flow pattern best illustrated by that shown in Appendix B for Well PP013. The flow rate measured near the top of the screen was only slightly less than the injection rate of approximately 1.0 gpm. However, flow rates measured between depths of 19 and 28 ft were considerably less. The most plausible explanation for this trend is that flow injected down the well exited the well near the top of the screen, flowed downward through a void around the outside of the screen, and reentered the screen slightly above a depth of 28 ft. The water obviously did not enter the upper geologic formation or it would not have reentered the screen at the bottom of this formation. As discussed previously, this response is most likely associated with the nonstandard well completion requirements for the direct-push wells and the resulting difficulties of installing an effective annular seal. These EBF testing results were instrumental in identifying the direct-push completions as suspect and led to the abandonment or reconfiguration of all wells installed using the Geoprobe rig.

Although resolution in the A1 zone was compromised during EBF testing along the barrier alignment by voids in the annular seals in these temporary well installations, one obvious conclusion is that the A1 zone is much less permeable than the A2/A3 zone. This general conclusion is consistent with results obtained from the pilot test well network. To provide some indication of the vertical distribution of horizontal hydraulic conductivity in the A1 zone, data were inspected from several pilot test site wells that were completed using standard techniques. Although insufficient data were available for a geostatistical analysis of permeability distribution in the A1 zone, data from the pilot test well network indicated a general trend of increasing hydraulic conductivity with depth. Due to the lack of information for the A1 zone along the remainder of the barrier alignment, this same distribution was assumed.

In contrast to the data in the A1 zone, the data collected from the A2/A3 zone in all wells appears valid. Again, consider the profile of flow rates of Well PP013 shown in Appendix B. The injected flow profile between depths of 28 and 33 ft appears confusing until the effect of ambient flow is included. The resulting net induced flow profile obtained by subtracting the ambient flow rate from the injected flow rate recorded at corresponding depths reveals a consistent and logical pattern. The resulting profile of hydraulic conductivity reveals a zone of highly permeable material between depths of 28 and 31 ft. This type of variability in the profile was observed at all test locations and was analyzed using geostatistical techniques. These data were used to construct alternative conceptual models that reflected the observed heterogeneities. A discussion of these geostatistical analyses and the conductivity distribution used in the barrier injection design analysis are provided in Sections 4.1 and 4.2, respectively.

3.4 Injection and Operational Monitoring Well Installation

As discussed in Section 3.1, once the temporary well installations had been sampled and EBF tests had been conducted at each location, the wells were over-drilled with the sonic rig, removed, and the locations completed again as the deep injection well at each injection well pair (Figure 3.7). This figure shows the screened intervals of both the upper and lower injection wells, which were designed based on information obtained from the temporary characterization wells. The upper and lower well of each pair were placed approximately 3 ft apart. A plan view map of the injection and operational monitoring well layout is provided in Figure 3.8. Table 3.1 contains well construction summary information for all wells used in the emplacement and monitoring of the ISRM permeable reactive barrier. Detailed well construction information is contained in the geologic logs and well installation reports in Appendix A.

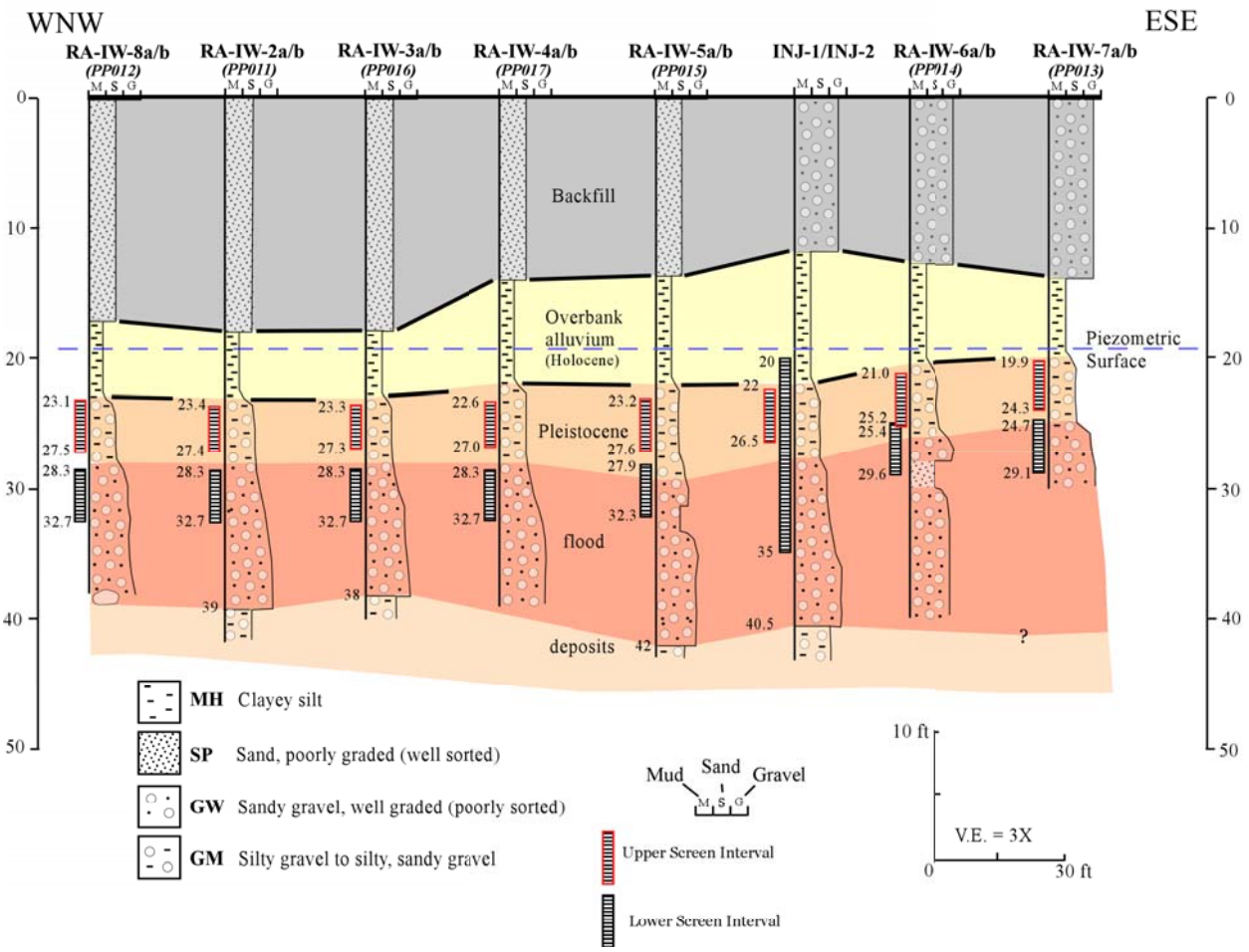

Figure 3.7. Geologic Cross-Section Showing the Screened Intervals of Injection Wells Along the ISRM Barrier Alignment

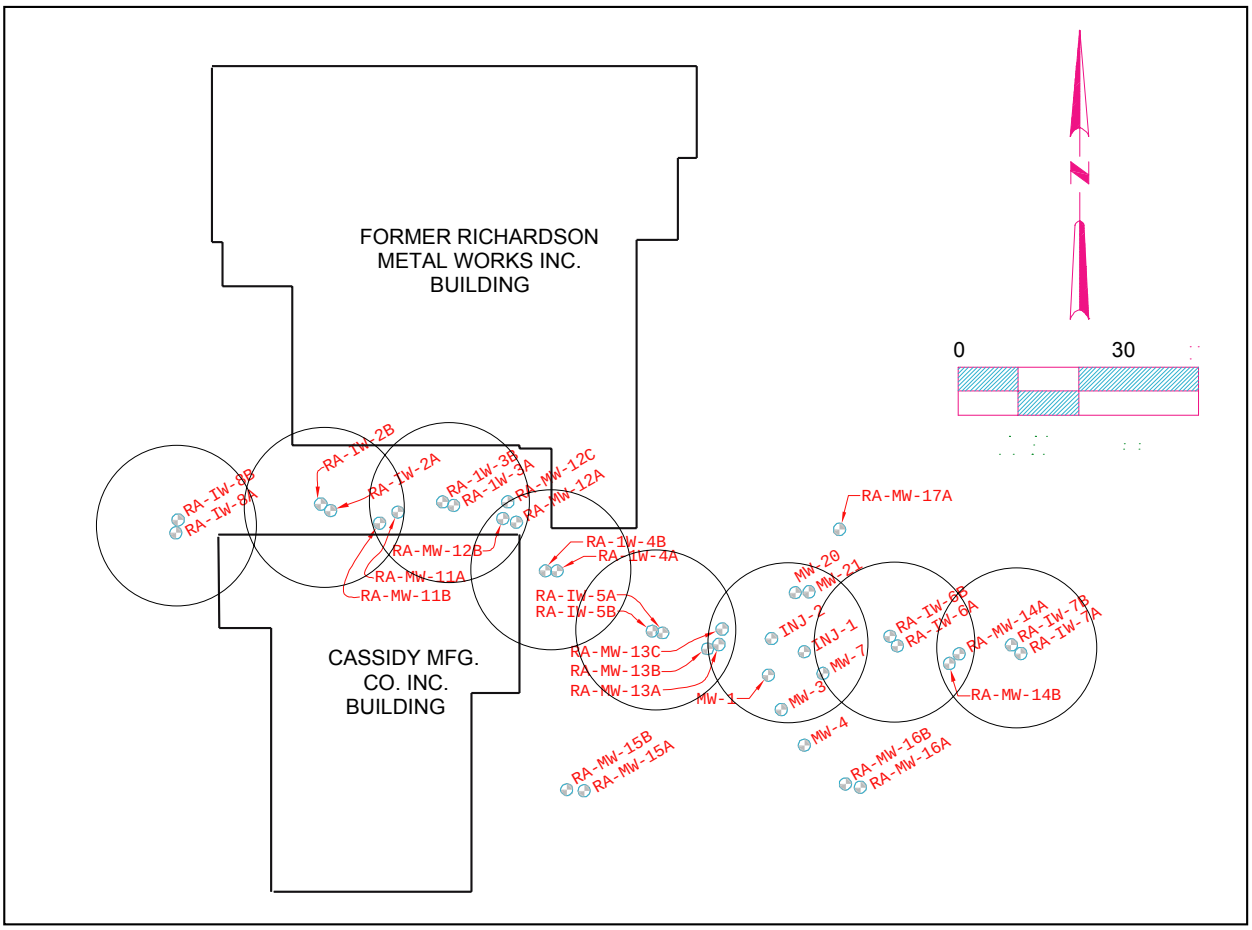

Figure 3.8. Well Location Map

Injection wells were installed in two separate drilling campaigns. The first three injection wells (2/ab, 3a/b, and 4a/b) were installed, and treatment zone emplacement operations were conducted in the 2a/b and 3a/b well pairs, prior to installation of the remaining injection wells. This phased drilling approach was employed to verify that the nominal well spacing of 30 ft, selected based on a conservative interpretation of results from the pilot-scale injection test, provided sufficient coverage (i.e., adequate reductive capacity within the overlap zones). Based on results from the first treatment zone emplacement field campaign, spacing between the remaining injection well pairs was maintained at 30 ft.

Injection wells used for emplacement of the barrier were, with only one exception, installed using the sonic method (INJ-2 was installed using hollow-stem auger). During these installations, a 10-in. borehole was advanced to total depth and completed with 6-in. PVC casing and screen. Screen material consisted of 20-slot continuous wire wrap (v-wire) screen and was set in a 10/20 Colorado silica sand filter pack. Operational monitoring wells were installed using

Table 3.1. Well Construction Summary Information

Well Number	Drilling Method	Casing Diameter (in)	Screen Interval (ft bgs)	Northing	Easting
Pilot Test Well Network					
INJ-1	Sonic	6	20 - 35	112447.61	1091616.21
INJ-2	Auger	6	22 - 27	112450.91	1091608.07
MW-1	Auger	2	19.5 - 34.5	112441.82	1091607.30
MW-3	Auger	2	22 - 37	112433.24	1091610.54
MW-4	Auger	2	20 - 35	112424.34	1091616.25
MW-5	Decommissioned	2	20 - 35	112464.46	1091631.93
MW-6	Reconfigured as RA-MW-13C				
MW-7	Sonic	2	42 - 47	112442.22	1091620.89
MW-9	Reconfigured as RA-MW-17A				
MW-10	Decommissioned	2	20 - 35	112414.65	1091603.09
MW-20	Auger	2	22 - 27	112462.35	1091613.99
MW-21	Auger	2	30 - 35	112462.58	1091617.43
MW-22	Decommissioned	2	35 - 40	112460.86	1091609.46
Remedial Action Well Network					
RA-IW-2A	Sonic	6	23.4 - 27.4	112482.82	1091498.21
RA-IW-2B	Sonic	6	28.3 - 32.7	112484.49	1091495.75
RA-IW-3A	Sonic	6	23.3 - 27.3	112484.11	1091528.87
RA-IW-3B	Sonic	6	28.3 - 32.7	112484.97	1091526.11
RA-IW-4A	Sonic (Replacement)	6	22.6 - 27.0	112467.78	1091554.62
RA-IW-4B	Sonic (Replacement)	6	28.3 - 32.7	112467.82	1091551.73
RA-IW-5A	Sonic	6	23.2 - 27.6	112452.33	1091580.90
RA-IW-5B	Sonic	6	27.9 - 32.3	112452.78	1091578.33
RA-IW-6A	Sonic	6	21.0 - 25.4	112449.10	1091639.46
RA-IW-6B	Sonic	6	25.2 - 29.6	112451.53	1091637.59
RA-IW-7A	Sonic	6	19.9 - 24.3	112447.22	1091670.20
RA-IW-7B	Sonic	6	24.7 - 29.1	112449.32	1091667.86
RA-IW-8A	Sonic	6	23.1 - 27.5	112477.29	1091459.63
RA-IW-8B	Sonic	6	28.3 - 32.7	112480.54	1091460.17
RA-MW-11A	Auger	2	22.9 - 27.6	112482.47	1091514.95
RA-MW-11B	Auger	2	28.3 - 32.9	112479.76	1091510.42
RA-MW-12A	Auger	2	23.2 - 27.9	112479.92	1091544.46
RA-MW-12B	Auger	2	28.3 - 33.0	112480.85	1091541.13
RA-MW-12C	Auger	2	34.5 - 39.0	112484.97	1091542.35
RA-MW-13A	Auger	2	22.5 - 27.1	112449.48	1091594.97
RA-MW-13B	Auger	2	27.3 - 31.9	112448.39	1091592.13
RA-MW-13C	Auger	2	34.6 - 39.5	112453.33	1091595.78
RA-MW-14A	Auger	2	20.3 - 25.1	112447.10	1091654.85
RA-MW-14B	Auger	2	25.5 - 30.0	112444.72	1091652.41
RA-MW-15A	Auger	2	22.1 - 26.6	112412.99	1091561.36
RA-MW-15B	Auger	2	27.7 - 32.5	112413.29	1091557.10
RA-MW-16A	Auger	2	22.2 - 26.7	112413.87	1091630.20
RA-MW-16B	Auger	2	27.9 - 32.5	112414.70	1091626.50
RA-MW-17A	Geoprobe/Auger	2	21.7 - 26.2	112478.04	1091624.86

the hollow-stem auger method. A 6-in. borehole was advanced to total depth and completed with 2-in. PVC casing and screen. Screen material consisted of 10-slot continuous wire wrap (v-wire) screen and was set in a 20/40 Colorado silica sand filter pack.

All site monitoring wells were developed prior to initial groundwater sampling. Well development was conducted in two phases. The first phase consisted of limited bailing and/or surging, as required, during well completion (i.e., after placing the filter pack but before placing the annular seal) to settle the sandpack and remove fine-grained material generated during drilling. Following well completion, an appropriately sized pump was installed, and the wells were pumped and surged until any remaining fine-grained material was removed and the well had achieved an acceptable yield and turbidity level. Several of the injection well installations, particularly those completed in the A1 zone, showed a limited response to a secondary, more rigorous development regime (i.e., aggressive surge blocking, jetting, and sand pumping). Due to the failure of these methods to achieve an acceptable well yield, an inflatable packer was installed, and pressurized water injection was used to develop the screen intervals. Although substantial well screen inefficiency (i.e., skin effect) still remained in many of the wells following this procedure, the yields were improved sufficiently to meet project requirements.

Several of the monitoring wells installed for the pilot test were installed using the direct-push (Geoprobe) method. However, as discussed previously, during site-specific characterization of the full barrier alignment, it was determined that the direct-push wells did not provide an adequate annular seal throughout the upper, more fine-grained portion of the aquifer, and subsequently these wells were abandoned or reconfigured using standard completion techniques. In addition, the original 4a/b injection well pair had to be abandoned and redrilled nearby due to a defective annular seal that was identified during pressurized injection development at this location. Abandonment consisted of over-drilling each well installation, removing the PVC casing and screen material, and sealing the borehole with bentonite. Installation and completion of injection and operational monitoring wells were conducted in accordance with Washington Administrative Code Standards ("Minimum Standards for Construction and Maintenance of Wells," WAC 173-160).

4.0 Barrier Design Analysis

This section contains a description of the geostatistical analysis and reactive transport modeling that was conducted to develop a barrier emplacement strategy. These analyses were based on the results from characterization activities conducted along the barrier alignment discussed in Section 3.

4.1 Geostatistical Analysis

As discussed in Section 2, the conceptual model developed during the ISRM pilot test assumed homogeneous and constant hydrogeologic conductivity distributions for each of three distinct sedimentary layers comprising the A aquifer (A1, A2, and A3 zones). However, interpretation of additional EBF tests conducted after the pilot-scale field testing (Section 3.3) indicated the existence of significant spatial heterogeneity in hydraulic conductivity within each of these sedimentary layers. The geostatistical analysis discussed in this section was performed to construct alternative conceptual models that reflect these observed heterogeneities through stochastic simulation. A rectangular study domain was used that extended vertically from depths of 25 to 40 ft and extended 30 ft horizontally from each of the two boreholes on both ends of the profile (PP012 and PP013). A small portion of the A1 zone was within the rectangular study domain; therefore, a digital boundary separating the A2/A3 zones from the A1 zone was determined based on the geological profile shown in Figure 4.1. Data falling within the A2/A3 zones were used to evaluate the spatial heterogeneity of the zones and as the conditioning data for the geostatistical simulations.

The EBF data were originally reported as relative conductivities normalized to unity for each borehole. Because the geostatistical analysis focused only on the two lower zones present at the site, data above these two zones were truncated. The EBF data from the two lower zones were then renormalized to unity. The relative conductivities of the boreholes were scaled based on the average absolute conductivity estimate for the A2/A3 zones (6600 ft/d). Vertical and horizontal variograms were calculated for the absolute hydraulic conductivity data after they were transformed to normal scores (Deutsch and Journel 1998). There were enough data available to calculate a reliable experimental vertical variogram and fit a spherical variogram model (Deutsch and Journel 1998) to it, but because of the small number of boreholes at the site, the horizontal variogram had few supporting data, and the horizontal variogram model had to be estimated using an assumption of the anisotropy ratio between the horizontal and vertical continuity. A horizontal-to-vertical anisotropy ratio of 20:1 was selected based on the current conceptual understanding of the site and knowledge of the depositional environment. The vertical variogram had a range of 3.5 ft, suggesting a horizontal range of 70 ft. Figure 4.2 shows the experimental variograms and the variogram models fit to them. The estimated horizontal variogram model generally agrees with the few data available in the horizontal experimental variogram, suggesting that it was not an unreasonable assumption. If additional work is

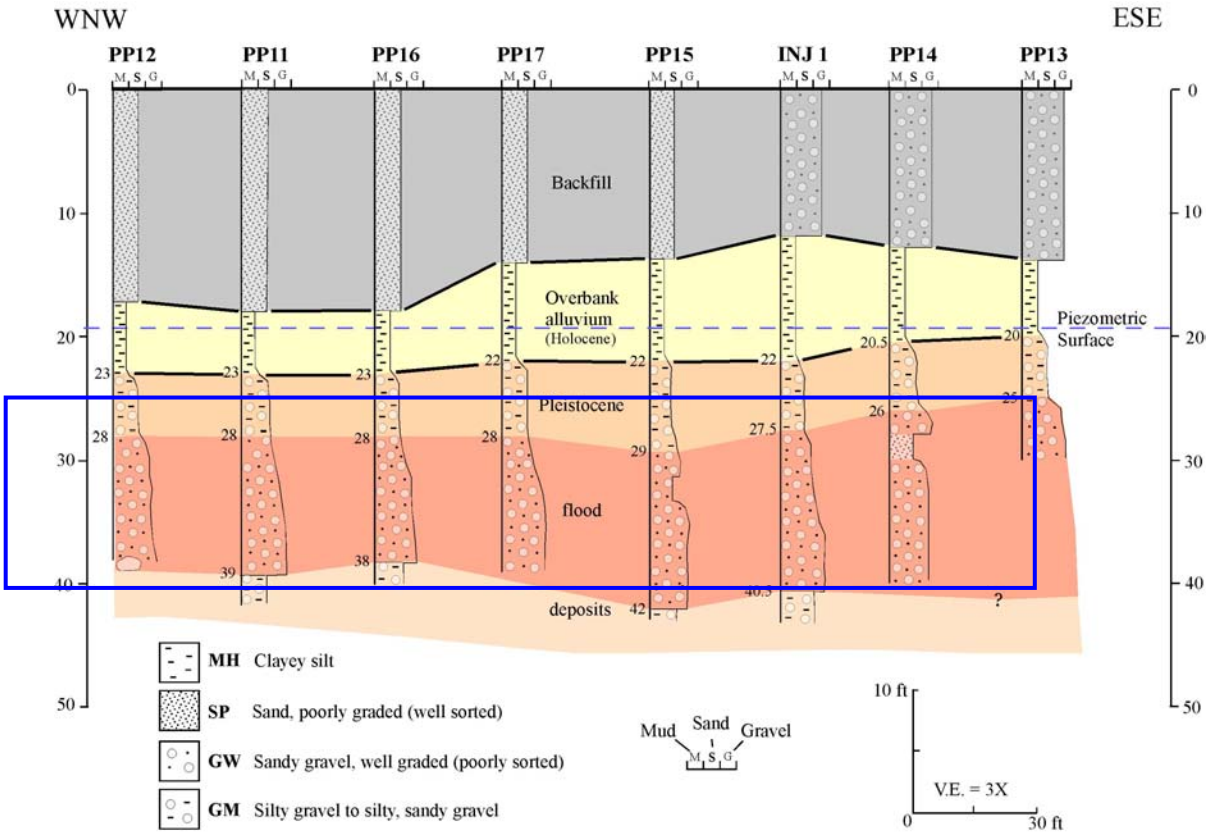

Figure 4.1. Geological Profiles of Boreholes Showing Outline of Geostatistical Modeling Domain

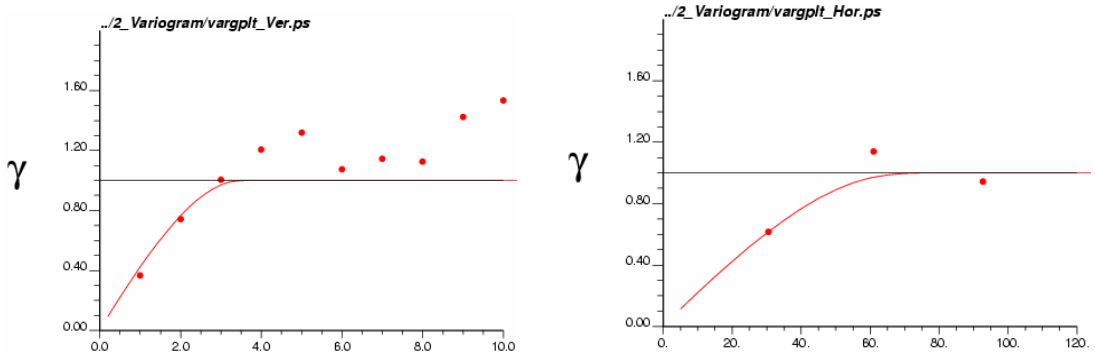

Figure 4.2. Normal Score Variograms and Models for Hydraulic Conductivity Data Estimated from Flow Meter Data. Vertical variogram on the left, horizontal on the right. The dots represent experimental variogram values; solid lines represent spherical variogram models fit to experimental variograms.

performed, it would be useful to vary the assumed anisotropy ratio (and thus the estimated horizontal continuity) to determine the effect it would have on the flow and transport modeling results.

The variogram models were used as input to generate a series of sequential Gaussian simulations. The simulation grid had a resolution of 1 ft horizontally and 0.5 ft vertically. Each simulation realization consists of 8556 (216 by 31) points and a total of 101 realizations were generated. Figure 4.3 shows two realizations as examples. Figure 4.4 shows the map of the mean values of the hydraulic conductivity derived by averaging the values at each grid node for the 101 realizations (known as the E-type estimate).

The simulated hydrological conductivity fields were used in numerical models to evaluate the flow and transport behavior. All simulated realizations are equally probable scenarios of the hydrological conductivity, but each realization will result in slightly different flow and transport behavior. Processing the suite of all realizations in the numerical flow and transport model would allow assessment of the uncertainty in the flow behavior. However, it is computationally intensive and not within the scope of this project to process all the individual realizations through the reactive transport model. The E-type estimate, which is the average of the simulated values at each node of the cross section and similar to those obtained from other interpolation methods like kriging or fitting splines to the data, is a smoothed representation of the data. Unlike the individual stochastic realizations, it does not capture the full spatial variability observed in the data. In order to run a limited number of realizations that would provide information on the variability that might be expected in the reactive transport model, the realizations were ranked and the ranking used to identify the extremes that bracket the expected range in spatial distributions of hydraulic conductivity at the site. A detailed discussion of the geostatistical analysis, including ranked conductivity distributions at each injection well location along the barrier alignment, is provided in Appendix C. Simulation of flow and reactive transport using results from this geostatistical analysis are discussed in the following sections.

4.2 Predictive Simulations of Treatment Zone Emplacement

Numerical simulations were conducted to support design of the sodium dithionite injections and resulting Fe(III) reduction in sediments at the FHC Site. These 2D, radial coordinate simulations were conducted to determine appropriate flow rates, durations, and reagent concentrations to use during the barrier emplacement operations. Simulations were conducted using the STOMP code, a three-dimensional (3D), integrated finite difference model for multi-fluid flow, solute transport, and heat transfer in variably saturated porous media (White and Oostrom, 2003). Mode 1 of the code was used for this work. In this mode the code solves mass balance equations for a single fluid phase (water), and all associated solutes under isothermal conditions.

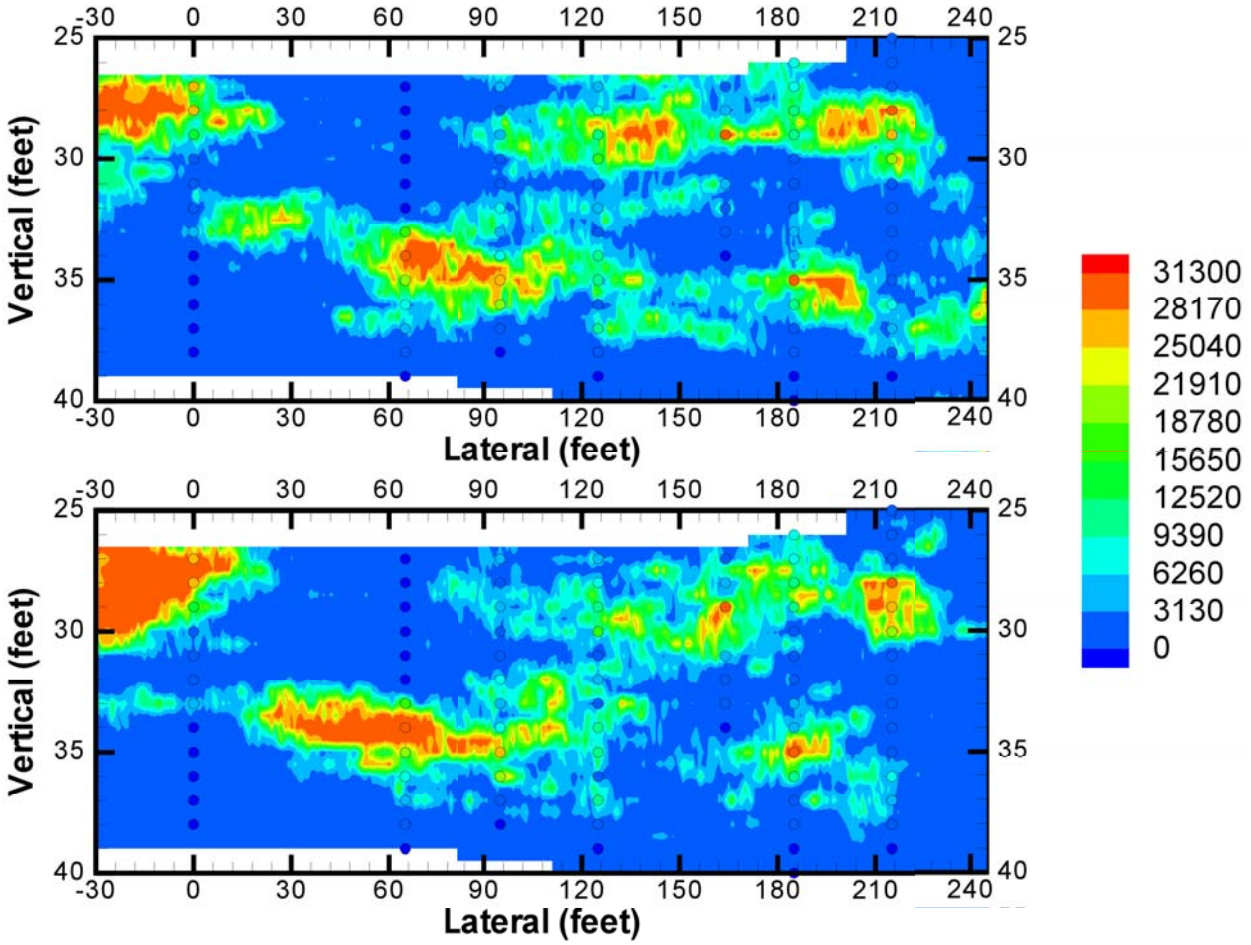

Figure 4.3. Two Example Realizations of the Hydraulic Conductivity from the Suite of 101 Stochastic Realizations that Were Generated

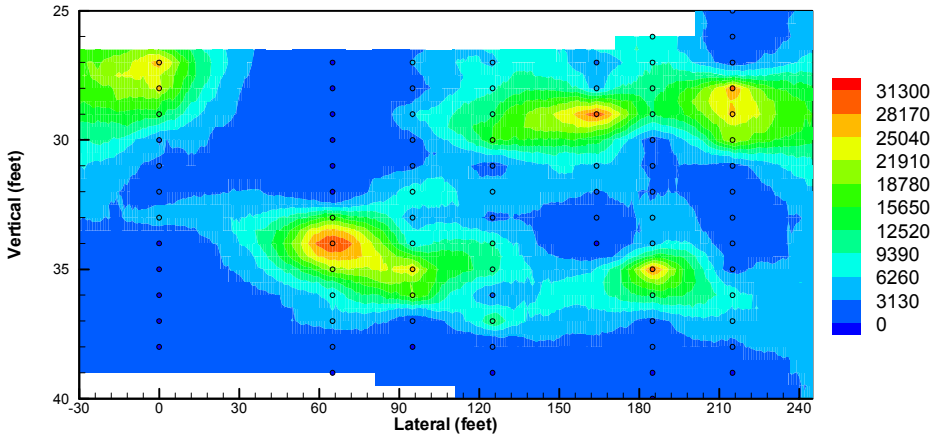

Figure 4.4. Map of the Average Simulated Hydraulic Conductivity at Each Node

As discussed previously, the injected reagent consisted of sodium dithionite ($Na_2S_2O_4$) in a potassium carbonate (K_2CO_3) buffer solution. The concentrations of these solutes were high enough to cause significant increases in solution density, which was approximated in the model using a concentration-dependent solution density function, shown in Figure 4.5. Fe(III) was also modeled as a solute but was effectively represented as a solid-phase constituent by using a large equilibrium partitioning coefficient (20,000 m^3/kg). The initial quantity of solid-phase Fe(III) available for reduction by dithionite was estimated in bench scale tests using core samples collected from the site (Section 2.3).

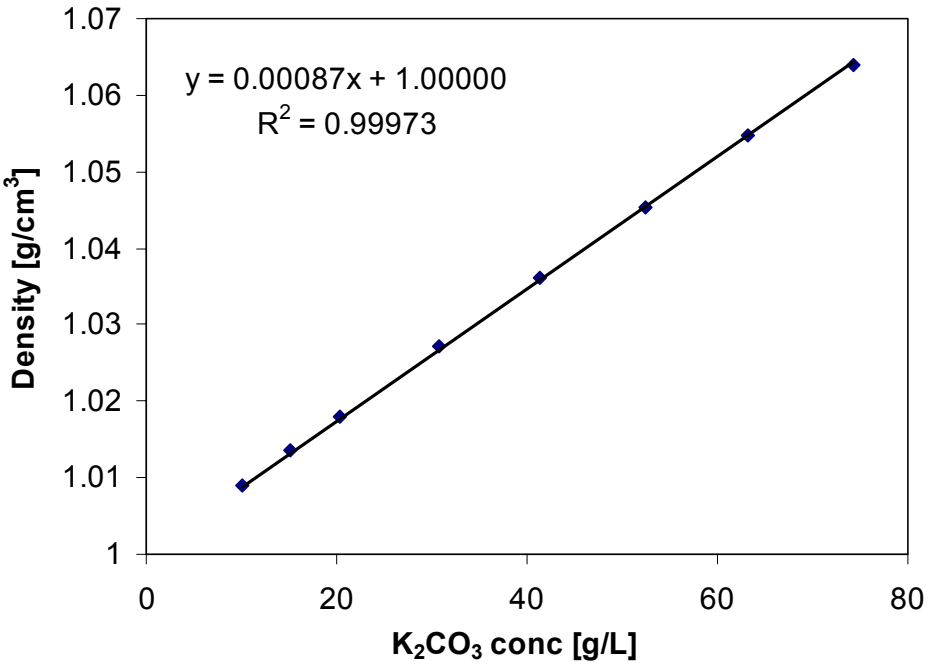

Figure 4.5. Concentration-Dependent Solution Density Function (data from Lide 1996).

During hydrogeologic characterization of the barrier alignment, A aquifer sediments were differentiated into the A1 zone (Holocene age, over-bank alluvium) and the combined A2/A3 zone (Pleistocene age, flood deposits). The A1 zone at the site is overlain by a locally confining silt layer (see generalized conceptual model in Figure 3.3). The physical and hydraulic properties for the A aquifer were estimated from the analysis of core samples and pump test data (Sections 2.2 and 2.4). The vertical distribution of horizontal hydraulic conductivity and estimates of the magnitude of formation heterogeneity was inferred from EBF testing results (Section 3.3 and Appendix B).

Figure 4.6 depicts the vertical hydraulic conductivity distribution used in the 2D radial design analysis simulations. The modeled domain was 21 ft high by 394 ft in radius. The uppermost unit represented in the modeled domain, located above a depth of approximately 22 ft bgs, was the Holocene-age over-bank alluvium. This alluvium was assigned a relatively low isotropic

hydraulic conductivity value to reflect its locally confining nature. The Pleistocene-age A1 unit underlies the alluvium between depths of approximately 22–27 ft bgs. Based on limited site characterization and pump test data from the pilot-scale test, the A1 unit was assigned hydraulic conductivity values in the horizontal direction that ranged from 50–300 ft/d with higher conductivities at deeper depths to approximate a fining-upward sequence of sediments. An anisotropy ratio of 1:100 was assumed for unit A1. The hydraulic conductivities for the underlying A2/A3 units were estimated from the E-type estimates generated from the EBF data (Section 4.1). The E-type estimates for a subdomain of the larger K field, spanning 15 ft of either side of the 3a/b injection wells, were averaged in the horizontal direction to generate the depth-dependent K profile shown in Figure 4.6. An anisotropy ratio of 1:100 was also assumed for the A2/A3 units. Additional model parameters, which for simplicity were mapped based on the original layered conceptual model, are provided in Table 4.1.

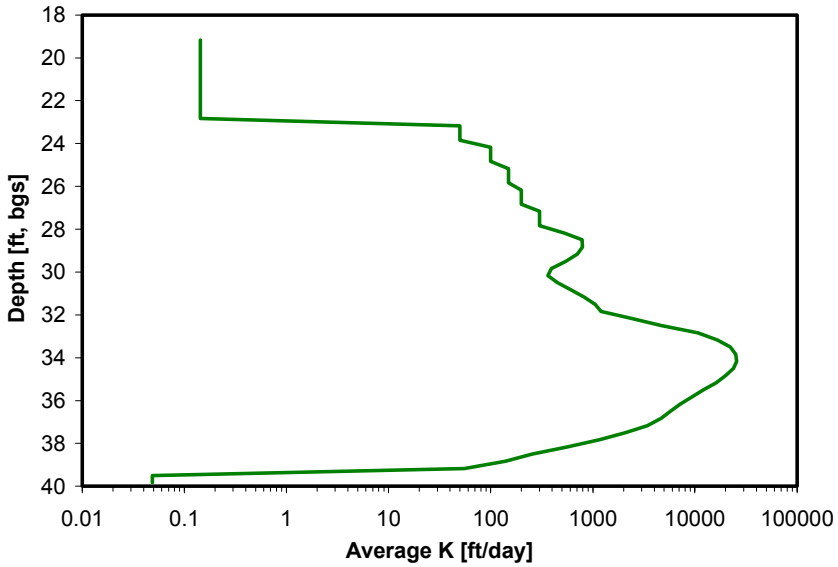

Figure 4.6. Average Hydraulic Conductivity Profile Used for Design Simulations in 2D Radial Model

Table 4.1. Dispersivities, Porosities, and Initial Fe(III) Concentrations Used for 2D Radial Model

Aquifer zone	Long. and trans. dispersivities [m]	Porosity	Initial Fe(III) conc. [mol/L bulk]
A1	0.5, 0.05	0.17	0.103
A2	0.5, 0.05	0.12	0.093
A3	0.5, 0.05	0.19	0.069

One primary design parameter considered during development of the injection strategy was the reagent allocation between the two zones targeted for treatment. Due to the relatively low permeability of the A1 zone relative to the A2/A3 zone, groundwater velocities in the A1 zone would be significantly slower than those in the deeper zones, indicating the need for less treatment in the A1 zone. However, the velocity advantage in the A1 zone is at least partially offset by its higher hexavalent chromium concentrations. To investigate the relative importance of these two competing factors, a simple spreadsheet model was constructed that assumed oxidizing species [i.e., DO and Cr(VI)] concentrations based on average baseline conditions and relative groundwater flux based on hydraulic property estimates. Based on this analysis, it was estimated that the A1 zone should receive approximately 25% as much treatment capacity as the A2/A3 zone to generate uniform treatment zone longevity. This reagent allocation was maintained throughout the barrier design analysis and emplacement operations.

Figures 4.7 through 4.9 show simulated total dissolved solids (TDS) concentrations, dithionite concentrations, and reduced iron concentrations, Fe(II), respectively, for selected simulation cases that were used in the design process. Predictions are shown for TDS and dithionite concentration six hours after the injection started and for Fe (II) concentration at the end of the residence phase (i.e., once all the injected reagent has reacted). Results from additional times throughout the injection and residence phases are contained in Appendix D. The conditions specified for Case 10 are approximately the same as were used during the injections at the RA-IW-3a/b well pair. The high TDS concentrations, which are primarily due to the high concentration of the buffer solution, can result in density sinking of the reagent during all phases of the treatment. Flow rates, durations, and solution concentrations were adjusted in various simulation cases within practical constraints imposed by field operating conditions and aquifer permeability to maximize the uniformity of coverage of the Fe(II) distribution.

Due to the difficulties associated with designing and conducting hydraulic tests that provide a definitive anisotropy value, there is generally considerable uncertainty in this property. Improved understanding of this parameter is important to effective deployment of the ISRM technology because it helps to mitigate the effects of density sinking. A general rule of thumb that is frequently assumed for numerical modeling of saturated groundwater flow is that the hydraulic conductivity in the horizontal or radial direction, Kx, is a factor of 10 greater than the hydraulic conductivity in the vertical direction, Kz. However, hydraulic test data and both tracer and dithionite transport data from the ISRM pilot test (Section 2) indicated that the anisotropy ratio of formation materials composing the A aquifer at FHC may be closer to a factor of 100 than a factor of 10.

Numerous simulations were conducted to develop a reasonable injection strategy based on estimates of hydrologic and geochemical properties at the site and the assumed anisotropy ratio of 100. This baseline injection strategy is represented by case 10 in Figures 4.7 through 4.9. The additional two cases shown in these figures (and at additional times in Appendix D) were developed to test the sensitivity of the system to anisotropy and develop an operational strategy

Case 10

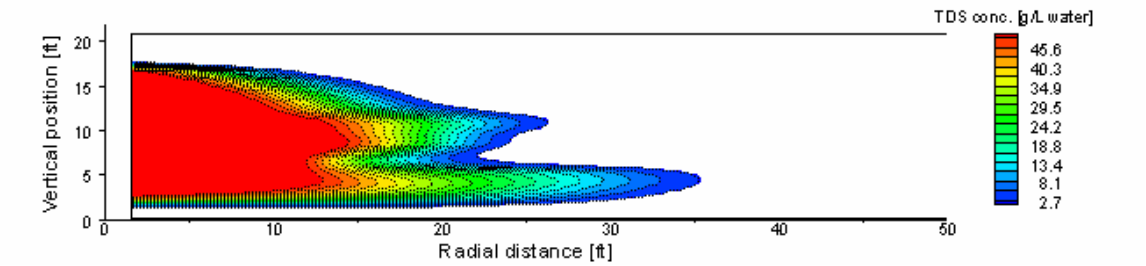

Case 12

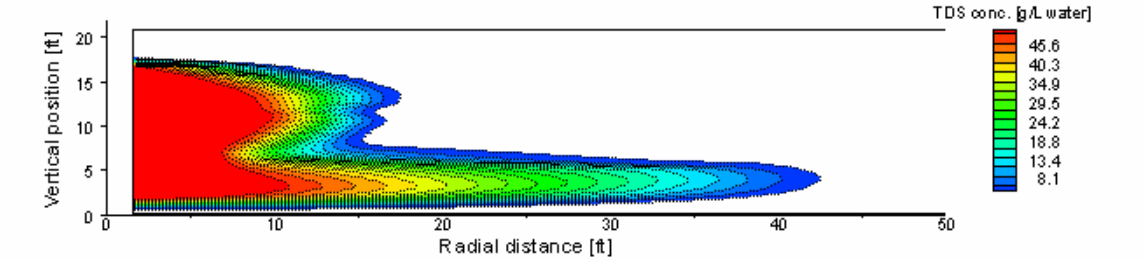

Case 14

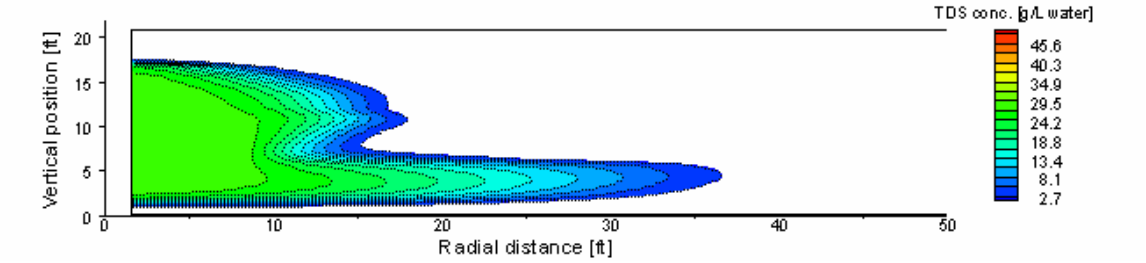

Figure 4.7. Predicted TDS Concentration Distributions (g/L) Around Well PP016 at 6 hr for Simulation Cases 10, 12, and 14 (top to bottom). Dithionite injectate concentrations are 0.08, 0.08, and 0.04 M for cases 10, 12, and 14, respectively. Flow rates are 6.94 gpm from 0-24 hr (~10,000 gal) in unit A1, and 27.75 gpm from 0-24 hr (~40,000 gal) in unit A2, for cases 10 and 12, and 6.94 gpm from 0-48 hr (~20,000 gal) in unit A1, and 27.77 gpm from 0-48 hr (~80,000 gal) in unit A2 for case 14. For case 10, units A1 and A2 are both layered with Kv=Kh/100. For cases 12 and 14, unit A1 is layered with Kv=Kh/100, and unit A2 is layered with Kv=Kh/10.

Case 10

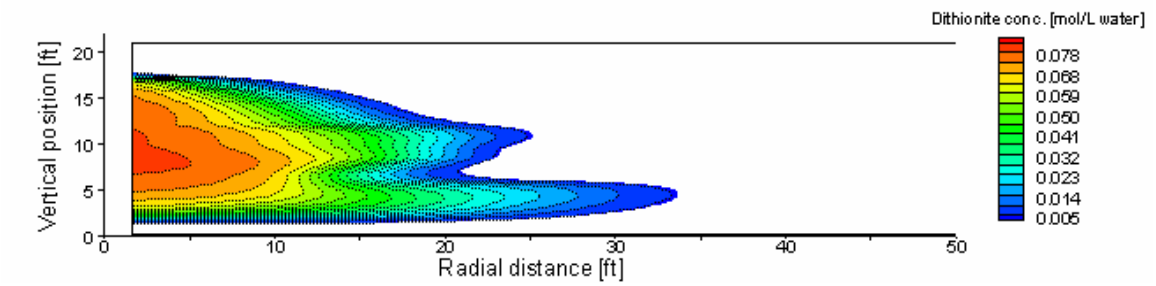

Case 12

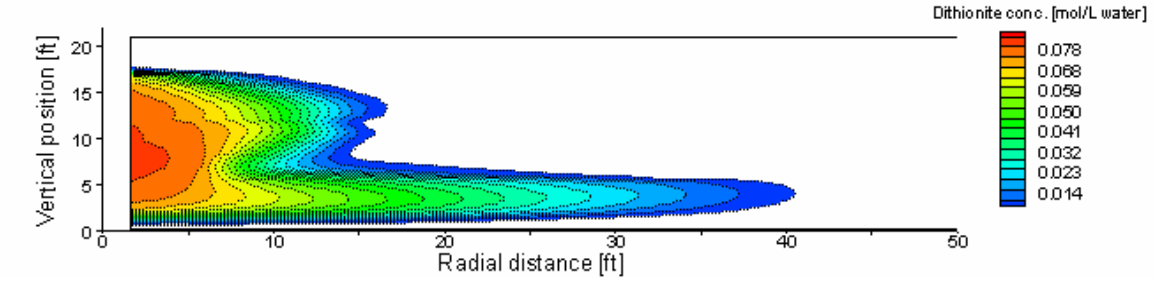

Case 14

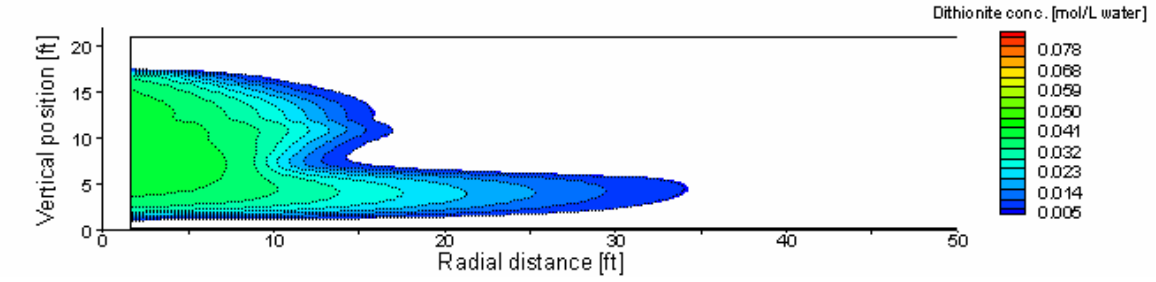

Figure 4.8. Predicted Dithionite Concentration Distributions (mol/L) Around Well PP016 at 6 hr for Simulation Cases 10, 12, and 14 (top to bottom). Dithionite injectate concentrations are 0.08, 0.08, and 0.04 M for cases 10, 12, and 14, respectively. Flow rates are 6.94 gpm from 0-24 hr (~10,000 gal) in unit A1, and 27.75 gpm from 0-24 hr (~40,000 gal) in unit A2, for cases 10 and 12, and 6.94 gpm from 0-48 hr (~20,000 gal) in unit A1, and 27.77 gpm from 0-48 hr (~80,000 gal) in unit A2 for case 14. For case 10, units A1 and A2 are both layered with Kv=Kh/100. For cases 12 and 14, unit A1 is layered with Kv=Kh/100, and unit A2 is layered with Kv=Kh/10.

Case 10

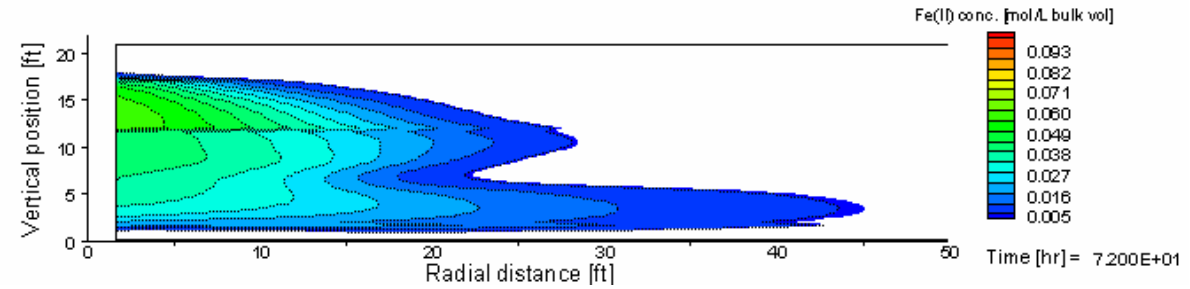

Case 12

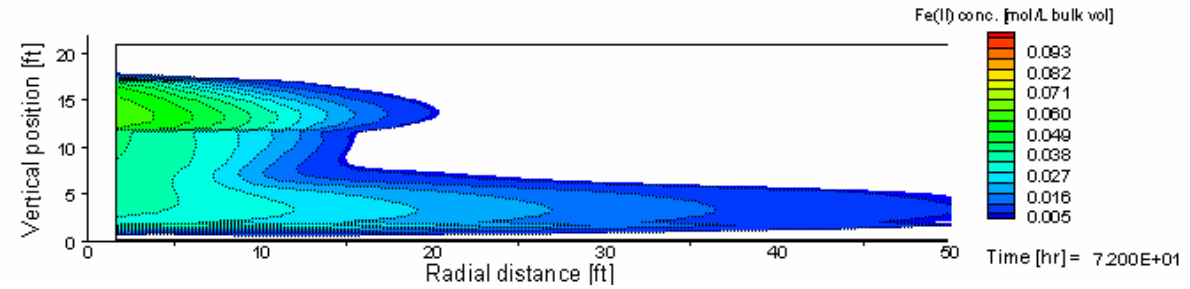

Case 14

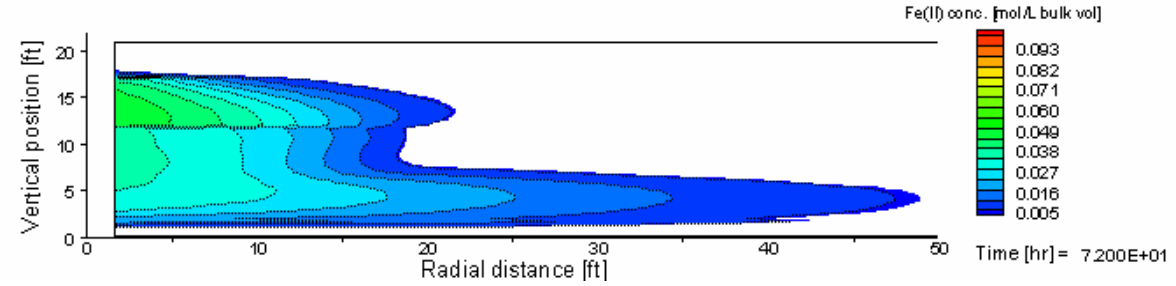

Figure 4.9. Predicted Fe(II) Concentration Distributions (mol/L bulk vol) Around Well PP016 at 72 hr for Simulation Cases 10, 12, and 14 (top to bottom). Dithionite injectate concentrations are 0.08, 0.08, and 0.04 M for cases 10, 12, and 14, respectively. Flow rates are 6.94 gpm from 0-24 hr (~10,000 gal) in unit A1, and 27.75 gpm from 0-24 hr (~40,000 gal) in unit A2, for cases 10 and 12, and 6.94 gpm from 0-48 hr (~20,000 gal) in unit A1, and 27.77 gpm from 0-48 hr (~80,000 gal) in unit A2 for case 14. For case 10, units A1 and A2 are both layered with Kv=Kh/100. For cases 12 and 14, unit A1 is layered with Kv=Kh/100, and unit A2 is layered with Kv=Kh/10.

that could be used if the anisotropy ratio was smaller than expected, resulting in an unacceptable degree of density sinking. In case 12, the anisotropy ratio of the A2 zone was decreased from 100 to 10 to illustrate the magnitude of density sinking that would occur. This information was developed to guide field operations by providing predictions of reagent arrival at the various monitoring points under these reduced anisotropy conditions. Of particular note is the early arrival in the A3 zone for the low anisotropy case. If conditions comparable to case 12 were encountered during emplacement operations, need for an operational change would be indicated. The simulation results shown in case 14 represent the proposed operational change under these lower anisotropy conditions. To reduce the effects of density sinking, reagent concentration would be decreased to one-half the original value, and the injection duration would be extended by a factor of two. As indicated, this approach does help mitigate the decreased treatment extent in the upper portion of the A2/A3 zone under the low anisotropy conditions and would likely be adopted if these conditions were encountered in the field.

Following the phase 1 remedial action treatment at the 3a/b well pair, which provided confirmation that an anisotropy ratio of 100 was a reasonable estimate, additional design analysis was conducted in an attempt to further refine the injection strategy. The Fe(II) distributions depicted for simulation cases 10, 12, and 14 in Figures 4.7 through 4.9 suggested that a two-stage injection strategy might mitigate some of the plume sinking behavior and allow for more uniform spatial coverage of the reduced iron zone. Figure 4.10 depicts results for simulation case 15, in which a two-stage injection strategy was used, with higher dithionite concentrations used during the first stage and lower concentrations during the second stage. Comparing this figure with results from Case 10 in Figure 4.9 indicates a more uniform coverage is predicted for the two-stage injection strategy. Based on these results, this modified injection strategy was used at most of the other well pairs (see Table 6.4). Comparison of these predictive simulations with observed arrival responses at selected operational monitoring wells is discussed in Section 6.2.

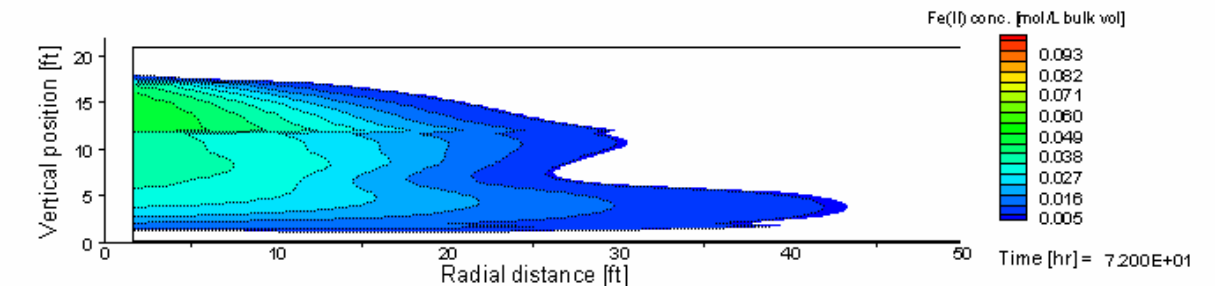

Figure 4.10. Predicted Fe(II) [mol/L bulk vol.] Concentration Distribution Around Well PP016 at 72 hr for Simulation Case 15. Dithionite injectate concentrations are 0.08 M from 0-12 hr, and 0.04 M from 12-36 hr, in both units A1 and A2. Flow rates are 6.94 gpm (~15,000 gal) and 27.75 gpm (~60,000 gal) in units A1 and A2, respectively. Units A1 and A2 are both assigned Kv=Kh/100.

4.3 Emplacement Strategy

The design analysis discussed above was used to develop an operational approach for installing an ISRM permeable reactive barrier at the FHC site. The analysis provided a framework for testing the effects of various hydrogeologic and operational parameters on treatment efficiency. Treatment zone emplacement was conducted using the same push-pull methodology used in the pilot-scale testing of the technology. The full-scale ISRM permeable reactive barrier was installed by coalescing a series of individually emplaced treatment zones to form a continuous linear barrier. A nominal well spacing of 30 ft was selected based on a conservative interpretation of results from the pilot-scale injection test. This nominal spacing was used during installation of the initial remedial action injection wells and was assumed in the initial design analysis. Based on results from the first two remedial action treatments, this 30-ft well spacing was specified for the remaining length of the barrier alignment.

As discussed, due to the differences in permeability between the A1 zone and upper portion of the A2/A3 zone, which combined composed the targeted treatment zone, injections had to be conducted using two separate injection wells, one targeting the A1 zone and the other targeting the upper portion of the A2/A3 zone. A detailed description of the ISRM permeable reactive barrier emplacement at FHC is contained in Section 6.

5.0 Field Site and Equipment Setup

This section includes a description of the site utilities, monitoring equipment, analytical equipment, injection equipment, and the integration of these components into the operational systems required to deploy the ISRM technology at the FHC site.

5.1 Site Utilities

Site utility requirements for deployment of the ISRM technology include access to water, electrical power, and wastewater disposal. A substantial source of water was needed to make up the injection solutions. At the FHC site, a nearby fire hydrant supplied the water needed for dilution of the concentrated dithionite solutions; each test used on average ~70,000 gallons of water at rates as high as 35 gpm. No onsite storage tanks were required because the concentrated reagent was pumped directly from the tanker truck that delivered the chemical.

Electrical power was required to operate site facilities, including a mobile laboratory and associated analytical equipment, process trailer, and injection/monitoring equipment. An appropriately sized electrical service panel was installed at the site that met all electrical requirements.

Wastewater was disposed to the City of Vancouver's sanitary sewer system under special wastewater discharge authorization (number 2002.11). The permit was obtained by EPA and authorized the ISRM crew to discharge a certified non-hazardous "special wastewater" to the city's sanitary sewer system in compliance with the Pretreatment Program (Vancouver Municipal Code Chapter 14.10), applicable provisions of federal and state regulations, and conditions contained in the discharge authorization. Specific conditions listed in the authorization included a range of permissible discharge dates, a maximum volume, a maximum rate, and several notification requirements.

5.2 Monitoring Equipment

Dedicated Grundfos® RediFlo2 sampling pumps were installed in all site monitoring wells. The sample tubing from each of these sampling pumps was routed inside an onsite mobile laboratory and connected directly to a sampling manifold. Sample pumps were operated using a manufacturer-supplied variable-speed control box (converts standard 110-V single-phase power to three-phase power to meet the requirements of Rediflo2 sampling pumps) and a project-developed multichannel interface (pump switch box) that allows multiple sample pumps to be operated from a single control box.

A project-developed sampling manifold was used to collect samples from the various monitoring wells. This approach routes all sample streams into a central manifold for

monitoring field parameters (in a flow-through monitoring assembly) and collecting groundwater samples (Figure 5.1). The advantage of this type of system is that all field parameter measurements are made using a single set of electrodes, which improves data quality and the ability to compare spatially distributed measurements. Consistent labeling between the sampling manifold and pump switch box simplifies selection of the well to be sampled and reduces the chance of operator error during the frequent sampling associated with the injection tests.

Field parameters were monitored using pH, ORP, temperature, electrical conductivity, and dissolved oxygen electrodes installed in a flow-through monitoring assembly. The flow-through assembly was designed to minimize the amount of "dead space" within the monitoring chamber and results in flow-through residence times of less than three seconds under standard monitoring conditions. Purge volumes pumped prior to sample collection were determined by monitoring the stabilization of field parameters. The field parameter monitoring electrodes and their specifications are shown in Table 5.1.

Pressure transducers (10 and 20 psi, 0.1% of full-scale accuracy) were installed in selected wells to monitor pressure response during hydraulic and dithionite/tracer injection tests and recorded continuously using a Campbell Scientific data logger. Water levels were measured using a high-accuracy, National Institute of Standards and Technology traceable, non-stretch, metal-taped, water level meter marked in 0.01-ft gradations.

Table 5.1. Field Parameter Monitoring Electrode Specifications

Parameter	Manufacturer/Model #	Range	Accuracy/Reproducibility
pH	Oakton/WD-35615	pH 2–16	±0.05 pH
ORP	Metron/10-565-3116		
Temperature	Oakton/WD-35607	0.0–100°C	±0.5°C
EC	Oakton/WD-35607	0.0–199.9 mS	± 50 µS
Dissolved oxygen	Orion/810	0–20 ppm	± 0.1 ppm

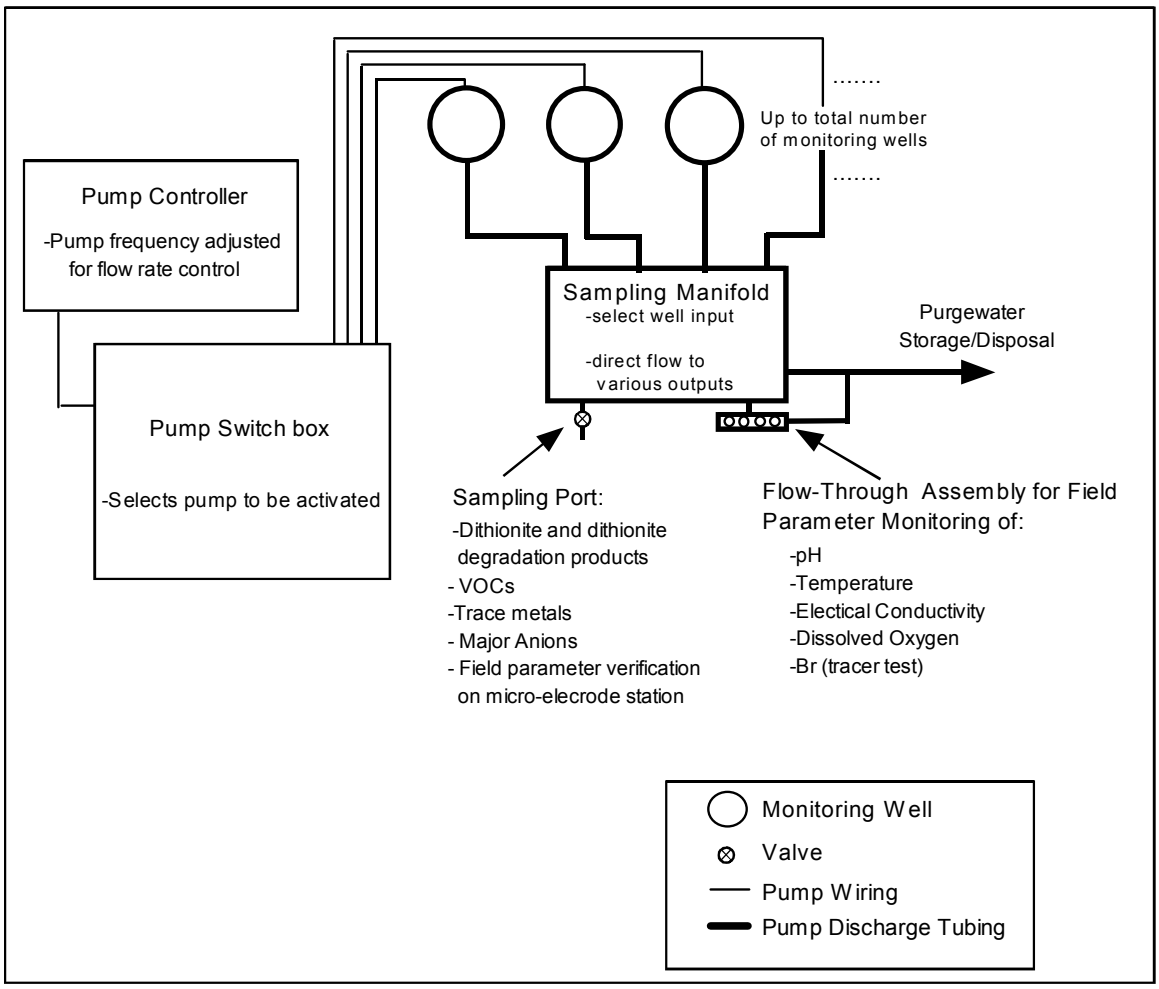

Figure 5.1. Schematic Drawing of the Groundwater Sample Acquisition System

5.3 Analytical Measurements

A comprehensive series of analytical measurements were made throughout the project in support of the field objectives. These included measurements made in Battelle's mobile laboratory during the injection/withdrawal tests, baseline and post-emplacement performance assessment monitoring performed in EPA's mobile laboratory, and samples submitted to EPA and contract analytical laboratories.

During the injection/withdrawal activities, dithionite measurements were performed in Battelle's laboratory using an ultraviolet absorption system with an on-line automatic dilution capability. Field measurements of dithionite were needed because of the inherent instability of that reagent, rendering analysis in an offsite laboratory impractical. Dithionite calibration standards were freshly prepared from pure reagent materials.

Trace metal samples were collected in 500-mL acid washed plastic bottles. Concentrated Ultrex nitric acid was used as a preservative. Baseline and performance assessment trace metals samples were analyzed by inductively coupled plasma-optical emission spectroscopy (ICP-OES; EPA 6010). Withdrawal samples were also analyzed for total sulfur ICP-OES. Ion chromatography was performed on unpreserved samples collected in 100-mL plastic bottles using EPA Method 300.0. In addition to these analytical measurements, samples were also analyzed onsite for Cr(VI) using a spectrophotometric method.

5.4 Injection and Withdrawal Equipment

The injection manifold (Figure 5.2) consisted of an injection pump and appropriately routed piping, valving, and flow rate monitoring equipment. The manifold is used to control (both rate and concentration), monitor, and sample the injection solutions; it is constructed of 316 stainless steel and used stainless steel ball valves for both diversion/shutoff and flow control valves.

A 0.75 hp Grundfos stainless steel multistage centrifugal pump (Model# CRN2-30) was used to inject the concentrated solution. Because the permeability of the targeted aquifer zone (A1) was relatively low and the static depth to water (~20 ft) relatively shallow, an inflatable packer (stainless steel with rubber bladder) was required to pack off the screened interval and prevent injected fluid from overflowing the casing. The injection tubing that extended from the well head to the top of the inflatable packer was made of 1.5-in.-diameter stainless steel pipe.

Omega Engineering turbine flow meters were installed to measure the flow rate of the various streams and the total injection flow rate. Both 1- and 2-in.-diameter flow meters were available to provide flexibility in the injection design. Appropriately sized flow meters were used to monitor the dilution water, concentrated tracer/dithionite solutions, and total injection rates. These flow meters were continually logged using a Campbell Scientific data logger.

Appropriately sized Grundfos stainless steel submersible extraction pumps were used during the withdrawal phase of the tests. The extraction pumps were installed on 1-in.-diameter reinforced rubber hose.

5.5 Description of Equipment Integration/Operation

The dithionite injection operations were conducted using the equipment described above and illustrated in Figures 5.1 and 5.2. The desired injection concentration was achieved by mixing the concentrated dithionite solution with dilution water from the pressurized source. Injection pressure for the concentrated solutions and dilution water was provided by the stainless steel injection pump and the pressurized water supply (e.g., fire hydrant), respectively. The two injection streams were mixed within the injection manifold and injected across each well's screen interval through a perforated section of pipe.

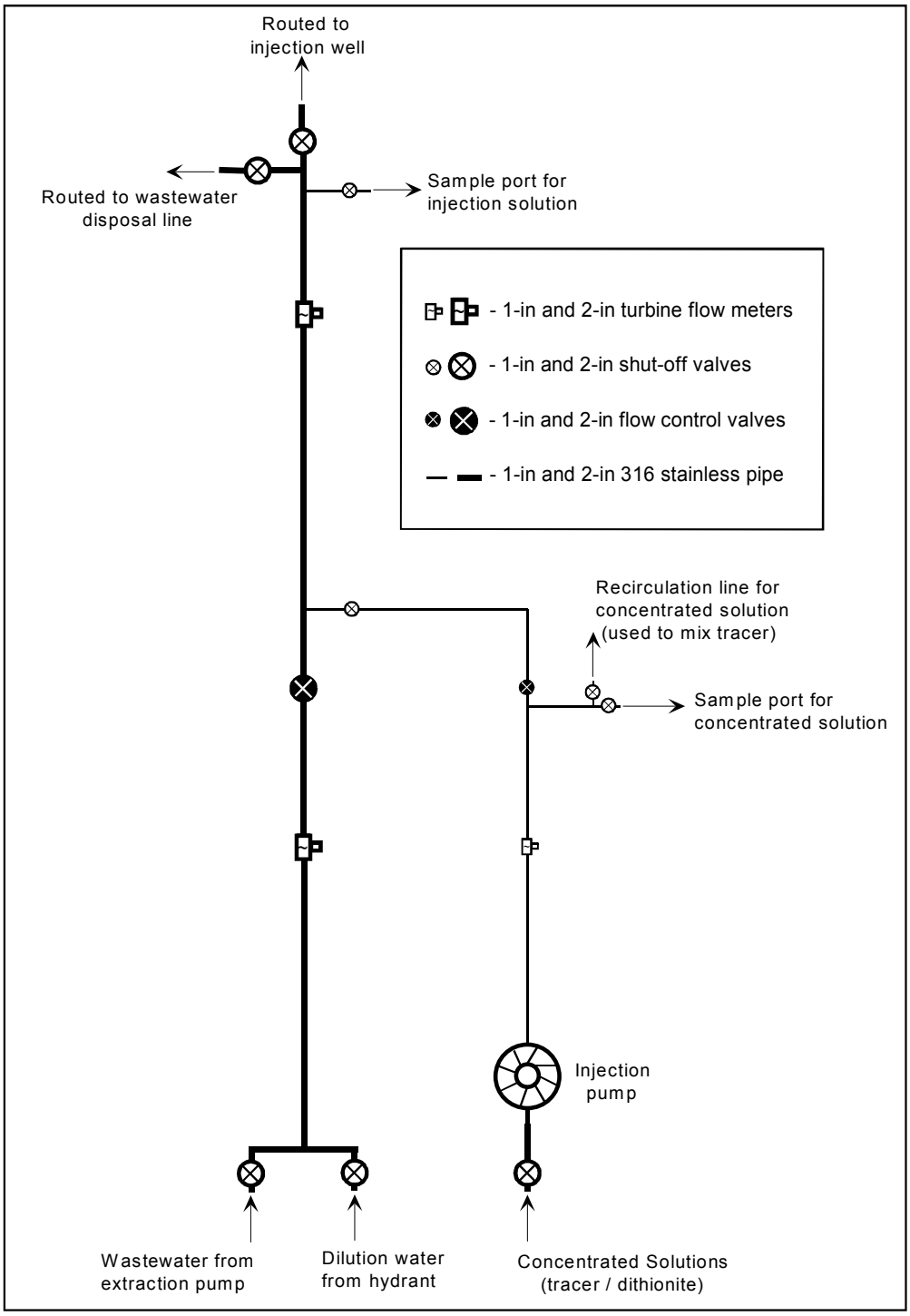

Figure 5.2. Schematic Drawing of the Dithionite Injection System

All injection flow rates (concentrated solution, dilution water, total, upper and lower injection well proportions) were monitored with turbine flow meters and controlled by manually adjusted flow control valves. Sample ports were located on the manifold so that samples of the concentrated and injection solutions could be collected throughout the injection test.

Following the injection and residence phases of the first two injection well pairs treated, the remaining dithionite and reaction products were removed through the central injection well with a submersible extraction pump. Wastewater generated during the withdrawal phase was routed back through the injection manifold to a wastewater disposal line that discharged to the sanitary sewer. Withdrawal water was routed back through the injection manifold so that the same flow monitoring and control equipment used to monitor/control the injection could be used to monitor and control the withdrawal.

Groundwater sample collection during barrier emplacement operations was conducted using the equipment described in Section 5.2 and illustrated in Figure 5.1. The groundwater sampling equipment consisted of dedicated variable-speed submersible sampling pumps installed in all site monitoring wells with sample tubing and control wiring routed to a central location inside the onsite mobile laboratory, where groundwater field parameters were monitored (in a flow-through monitoring assembly) and groundwater samples collected. The advantage of this type of system is that all field parameter measurements were made using a single set of electrodes, which improves data quality and comparability of spatially distributed measurements.

6.0 ISRM Permeable Reactive Barrier Emplacement

This section provides a description of the ISRM permeable reactive barrier emplacement, a discussion of emplacement results, and a comparison of predicted and observed reagent arrivals at selected monitoring wells. Information presented in this section provides the basis for estimating the spatial distribution of reduced iron along the barrier alignment.

6.1 Emplacement Description

This section describes the emplacement of the ISRM permeable reactive barrier. A detailed description of the initial remedial action treatment zone emplacement (3a/b well pair) is provided in Section 6.1.1. A summary of the remaining treatment zone emplacements is provided in Section 6.1.2.

The objective of the ISRM component of the FHC remedial action was to create a permeable reactive barrier, or reduced iron zone, in the A1 and the upper portion of the A2/A3 zones of the A aquifer. The purpose of the reduced iron zone is to remediate hexavalent chromium in groundwater migrating through the reactive barrier. This full-scale ISRM permeable reactive barrier was installed by coalescing a series of individually emplaced treatment zones created using the same methodology employed during the pilot-scale field test (Section 2). During emplacement of each treatment zone, a sodium dithionite solution containing a potassium carbonate pH buffer was injected into the aquifer simultaneously in two centrally located wells, one targeting the A1 zone and the other targeting the upper portion of the A2/A3 zone, to reduce the naturally occurring Fe(III) to Fe(II). Eight field tests were conducted in three separate field campaigns between late May and early August 2003. Table 6.1 shows the injection well pair numbers and test dates for each of the individual barrier emplacement operations conducted.

Table 6.1. ISRM Full-Scale Injection/Withdrawal Well Numbers and Field Test Dates

Injection Campaign	Injection/Withdrawal Well Numbers	Test Date
1	3a and 3b	May 27–June 1, 2003
1	2a and 2b	June 2–9, 2003
2	4a and 4b	July 10–13, 2003
2	5a and 5b	July 14–15, 2003
2	INJ-1 and INJ-2	July 16–18, 2003
3	6a and 6b	August 4–6, 2003
3	7a and 7b	August 6–8, 2003
3	8a and 8b	August 9–10, 2003

Treatment zone emplacement operations were performed in two centrally located wells by using an injection/withdrawal (or push-pull) approach. The push-pull approach consists of three phases: injection, residence, and withdrawal. During the injection phase, the sodium dithionite solution was pumped into the two injection wells and allowed to react with the aquifer sediments. The residence phase, which occurs after injection stops but before withdrawal, provides additional time for the reagent solution to react. During the withdrawal phase, which was conducted for the 3a/b and 2a/b emplacements only (see discussion below), groundwater was extracted from the aquifer by pumping from the same wells used for injection.

6.1.1 Treatment Emplacement at Wells 3a and 3b

Treatment zone emplacement is discussed here in detail for the first remedial action injection at wells 3a and 3b and is followed by a summary for the remaining seven treatment zone emplacements (Section 6.1.2). In general, remedial action injections were conducted in a manner similar to the initial pilot scale injection (Section 2.6). A summary of the injection/ withdrawal test at the 3a/b well pair is provided in Table 6.2. Relative well locations and screen depth interval information are provided in Figure 3.9 and Table 3.1, respectively. During emplacement of this treatment zone on May 27, 2003, approximately 5,734 gallons of concentrated sodium dithionite solution containing a potassium carbonate pH buffer was delivered to the site via tanker truck. Prior to shipment to the FHC site, the dithionite solution was chilled during the dissolving process and the headspace of the tank was blanketed with nitrogen gas to prevent oxidation by atmospheric oxygen. The molar concentration of the potassium carbonate buffer was four times that of the sodium dithionite to maintain a high pH for enhancing the stability of the dithionite. A pH of approximately 11 was maintained during solution injection.

As was done during the pilot scale testing of the ISRM technology at FHC, the concentrated reagent was pumped directly from the tanker truck and diluted inline using the local municipal water supply from a nearby fire hydrant. The volume of concentrated reagent in the tanker truck, estimated based on tank level measurements, was used to determine the rate of flow (of concentrated reagent) from the tanker truck that would provide the specified concentration, injection rate, and total injection volume. The diluted dithionite injection concentration was monitored closely at the beginning of the test and at regular intervals throughout the test to verify that the delivered tanker volume, reagent mass, and purity met design specifications. To enhance stability, a blanket of argon gas was maintained in the headspace of the tanker truck during injection to minimize reagent degradation from contact with atmospheric oxygen.

6.1.1.1 Injection Phase

As indicated in Table 6.2, the average reagent concentration used in the 3a/3b injection was 0.08 M sodium dithionite with a 0.32 M potassium carbonate pH buffer. A concentrated reagent flow rate of 4.1 gpm from the tanker truck was diluted with 31 gpm of fire hydrant water for a

Table 6.2. Summary of the First ISRM Full-Scale Dithionite Injection/Withdrawal Test at the FHC Site (Wells 3a and 3b)

Test Parameter	Value
Injection Phase	
Reagent Mass	6,000 lb 95% purity sodium dithionite ($Na_2S_2O_4$) 15,000 lb potassium carbonate (K_2CO_3)
Tanker Truck Volume	5,734 gal
Total Injection Flow Rate	35.0 gal per min
Tanker Truck Flow Rate	4.0 gal per min
Fire Hydrant Flow Rate	31.0 gal per min
Injection Concentration	0.084 moles/L $Na_2S_2O_4$
Injection Duration	1,435 min (23.9 hr)
Injection Volume	50,220 gal
3a Injection Flow Rate	7.0 gal per min
3a Injection Volume	10,040 gal
3b Injection Flow Rate	28.0 gal per min
3b Injection Volume	40,180 gal
Residence Phase	
Duration	2,730 min (45.5 hr)
Withdrawal Phase	
Total Withdrawal Volume	44,592 gal
Total Mass of Dissolved Solids Removed	1,353 kg (2,976 lb)
Total Mass of Sulfur Removed	131.9 kg (290.1 lb)
Estimated % recovery	15%
3a Withdrawal Flow Rate	3.0 gal per min
3a Withdrawal Volume	5,823 gal
3a Withdrawal Duration	1,920 min (32 hr)
3b Withdrawal Flow Rate	20.5 gal per min
3b Withdrawal Volume	39,420 gal
3b Withdrawal Duration	1,920 min (32 hr)

total injection rate of 35.1 gpm. After mixing, this injection rate was split and injected into wells 3a (~7 gpm) and 3b (~28 gpm). Well 3b, which is completed in the upper portion of the A2/A3 zone, can sustain a much higher yield than well 3a, which was completed in the overlying A1 zone. A total volume of 50,220 gallons of reagent was injected into wells 3a and 3b over 1,435 minutes (23.9 hours). Aqueous samples were initially collected at roughly five-minute intervals in a rotating sequence beginning with the injection stream and then with monitoring wells 12a, 12b, 12c, 11a, and 11b (or approximately every 0.5 to 0.75 hour for the injection stream and each monitoring well). Wells 2a and 2b, located the farthest from the injection wells and not expected to show any effect initially, were sampled every other rotation, or approximately every 1 to 1.5 hours. During the latter part of the injection phase samples were collected less frequently (about every 1 to 2 hours) from the injection stream and each monitoring well.

Samples were analyzed in an onsite mobile laboratory for sodium dithionite and field parameters (electrical conductivity, temperature, pH, DO, and ORP). Dithionite was measured using two automated high-performance liquid chromatography (HPLC) systems. Because of its instability, dithionite must be measured at the site shortly after sample collection. Dithionite analysis of the injection stream was necessary to verify the design molar concentration of the reagent delivered to the aquifer. Figure 6.1 shows that dithionite molar concentration of the injection stream was approximately 0.084 M.

Dithionite analyses of samples collected from monitoring wells 11a, 11b, 12b, and 12c show that the reagent began to reach these locations in the early part of the injection test (Figures 6.2 through 6.5). Field measurements of EC act as a good conservative tracer and provide additional indication that the reagent reached these wells. As indicated, EC measurements generally show patterns similar to those of the dithionite measurements. Dithionite concentrations and EC increased in these wells to roughly 25 to 85% of the input molar concentration by the end of the injection test. The dithionite and EC patterns exhibited by monitoring well 12a appear to be an anomaly (Figure 6.4). As discussed in Section 6.2, dithionite and EC response at well 12a, which began to appear during the latter part of the injection test after the sampling strategy was changed on this well to employ an extend purge cycle, is most likely associated with this well being completed within a lens of relatively low permeability material. As expected, reagent did not reach wells 2a and 2b, which are located approximately 30 ft from the 3a/b well pair, during any phase of the treatment zone emplacement.

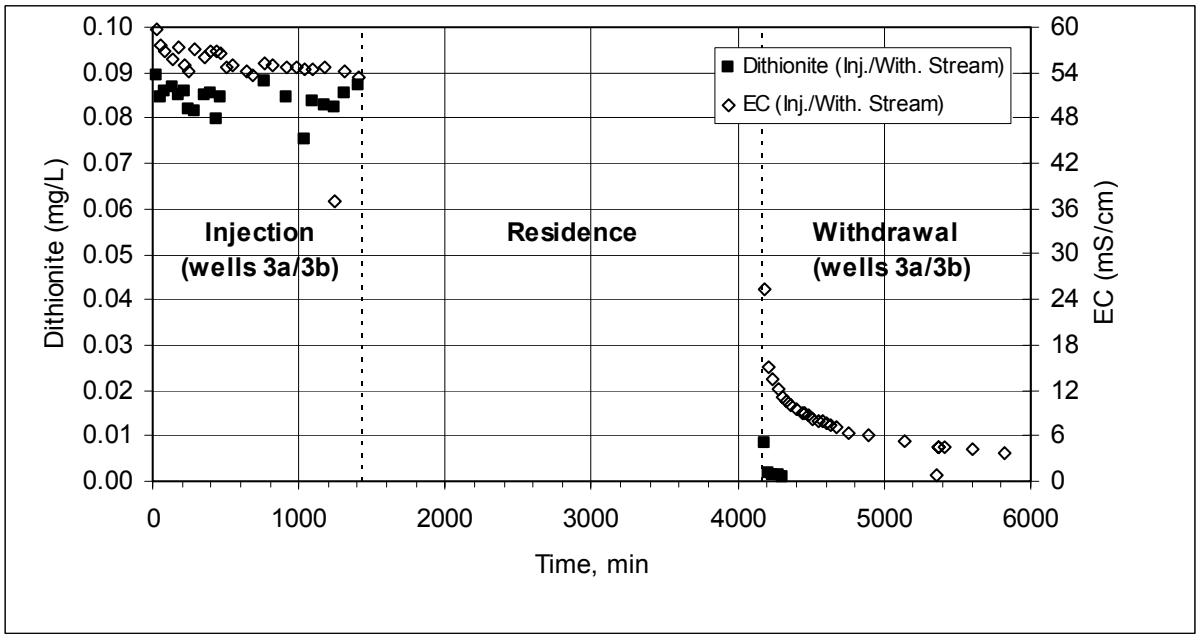

Figure 6.1. Dithionite and EC Measurements of the Injection and Withdrawal Streams During the RA-IW-3a/b Well Pair Treatment

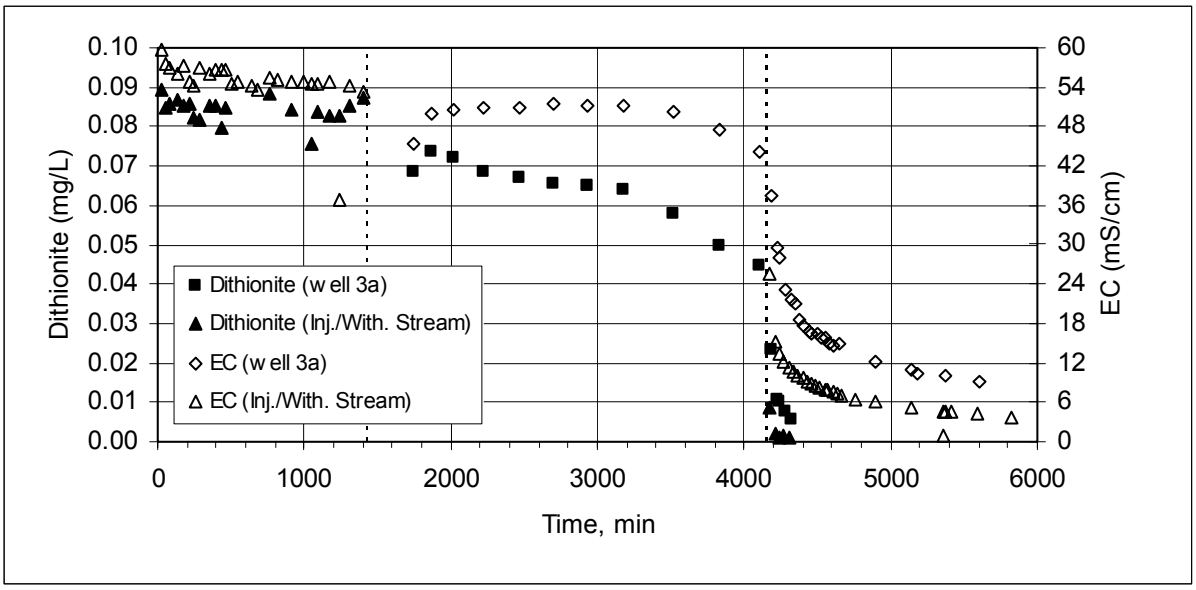

Figure 6.2. Dithionite and EC Measurements at Well RA-IW-3a and Injection and Withdrawal Streams During the RA-IW-3a/b Well Pair Treatment

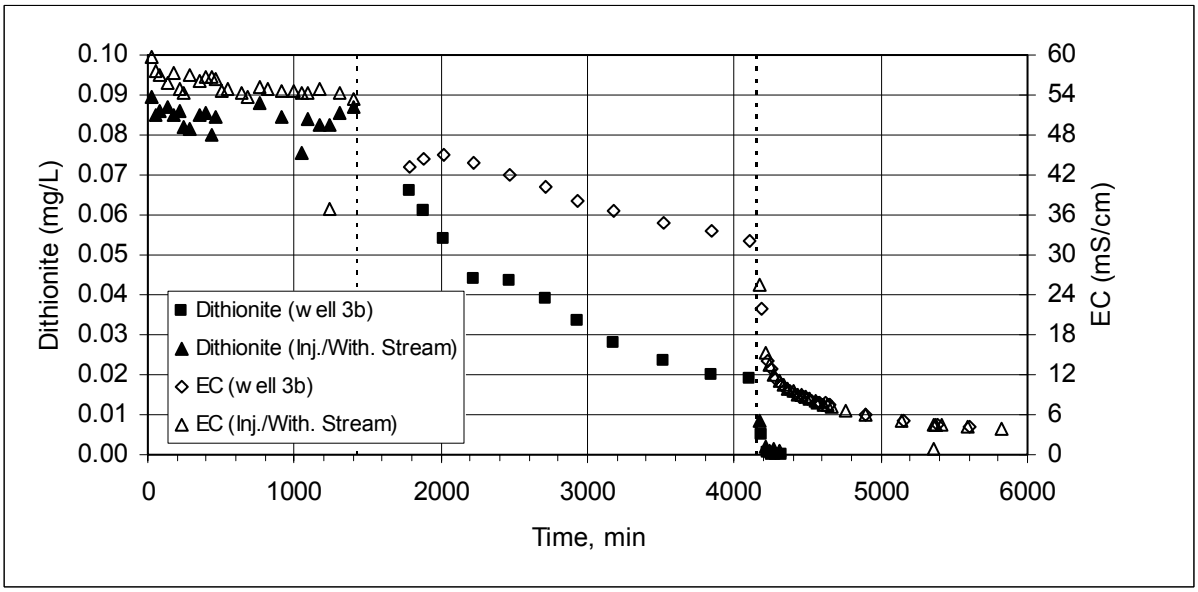

Figure 6.3. Dithionite and EC Measurements at Well RA-IW-3b and Injection and Withdrawal Streams During RA-IW-3a/b Well Pair Treatment

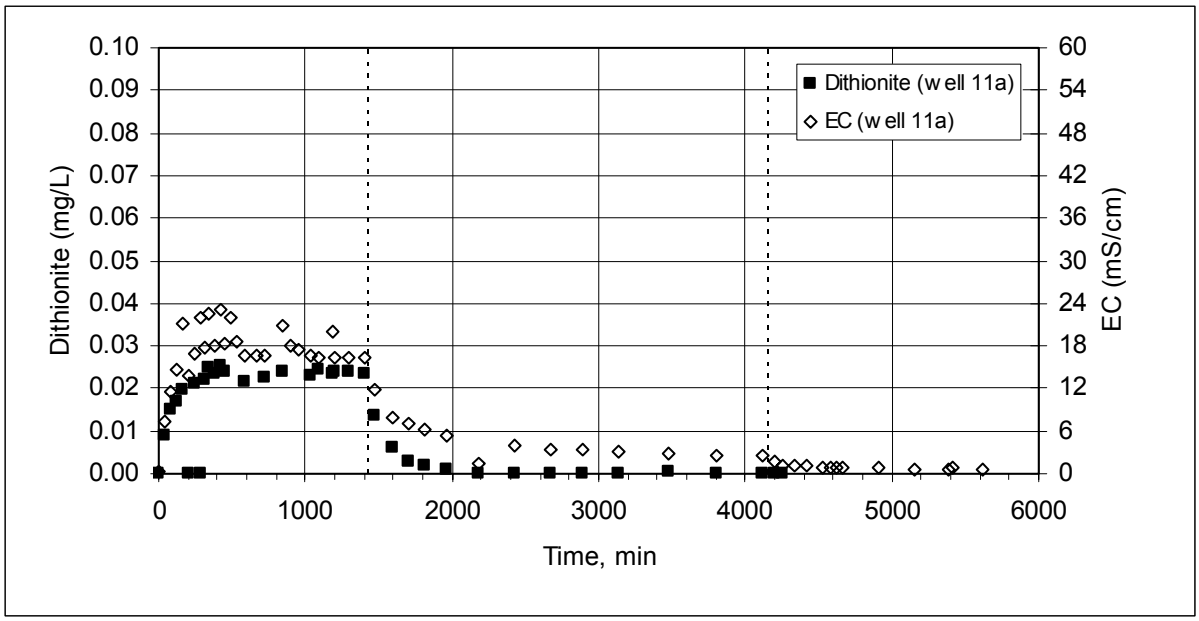

Figure 6.4. Dithionite and EC Measurements at Monitoring Well RA-MW-11a During the RA-IW-3a/b Well Pair Treatment

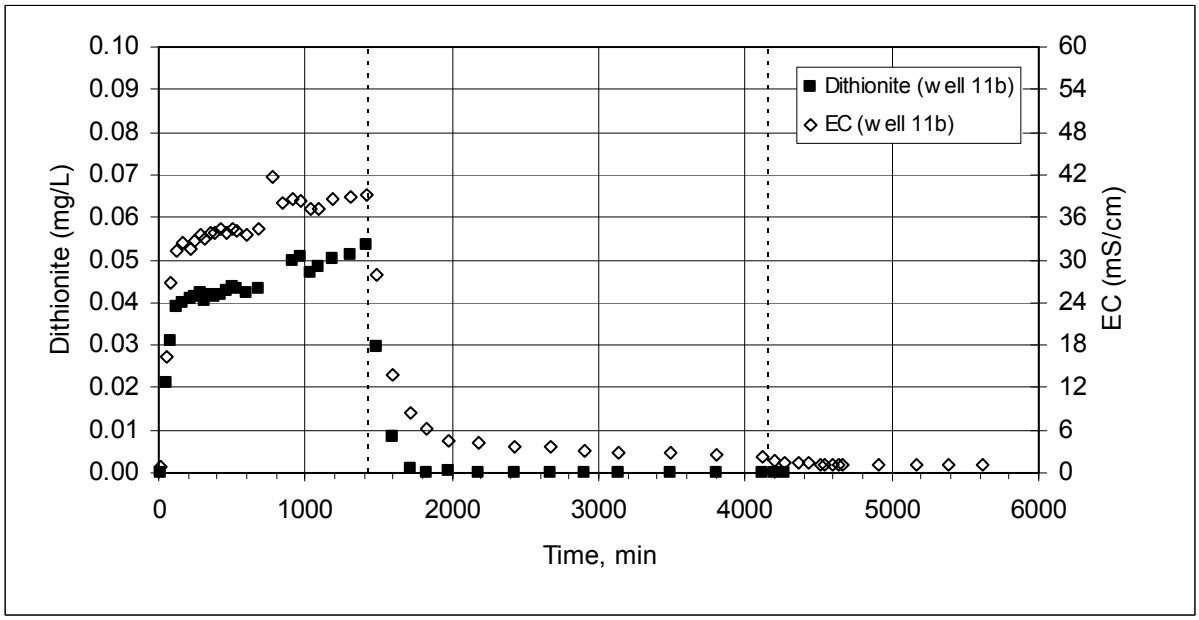

Figure 6.5. Dithionite and EC Measurements at Monitoring Well RA-MW-11b During the RA-IW-3a/b Well Pair Treatment

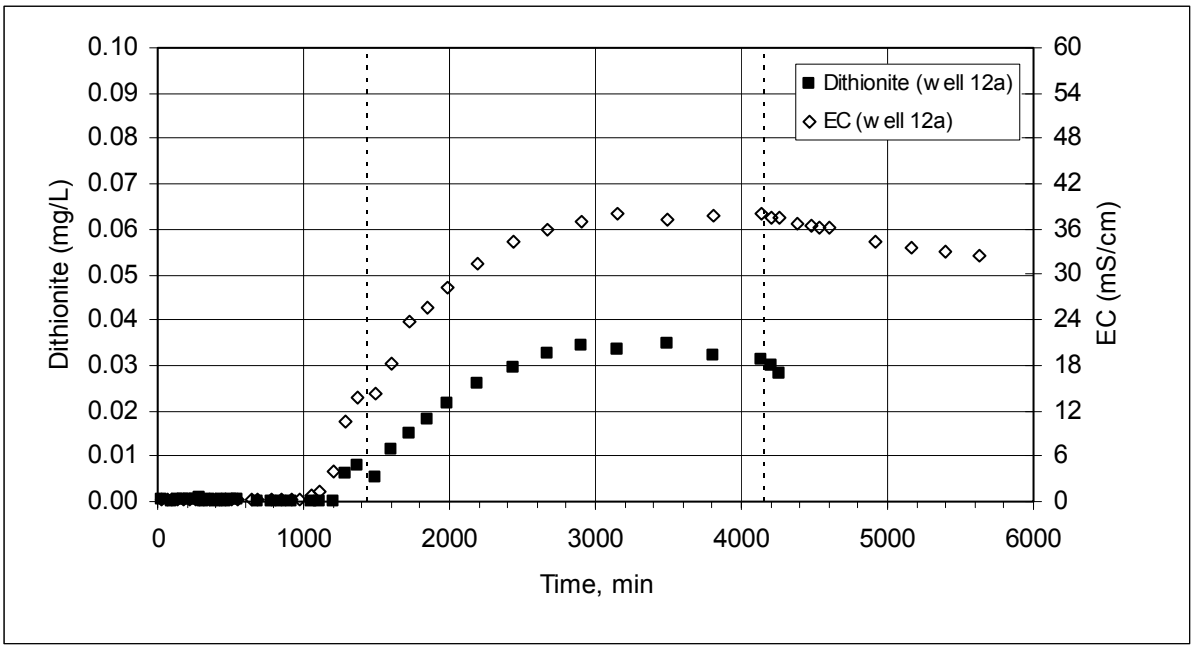

Figure 6.6. Dithionite and EC Measurements at Monitoring Well RA-MW-12a During the RA-IW-3a/b Well Pair Treatment

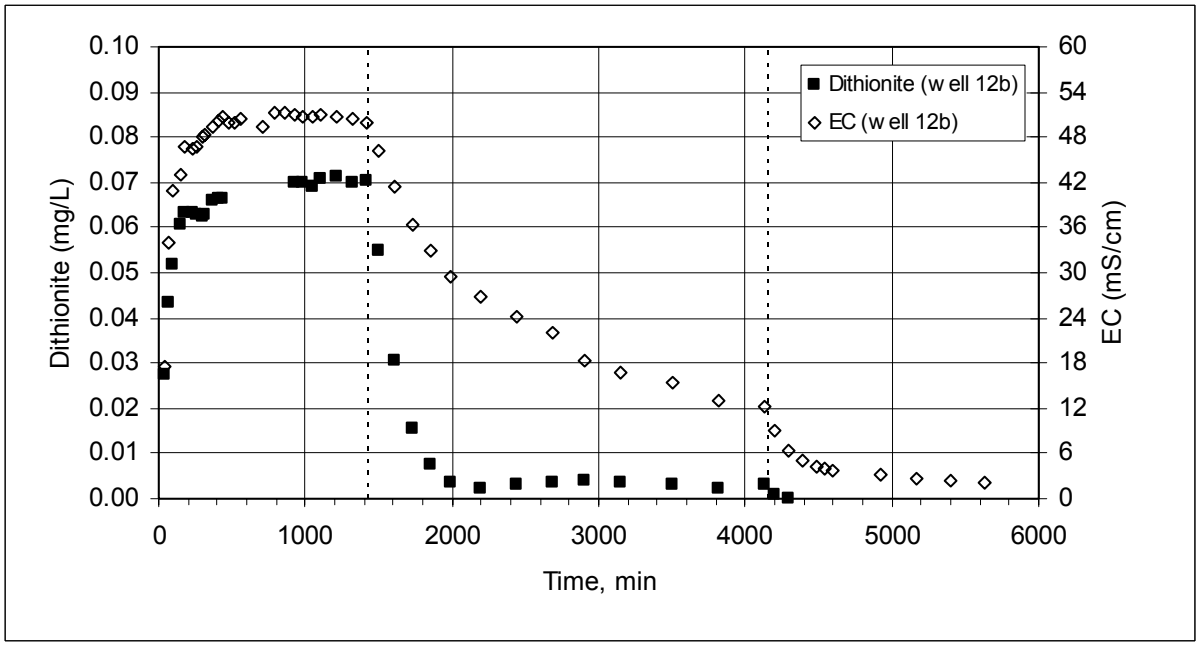

Figure 6.7. Dithionite and EC Measurements at Monitoring Well RA-MW-12b During the RA-IW-3a/b Well Pair Treatment

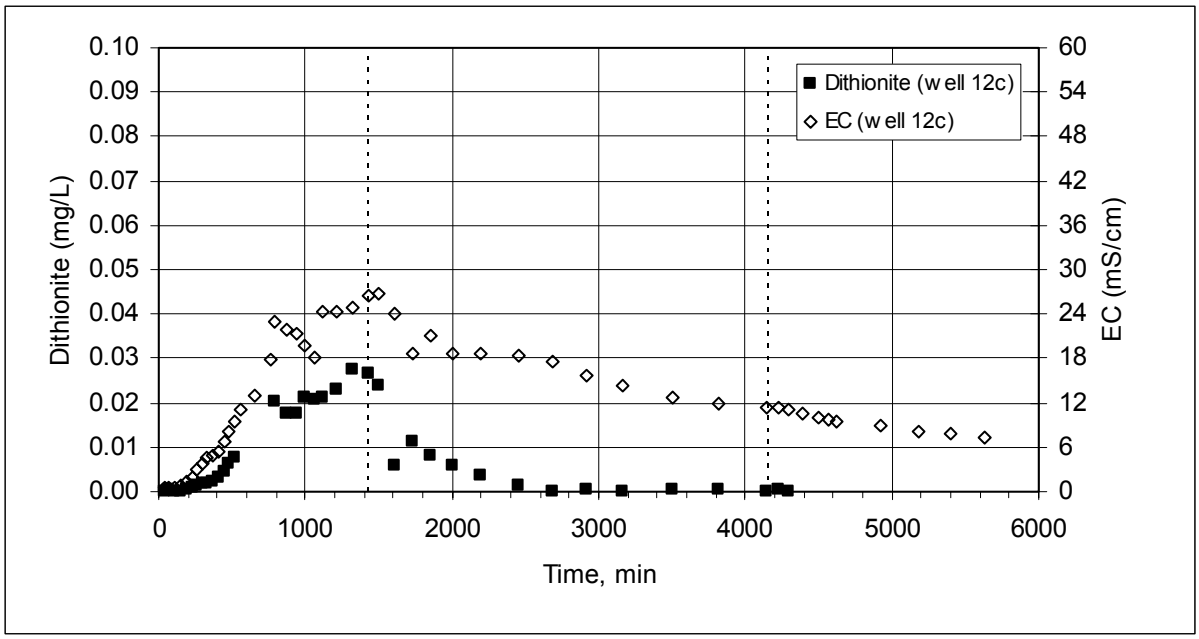

Figure 6.8. Dithionite and EC Measurements at Monitoring Well RA-MW-12c During the RA-IW-3a/b Well Pair Treatment

6.1.1.2 Residence Phase

Following the injection phase, the residence phase provided additional time for the dithionite to react with the aquifer sediments. Aqueous samples were collected from the monitoring wells during the residence phase and measured for dithionite and field parameters. The duration of the residence phase was based on the estimated field-scale dithionite reaction and degradation rates and observed dithionite concentration measurements from site monitoring wells. The duration of the residence phase was 2,730 minutes (45.5 hours); it took place between 1,435 and 4,165 minutes elapsed time since injection of the reagent began.

Sampling frequencies for the monitoring wells, including wells 3a and 3b, during this phase of the test began at 2-hr intervals and was decreased to 4-hr intervals by the end of this phase. Dithionite concentrations decreased to levels of 2.5% or less of the injection concentration in most monitoring wells by the end of the residence phase (Figures 6.4 through 6.8). Dithionite concentrations decreased to 56% of the injection concentration in well 3a and to 24% of the injection concentration in well 3b (Figures 6.2 and 6.3). These decreases in dithionite concentrations were due to reaction with ferric iron, disproportionation reactions, and density effects. As discussed previously, the exception to this general decreasing trend during the residence phase is well 12a, where dithionite began to show up near the end of injection and continued to increase throughout much of the residence phase (Figure 6.6). Dithionite concentrations and EC at well 12a leveled off after approximately 1,500 minutes into the residence phase (or t = 3,000 minutes since the beginning of the injection test).

6.1.1.3 Withdrawal Phase

During the withdrawal phase, 44,592 gallons of groundwater was pumped from wells 3a and 3b over a period of 1,920 minutes (32 hours) and disposed of to the City of Vancouver's sanitary sewer southeast of the field test site. This volume was slightly less than the injection volume (Table 6.2). The majority of the withdrawn groundwater was pumped from well 3b at a rate of 20.5 gpm, yielding an extraction volume of 39,420 gallons. The remainder of the volume, or 5,823 gallons, was extracted from well 3a at a rate of 3 gpm. Extraction from well 3a was limited due to the lower hydraulic conductivity materials composing the A1 zone and the resulting inability of this well to sustain a higher yield.

The sampling frequency of the withdrawal stream and the monitoring wells was ~1/2 hour during the beginning of the withdrawal phase and then was decreased to 4 hours after approximately 8 hours of pumping. Samples were collected at roughly five-minute intervals in a rotating sequence similar to the injection phase. Samples were also collected from wells 3a and 3b individually in addition to the withdrawal stream, which represents the combined pumping from the 3a/b well pair. During the withdrawal phase, dithionite concentrations and EC decreased to low levels in the withdrawal stream and most monitoring wells (Figures 6.1 through 6.8). Dithionite levels in the withdrawal stream and in the monitoring wells (with the exception of 12a) dropped below detection limits within approximately an hour of pumping; at that point, dithionite analyses were discontinued for the remainder of the withdrawal phase. Samples from injection wells 3a and 3b also showed a similar decreasing pattern in the dithionite concentrations and EC (Figures 6.2 and 6.3). Although dithionite concentrations in well 12a decreased during the withdrawal, the concentration was 35% of the injection concentration after about 1.5 hours of pumping. However, due to the anomalous nature of this well and operational factors associated with continued dithionite monitoring at this single well location, dithionite monitoring at 12a was discontinued. Continued monitoring of EC indicated that reagent and/or residuals at this well continued to be elevated by the end of the withdrawal phase.

Aqueous samples from the withdrawal stream were collected and analyzed for sulfur and total dissolved solids to determine mass recovery from the withdrawal phase. The total mass of sulfur removed during withdrawal was approximately 132 kg (290 lb), and the total mass removed based on the TDS data was 1,353 kg (2,976 lb). This compares to a total mass of 1,257 kg (2,766 lb) removed based on the field-measured EC data. Based on a comparison of these data with the total mass of reagent injected, it was estimated that approximately 15% of the total injected reagent mass was recovered during the withdrawal phase. This relatively poor recovery, which is consistent with the recovery response observed during the pilot test, is most likely associated with the heterogeneous nature of the formation materials at FHC and density sinking of the reagent.

Table 6.3 provides a comparison of baseline and post-treatment results for hexavalent chromium, EC, DO, pH, and ORP immediately following the 3a/b emplacement. These results

Table 6.3. Comparison of Pre- and Post-Treatment Water Quality Parameters at 3a/b Well Pair

Well Number	Hexavalent Cr (mg/L)	EC (µS/cm)	DO (mg/L)	pH	ORP (mV)
Baseline Monitoring					
RA-IW-2A	0.72	256	0.00	6.03	159
RA-IW-2B	2.12	402	0.52	6.38	160
RA-IW-3A	8.51	na	na	na	na
RA-IW-3B	5.86	na	na	na	na
RA-IW-11A	3.67	410	0.33	6.73	155
RA-IW-11B	4.05	400	0.00	6.66	134
RA-IW-12A	8.38	124	2.43	4.61	283
RA-IW-12B	8.46	174	2.10	5.71	262
RA-IW-12C	0.99	560	0.00	6.48	57
Post-Injection Monitoring					
RA-IW-2A[(a)]	na	296	na	7.71	-753
RA-IW-2B[(a)]	na	345	na	7.49	-733
RA-IW-3A[(b)]	na	8220	na	9.51	-653
RA-IW-3B[(b)]	na	3360	na	8.94	-673
RA-IW-11A[(b)]	na	532	na	7.85	-641
RA-IW-11B[(b)]	na	953	na	8.24	-636
RA-IW-12A[(b)]	na	30700	na	9.61	-744
RA-IW-12B[(b)]	na	1980	na	8.40	-732
RA-IW-12C[(b)]	na	6860	na	8.11	-698
RA-IW-12A[(c)]	0.00	6180	0.00	8.37	-184
RA-IW-12B[(c)]	0.00	3580	0.00	8.49	-113
RA-IW-12C[(c)]	0.00	1810	0.00	8.09	-175

na = Measurement not available
(a) Samples collected near end of injection phase.
(b) Samples collected near end of withdrawal phase.
(c) Samples collected approximately 1 month after injection test.

provide a preliminary indication of the treatment performance (Cr, DO, ORP) and an indication of how much spent reagent remained in the aquifer after completing the pilot-scale test (EC). As expected, EC increased from an average baseline value of 330 µS/cm to post-emplacement values that ranged as high as 10 to 20 times this value. The relatively large increase in well 12a is consistent with the anomalous response observed at this well. One month after the treatment, EC measurements in this well had decreased to more typical values, while EC measurements in 12b increased. This paired response likely indicates continued drainage of residuals from the relatively low-permeability materials in this region of the A1 zone. In general, residuals were significantly elevated in the A1 zone relative to the lower portion of the aquifer. These elevated residual concentrations are associated with the difficulty of withdrawing spent reagent from this relatively low-permeability material.

6.1.2 Summary of Treatment Emplacement at Remaining Wells

Table 6.4 is a summary of all eight remedial action barrier emplacement operations. The total reagent mass injected at each well pair was 6,000 lb $Na_2S_2O_4$ (sodium dithionite) and 15,000 lb K_2CO_3 (potassium carbonate buffer), for a total reagent mass of 168,000 lb. The total volume injected (reagent and dilution water) during emplacement of the ISRM permeable reactive barrier at FHC was 560,000 gallons. As discussed in Section 4.2, during the initial remedial action emplacement at the 3a/b well pair, the molar concentration of the reagent was maintained at approximately 0.08 M throughout the injection phase. This test confirmed that the actual formation anisotropy ratio was closer to the assumed value of 100 than to 10, which is a typical assumption (see discussion in Section 4.2). Following this test, additional design analyses were conducted in an attempt to further refine the injection strategy.

Table 6.4. Remedial Action Dithionite Injection Summary

Injection Well Pair	Injection Start Date	Concentrated Reagent Mass/Volume	Injection Concentration and Duration	Injection Rate (gpm)	Injection Volume (gal)
INJ-1/INJ-2	7/16/03	6,000 lb $Na_2S_2O_4$ 15,000 lb K_2CO_3 5,640 gal	0.084 M for 12 hr, 0.043 M for 22.7 hr	INJ-1 = 28.4 INJ-2 = 7.0 Total = 35.4	INJ-1 = 59,150 INJ-2 = 14,550 Total = 73,700
RA-IW-2a/b	6/2/03	6,000 lb $Na_2S_2O_4$ 15,000 lb K_2CO_3 5,680 gal	0.086 M for 12 hr, 0.046 M for 22.7 hr	IW-2b = 28.0 IW-2a = 7.0 Total = 35.0	IW-2b = 58,400 IW-2a = 14,500 Total = 72,900
RA-IW-3a/b	5/28/03	6,000 lb $Na_2S_2O_4$ 15,000 lb K_2CO_3 5,730 gal	0.084 M for 24 hr	IW-3b = 28.0 IW-3a = 7.0 Total = 35.0	IW-3b = 40,200 IW-3a = 10,000 Total = 50,200
RA-IW-4a/b	7/11/03	6,000 lb $Na_2S_2O_4$ 15,000 lb K_2CO_3 5,430 gal	0.082 M for 6 hr, 0.042 M for 30 hr, 0.025 M for 6.4 hr	IW-4b = 28.5 IW-4a = 6.4 Total = 34.9	IW-4b = 72,400 IW-4a = 16,300 Total = 88,700
RA-IW-5a/b	7/14/03	6,000 lb $Na_2S_2O_4$ 15,000 lb K_2CO_3 5,750 gal	0.084 M for 33.1 hr	IW-5b = 14.5 IW-5a = 10.5 Total = 25.0	IW-5b = 28,800 IW-5a = 20,800 Total = 49,600
RA-IW-6a/b	8/4/03	6,000 lb $Na_2S_2O_4$ 15,000 lb K_2CO_3 6,820 gal	0.079 M for 12 hr, 0.041 M for 25.7 hr	IW-6b = 28.0 IW-6a = 7.1 Total = 35.1	IW-6b = 63,400 IW-6a = 16,100 Total = 79,500
RA-IW-7a/b	8/6/03	6,000 lb $Na_2S_2O_4$ 15,000 lb K_2CO_3 5,760 gal	0.08 M for 15.7 hr, 0.044 M for 16.7 hr	IW-7b = 27.1 IW-7a = 7.9 Total = 35.0	IW-7b = 52,600 IW-7a = 15,400 Total = 68,000
RA-IW-8a/b	8/9/03	6,000 lb $Na_2S_2O_4$ 15,000 lb K_2CO_3 5,690 gal	0.081 M for 12 hr, 0.042 M for 23.7 hr	IW-8b = 28.6 IW-8a = 7.5 Total = 36.1	IW-8b = 61,200 IW-8a = 16,100 Total = 77,300

Results from these analyses suggested that a staged concentration injection strategy, with higher dithionite concentrations used during the first stage and lower concentrations during the second stage, could help mitigate the effects of density sinking of the reagent and allow for more uniform spatial coverage of the reduced iron zone. Based on these results, this modified

injection strategy was used at most of the other well pairs (see Table 6.4). One exception was the 5a/5b well pair where, due to limited well capacity and the resulting extended test duration for the two-stage approach, the injection was conducted using a constant concentration throughout the injection. Another slight variation was at the 4a/b well pair where, due to evidence of increased density sinking (see Figures E.14 and E.15 in Appendix E), a three-stage approach was adopted where concentrations were reduced sooner to help mitigate the effects of density sinking. The INJ-1/INJ-2 injection listed in Table 6.4 is the second injection operation conducted at this location. Due to the limitations associated with the pilot test treatment, which used only the A1 zone injection well (see discussion in Section 2.7), a second injection was conducted that adopted the improved injection strategy.

As discussed in Section 6.1.1, an estimated 15% of the total injected reagent mass was recovered during the withdrawal phase of the initial remedial action emplacement at the 3a/b well pair. This relatively poor recovery, which is consistent with the recovery response observed during the pilot test (~5%), is most likely associated with the heterogeneous nature of the formation materials at FHC and density sinking of the reagent. Following the occurrence of a similar recovery response at the second remedial action emplacement (2a/b well pair) and a consideration of cost relative to the benefits of removing this small percentage of spent reagent, it was decided, with EPA concurrence, that attempts to withdraw the spent reagent would be discontinued.

The dithionite injection BTCs from treatment zone emplacements at the various well pairs are provided in Figures 6.1 through 6.8 for the 3a/b injection and in Appendix E for the remaining injections. Inspection of the BTCs from each emplacement operation along the barrier alignment provides a qualitative measure of the spatial distribution of treatment. In general, these data indicate that a finite amount of treatment was achieved along the full barrier alignment, although in two cases, the iron distribution in the overlap zones between two injection well pairs may have been less than that predicted in the design simulations. These cases include the 2a/b injection, where very little response was observed at the 11a/b monitoring well pair and the 5a/b injection where only limited response was observed in the 13a/b monitoring well pair. These responses are indicative of the formation heterogeneities present at the FHC site and an example of the challenges associated with deploying an effective remedial technology at hydrogeologically complex sites. However, in both cases, the monitoring well pair in question did receive substantial treatment during the injection operation on the opposing side of the monitoring well pair (i.e., 3a/b for the 11a/b case and INJ-1/2 for the 13a/b case).

In an attempt to provide a more quantitative estimate of the spatial distribution of reduced iron achieved during the treatment zone emplacements, the 2D radial reactive transport model developed during the design analysis phase of the project was enlisted. A comparison of observed reagent arrivals at selected wells with arrival predictions based on these reactive transport simulations is provided in the following section and demonstrates a reasonably good fit between predicted and observed responses. Subsequently, this reactive transport model will be

used to estimate the spatial distribution of reductive capacity generated during barrier emplacement operations (Section 6.3). This model will also be used to provide bounding estimates of barrier longevity (Section 7.2).

6.2 Comparison of Predicted and Observed Reagent Arrivals

Figure 6.9 shows the dithionite arrival responses observed during the 3a/b injection for wells 11a, 11b, 12a, 12b, and 12c along with simulation results from the 2D radial model that was presented in Section 4.2. The simulations that were conducted for comparisons with the observed dithionite breakthrough curves used the E-type estimates from either the east or west sides of the injection well pair, depending on where the particular observation wells were located. Although the monitoring wells are all within approximately the same radial distance of the injection wells, the observed BTCs at these locations show significant differences. The differences between the observed BTCs and between the observed and simulated BTCs are assumed to be due primarily to aquifer heterogeneities not represented in the two-dimensional radial model.

The arrival response observed in 12a (Figure 6.9) is most likely associated with this well being completed within a lens of relatively low-permeability material. This same type of delayed response was observed during treatment of the injection well pair on either side of this monitoring location (i.e., 3a/b and 4a/b). During the 3a/b injection, the arrival response in 12a did not occur until after approximately 20 hours when the sampling strategy was changed on this well to employ an extend purge cycle, drawing the reagent into the lower-permeability material. The low permeability of the formation materials surrounding this well is also evidenced by the prolonged high reagent concentrations during the withdrawal phase at this well relative to the tailing response in the other wells. Also of interest is the response in well 12c, which is screened below the targeted treatment interval and indicates that geologic controls limiting vertical flow at this location were not adequately represented in the model (i.e., the model predicts more reagent sinking than was observed at this location).

Figure 6.10 shows the dithionite arrival responses observed during the 6a/b injection, which is near the east end of the barrier alignment, for wells MW-20, MW-21, RA-IW-7a and -7b, and RA-MW-14a and -14b. A two-stage injection strategy was employed during this injection, which is evident in the BTCs shown in the figure. Results in Figure 6.10 are similar to those obtained for the 3a/b well pair but indicated a somewhat less heterogeneous response. Note that the simulation results shown in Figures 6.9 and 6.10 have not been calibrated based on the observed arrivals but instead use the model parameterization that was developed based on available field characterization data.

Together, the arrival responses shown in Figure 6.9 and 6.10 illustrate the general effect of the presumed formation heterogeneities at the site. At well 11a, although breakthrough occurred

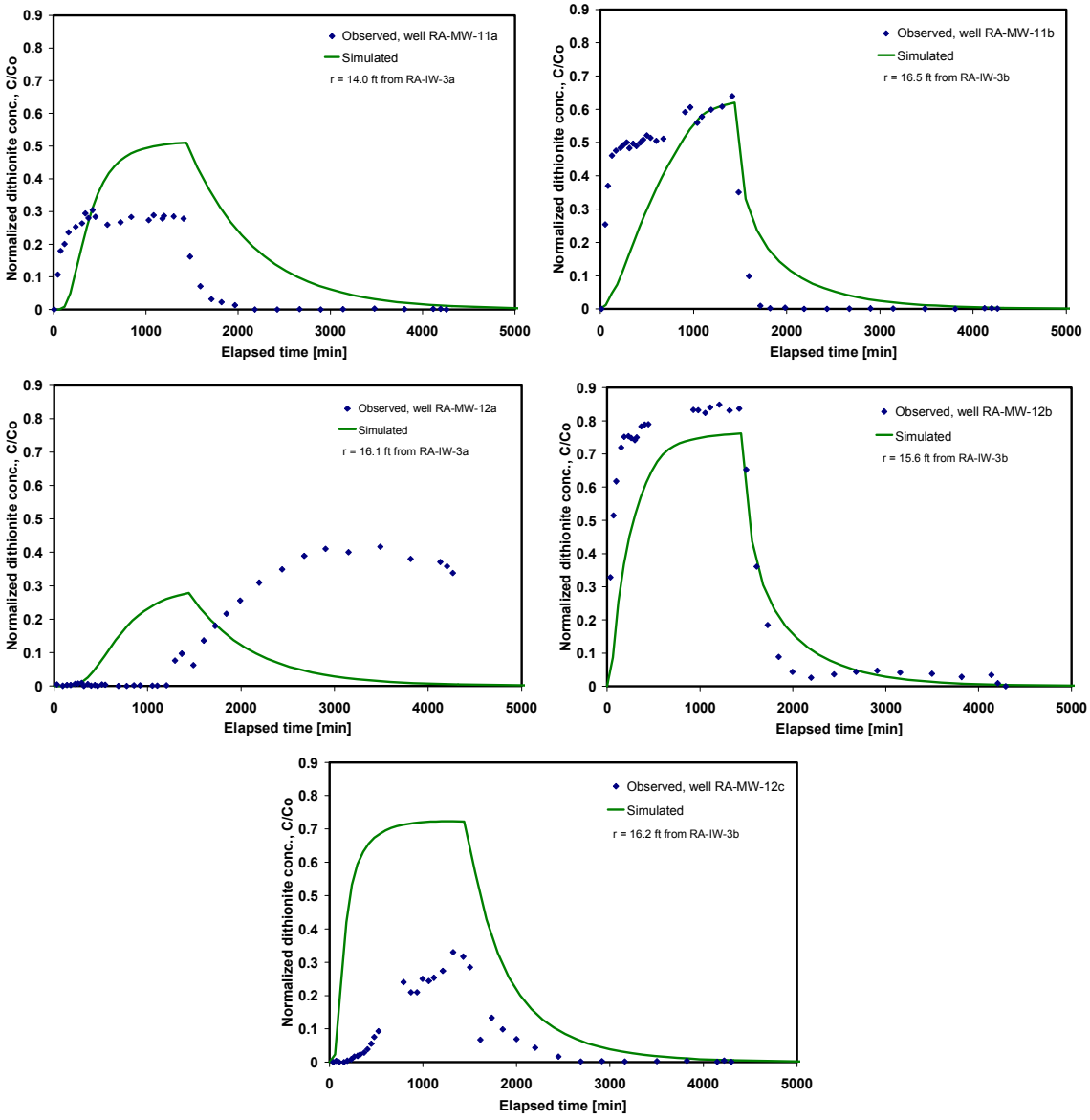

Figure 6.9. Observed and Simulated Dithionite Breakthrough Curves for Wells RA-MW-11a, -11b, -12a, -12b,and -12c (from left to right and top to bottom) Resulting from the Injection at RA-IW-3a/b Well Pair

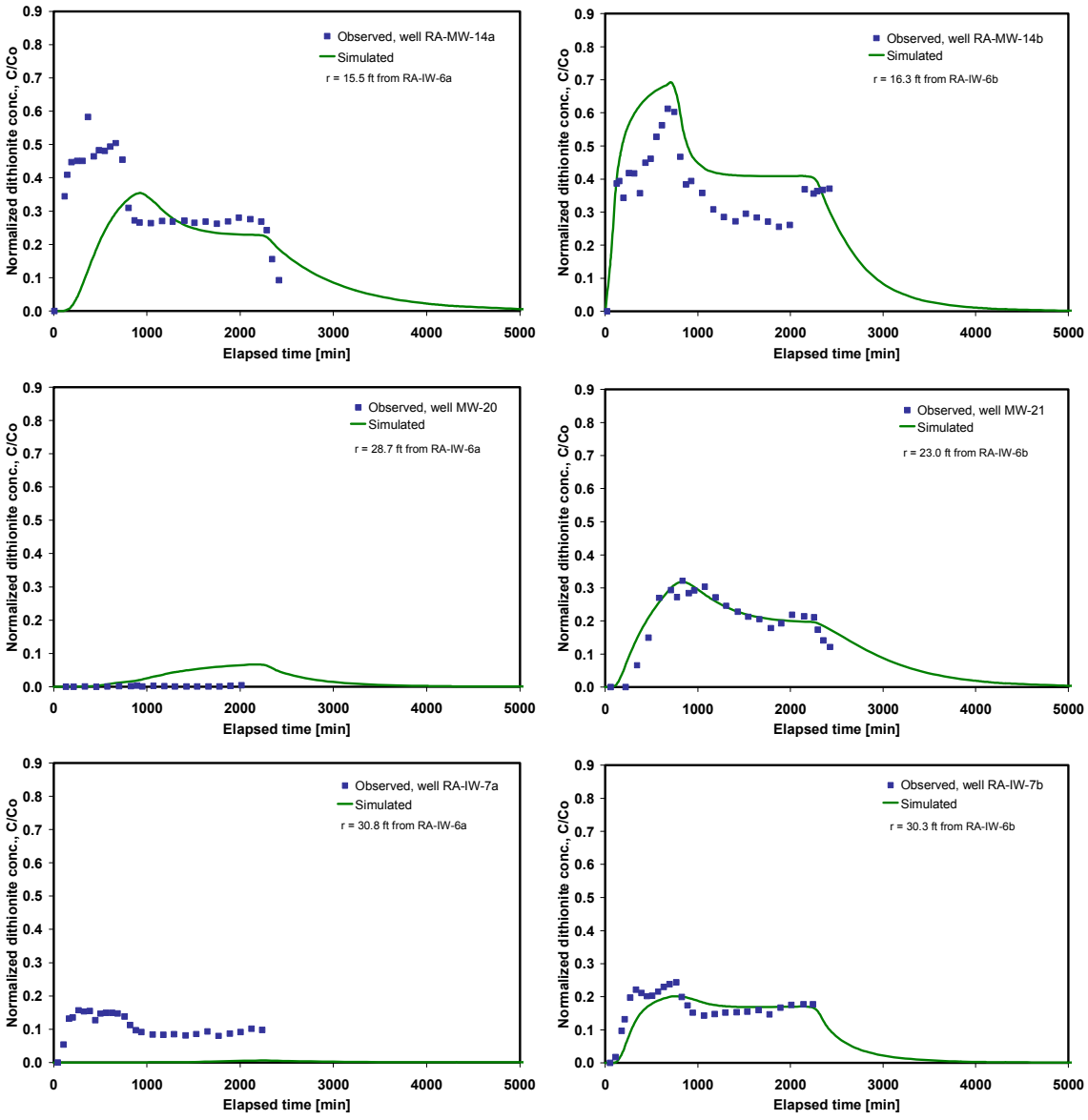

Figure 6.10. Observed and Simulated Dithionite Breakthrough Curves for RA-MW-14a, -14b, MW-20, MW-21, RA-IW-7a, and -7b (from left to right and top to bottom) Resulting from the Injection at RA-IW-6a/b Well Pair

early, indicating some degree of preferential flow to this location, the arrival response flattened out at a concentration less than the predicted response, indicating that the monitoring well may be influenced by higher permeability channels not impacted by the injection (i.e., preferential flow of clean water from outside the area of influence prevents the well from reaching the predicted reagent concentration). Conversely, the arrival at other locations was quicker, and in the case of 12b, reached maximum concentration much sooner than predicted, indicating that substantial preferential flow paths may exist between the injection well and the monitoring well. In general, the simulated BTCs for monitoring locations located in the A2/A3 unit match the

observed BTCs better than those for the A1 unit. This is presumably a result of the better site characterization data available for the A2/A3 zone and the improved model parameterization based on the geostatistical analyses of the EBF data.

The relatively good fit between the predicted and observed arrival responses at these locations indicates that the 2D radial reactive transport model constructed during this effort provides a reasonable representation of actual site conditions and subsequently will be a useful tool for estimating the distribution of reductive capacity that was generated during emplacement operations at the site. Of particular note is the generally good fit in the 'b' wells, which, as discussed in Section 4.2, are of primary importance due to the relatively high oxidizing species concentrations and flux rates in this zone. Comparison of predicted and observed responses in the 'a' wells indicates that the 2D radial model has the potential to over-predict reductive capacity in the A1 zone at some locations.

6.3 Emplacement Results and Discussion

Data from emplacement operations along the barrier alignment provide a good qualitative measure of the spatial distribution of treatment. In general, these data indicate that a finite amount of treatment was achieved along the full barrier alignment, although in two separate instances, the iron distribution in the overlap zones between two injection well pairs may have been less than that predicted in the design simulations. The observed responses were indicative of the formation heterogeneities present at the FHC site and provide an example of the challenges associated with deploying an effective remedial technology at hydrogeologically complex sites. However, in both cases, the monitoring well pair in question did receive substantial treatment during the injection operation on the opposing side of the monitoring well. And even under these non-ideal reduced-iron distribution conditions, it is likely that, given the relatively small hydraulic gradient at the site and the effectiveness of the source area treatment, even the lowest-capacity regions of the barrier will contain sufficient quantities of reduced iron to meet the remedial objectives documented in the proposed plan (i.e., installation of the ISRM barrier provides additional long-term protection of groundwater and downgradient groundwater during augering/injection of reductant into the source area soils and the plume hot-spot area.)

As discussed in Section 6.2, to provide a more quantitative estimate of the spatial distribution of reduced iron that was emplaced during the ISRM treatments, a 2D radial reactive transport model was enlisted. This model was developed during the design analysis phase of the project and was verified with dithionite arrival response data from two separate locations along the barrier alignment. The emplaced Fe(II) distribution was simulated at the 3a/b and 4a/b injection well locations (Figure 6.11). These locations were selected because 1) they are located within the central portion of the plume where characterization of barrier effectiveness and longevity is most critical, 2) their adjacent location allowed for the estimation of reductive capacity generated at each well and in the overlap zone between the two wells, and 3) the different injection strategies used at these two wells provided a comparison of the resulting reduced iron

distribution from a constant versus staged injection concentration approach. Due to project constraints, predictive simulations of reductive capacity were not conducted along the full length of the barrier; this additional simulation work, although useful for assessing the emplacement efficiency along the full length of the barrier, was not within the scope of this effort.

The 2D radial reactive transport model was used to simulate the Fe(II) distribution generated at each injection well pair by specifying the actual operational parameters used during treatment zone emplacement at these locations. These 2D reduced iron distributions generated using the radially symmetric model were projected onto a 3D grid using a radial to Cartesian coordinate transformation. The resulting 3D data from each of these emplacement operations were then superimposed to generate the overlapped reduced iron distribution resulting from the combined treatment at these two locations. Figure 6.11a shows the reduced iron distribution resulting from the 3a/b injection and Figure 6.11b shows the reduced iron distribution resulting from the 4a/b injection. Figure 6.11c shows the combined effect of the two emplacement operations.

Comparing Figure 6.11a and b demonstrates the benefits of the staged injection concentration approach (4a/b injection) that was adopted following the initial remedial action injections (Section 6.1.2) relative to the constant concentration approach used in the 3a/b injection. As indicated, the higher-concentration, shorter-duration injection in the 3a/b injection resulted in more reductive capacity near the injection well but less at greater radial distances. Conversely, the staged concentration approach used during the 4a/b injection, which started at the same maximum concentration but stepped it down for a longer injection duration, resulted in a more uniform iron distribution. As indicated previously, this multistage injection concentration approach was adopted after the initial remedial action injection campaign and was used at a majority of the well locations. A discussion of bounding estimates of barrier longevity based on the combined reduced iron distribution shown in Figure 6.11c is provided in Section 7.2.

Although the 2D radial model provided a reasonable representation of the ISRM barrier emplacement operations that were investigated, for highly heterogeneous sediments, 2D simulations may not always be adequate. To determine whether a fully 3D model could better represent the observed site conditions, a 3D model was also developed. Preliminary results indicated that the simulated dithionite arrivals for the 3D model did not match the observed arrival responses as well as those obtained using the 2D model. This is due in part to extrapolation of the 2D K field generated from the EBF data into the third dimension and the associated creation of artificially high connectivity of the K field in the third dimension. Another disadvantage of the 3D model is the coarser grid resolution required to discretize the model domain such that the simulations could be run in a reasonable amount of time. The larger model grid blocks that result from the coarser grid resolution tend to result in lower peak concentration values than the finer grids, which are better able to track sharp concentration fronts associated with injected solute pulses. These preliminary modeling results demonstrated the potential advantages of going to a fully 3D model, but additional investigation was not within the scope of this effort and was not pursued for inclusion in this report.

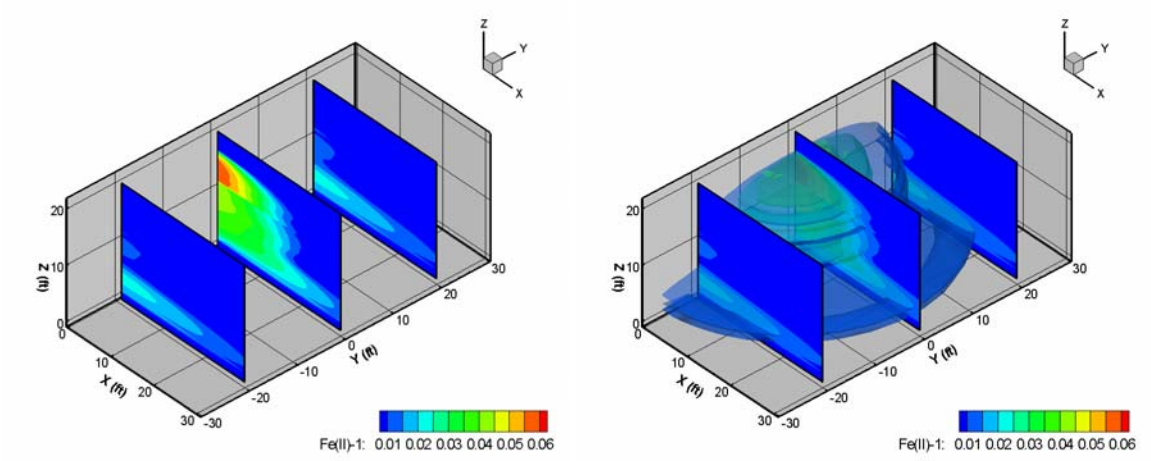

a)

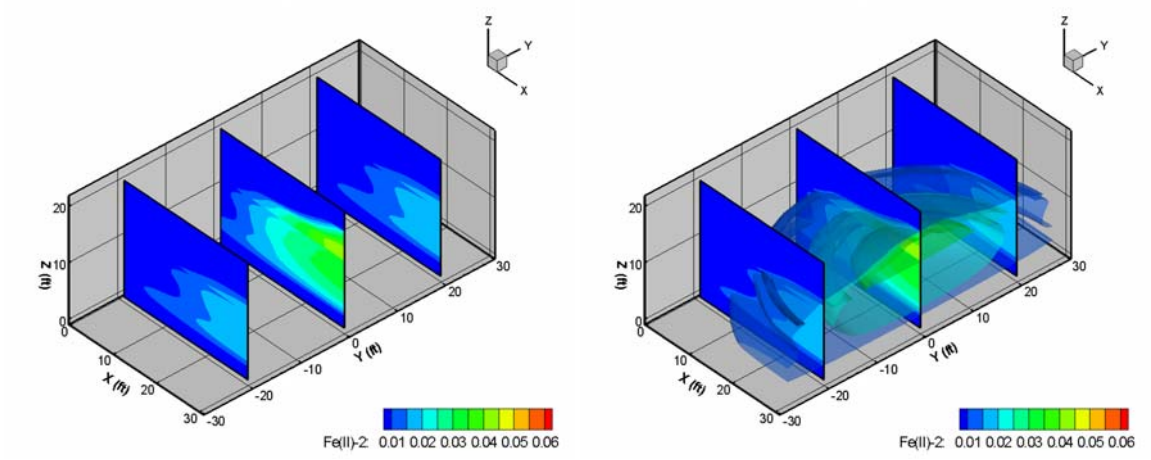

b)

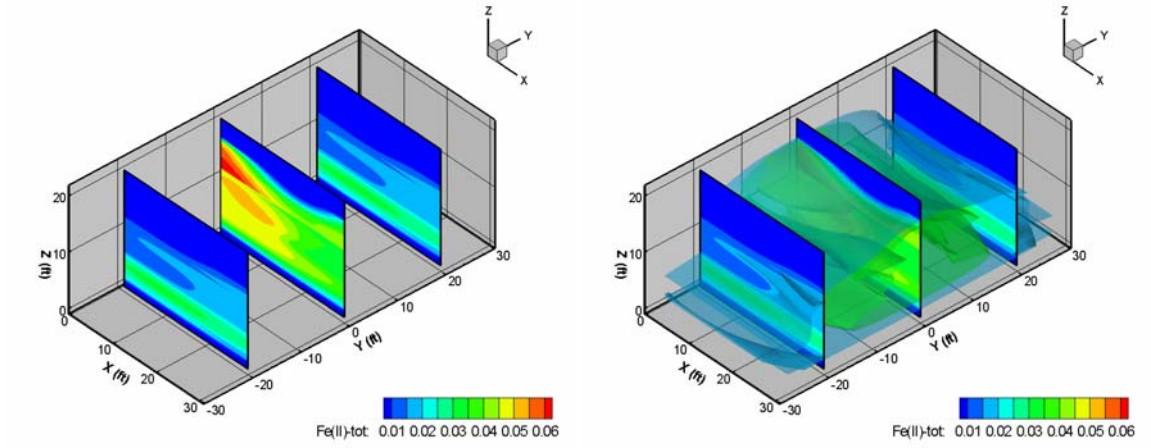

c)

Figure 6.11. Fe(II) Concentration Contours and Isosurfaces for a) 3a/b Injection, b) 4a/b Injection, and c) Combined Results for 3a/b and 4a/b. The y axis runs parallel to the barrier alignment with X = 0 and X = 30 corresponding to 3a/b and 4a/b well pairs, respectively.

7.0 Performance Assessment

This section contains a discussion of the preliminary performance monitoring results from selected injection and monitoring wells along the ISRM permeable reactive barrier alignment and a discussion of the estimated barrier longevity.

7.1 Preliminary Performance Monitoring Results

During an initial groundwater sampling event that was conducted in support of a long-term monitoring strategy designed to assess the performance of the ISRM permeable reactive barrier installation at FHC, EPA personnel collected aqueous samples from selected injection and monitoring wells along the barrier alignment. This first round of post-emplacement performance samples were collected October 14 through 17, 2003, two months after the barrier installation was completed. This sampling date was approximately four months after emplacement of the first remedial action treatment zone and one year after the initial pilot-scale test of the ISRM technology. Results from this sampling event are presented in Tables 7.1 through 7.3.

Table 7.1 summarizes the results for hexavalent chromium and field parameters (EC, DO, pH, and ORP) two months after completion of all barrier emplacement activities at the site. Baseline conditions for selected wells are provided in Table 6.3. These preliminary post-emplacement performance assessment monitoring results are consistent with results from the pilot test and the expected response for an ISRM treatment zone. Observed responses within the reduced iron treatment zone, relative to baseline conditions, included 1) a decrease in the DO concentration associated with the creation of a reducing environment, 2) a decrease in the ORP, 3) a small increase in the pH associated with the pH buffered reagent, 4) an increase in EC associated with treatment residuals, and 5) a decrease in hexavalent chromium concentration within the treatment zone to below detection limits.

Because the injected reagent is a high-pH, high ionic-strength reducing agent, it has the potential to mobilize some trace metals through several processes including reduction, amorphic dissolution, and cation exchange. Table 7.2 is a summary of the post-emplacement trace metals analysis results for filtered samples, which provide a measure of the concentration of dissolved metals in groundwater. Average post-treatment concentrations from the treated zone are shown for comparison with average baseline concentrations and with applicable primary and/or secondary MCL. Baseline conditions are represented by the average pre-injection values measured in all pilot test monitoring wells, as provided in Table 2.3. Comparison of the dissolved metals data in Table 7.2 with analysis results for unfiltered samples (Table 7.3) provides a measure of the amount of metals that are present in the particulate phase. These data indicate that for some elements, most notably aluminum, chromium, copper, and iron, trace metals are present in the particulate phase.

Table 7.1. Hexavalent Chromium and Field Parameter Results from the Initial Performance Assessment Sampling Event

Well Number	Hexavalent Cr (mg/L)	Temp (°C)	EC (mS/cm)	DO (mg/L)	pH	ORP (mV)
INJ-1	0.04U	15.6	2.41	0.47	8.1	-97
RA-IW-2b	U[(a)]	16.7	2.72	0.06	8.4	-412
RA-IW-3a	U[(a)]	17.5	4.73	0.06	8.9	-476
RA-IW-3b	U[(a)]	16.4	3.76	0.07	8.5	-415
RA-IW-4a	0.04U	15.4	2.87	0.16	9.3	-148
RA-IW-4b	0.04U	15.4	1.98	0.04	9.4	-225
RA-IW-8a	0.04U	15.0	0.81	0.94	7.5	-97
RA-MW-11a	U[(a)]	16.0	2.05	0.06	7.4	-391
RA-MW-11b	U[(a)]	15.1	2.63	0.04	8.7	-461
RA-MW-12a	U[(a)]	17.3	4.97	0.08	8.5	-442
RA-MW-12b	0.04U	15.9	3.17	0.03	8.2	-310
RA-MW-12c	0.04U	15.8	3.85	0.04	8.7	-308
RA-MW-13a	0.04U	15	5.19	0.21	7.7	-118
RA-MW-13b	0.04U	15.1	3.95	0.54	7.9	-169
RA-MW-14a	0.04U	14.1	4.57	0.24	7.8	-159
RA-MW-14b	0.04U	14	1.84	0.07	8.7	-174
RA-MW-15a	0.04U	14.7	0.68	0.25	7.3	-17
RA-MW-15b	0.04U	14.5	0.55	0.32	7.2	20
RA-MW-16a	0.04U	14.9	4.14	0.15	7.3	-60
RA-MW-16b	0.04U	14.5	2.73	0.11	7.4	-103
RA-MW-17a	0.04U	14.3	1.78	0.25	6.9	-18

(a) Strong matrix interference associated with source area reductant. Detection limit not determinable.
U = Not detected (<MDL).

As indicated in Table 7.2, iron increased to levels that exceeded the secondary MCL in several of the wells sampled following treatment. These values, although elevated, were significantly lower than the iron concentrations observed following the pilot test (Table 2.6). This difference is most likely associated with the timing of the two sampling events, with pilot test results being collected immediately following the treatment and these barrier performance results being collected approximately two months after the treatment, providing time for mobilized iron to become re-adsorbed onto formation sediments. Manganese, which exceeded the secondary MCL prior to any ISRM treatment at the site (Table 2.3), was impacted and on average increased to levels approximately 40 times the secondary MCL. This increase is similar to that observed following the pilot test. These increases indicate that, as expected, iron and manganese were mobilized by the reductive treatment. Another trace metal that showed indication of mobilization was arsenic, which at several locations within the treatment zone increased by approximately two to four times its primary MCL. Inspection of arsenic concentrations in the two downgradient monitoring well pairs (RA-MW-15a/b and 16a/b) indicates the elevated concentrations were isolated to the treatment zone. Additional elements

Table 7.2. Post-Emplacement Dissolved (filtered) Trace Metals Results from the Initial Performance Assessment Sampling Event

	Dissolved (filtered) Metals (µg/L)											
Well Number	**Ag**	**Al**	**As**	**Ba**	**Be**	**Ca**	**Cd**	**Cr**	**Co**	**Cu**	**Fe**	
RA-IW-2b	1.1 U	147	24.8	231	0.10 U	223000	0.60 U	3.6	12.8	8.6	31.6 U	
RA-IW-3a	1.1 U	159	12.1	391	0.10 U	739000	0.60 U	101	0.90 U	2.2	333	
RA-IW-3b	1.1 U	132	7	230	0.10 U	302000	0.60 U	30.9	21.0	1.3 U	178	
RA-IW-4a	1.1 U	182	12.8	150	0.10 U	42300	0.60 U	2.1 U	41.8	5.6 U	145	
RA-IW-4b	1.1 U	142	4.7	69.6	0.10 U	10200	0.60 U	1.0 U	77.7	1.7 U	219	
RA-MW-11a	1.9	153	22.1	438	0.10 U	211000	0.60 U	20.7	33.1	3.8 U	1260	
RA-MW-11b	1.2	125	41.9	108	0.10 U	324000	0.60 U	9	38.0	2.4 U	111	
RA-MW-12a	1.1 U	174	28.5	636	0.10 U	644000	0.60 U	192	3.5	3.4	358	
RA-MW-12b	1.1 U	159	14.1	163	0.10 U	100000	0.60 U	9.3	106	3.0	287	
RA-MW-12c	1.1 U	139	4.5	233	0.10 U	106000	0.60 U	3.3	126	4.0	794	
Avg Treat. Zone	1.2	151	17.3	265	0.10 U	270150	0.60 U	37.3	35.0	3.6	372	
Avg Baseline	0.56 U	18.8	2.6 U	29.2	0.20 U	46175	0.37 U	1274	0.88	1.4	12.0	
Primary MCL			10		4		5	100		1300		
Secondary MCL	100	50–200								1000	300	
	Dissolved (filtered) Metals (µg/L)											
Well Number	**Hg**	**K**	**Mg**	**Mn**	**Na**	**Ni**	**Pb**	**Sb**	**Se**	**Tl**	**V**	**Zn**
RA-IW-2b	na	223000	31200	1950	123000	43.8	2.8 U	6.2 U	4.2 R	5.3 U	1.0 U	34.7
RA-IW-3a	na	162000	13000	215	131000	165	2.8 U	6.2 U	4.2 R	5.3 U	2.1	339
RA-IW-3b	na	289000	26200	403	207000	74.2	2.8 U	6.2 U	4.2 R	5.3 U	3.8	146
RA-IW-4a	na	316000	18900	467	263000	44.1	2.8 U	6.2 U	4.2 U	5.3 U	2.0 U	5.2
RA-IW-4b	na	266000	6980	191	155000	6.9	2.8 U	6.2 U	4.2 U	5.3 U	1.0 U	2.0
RA-MW-11a	na	96500	49300	13400	157000	48.2	2.8 U	6.2 U	5.5	5.3 U	1.7	34.1
RA-MW-11b	na	115000	26500	1530	89200	67.1	2.8 U	6.2 U	4.2 U	5.3 U	2.7	76.4
RA-MW-12a	na	278000	3540	212	181000	128	2.8 U	8.5	4.2 R	5.3 U	2.2	373
RA-MW-12b	na	344000	25900	1150	191000	25.7	2.8 U	6.2 U	4.2 R	5.3 U	1.0 U	2.6
RA-MW-12c	na	694000	34100	586	236000	24.1	2.8 U	6.2 U	4.2 R	5.3 U	1.0 U	4.2
Avg Treat. Zone	na	278000	23600	2010	173000	62.7	2.8 U	7.1	4.4	5.3 U	1.9	102
Avg Baseline	0.49 U	3071	10212	192	9536	1.9	1.1 U	4.0	2.2	2.5 U	3.9	3.1 U
Primary MCL	2						15	6	50	2		
Secondary MCL				50								5000

na = Not analyzed.
U = Not detected (<MDL).
J = Reported value is an estimate. Analyte was detected, but has a large associated error.
R = Rejected.

Table 7.3. Post-Emplacement Total (unfiltered) Trace Metals Results from the Initial Performance Assessment Sampling Event

Well Number	Total (Unfiltered) Metals (µg/L)										
	Ag	**Al**	**As**	**Ba**	**Be**	**Ca**	**Cd**	**Cr**	**Co**	**Cu**	**Fe**
INJ-1	1.1 U	323	4.1 U	77.1	0.10 U	46500	0.60 U	4.2	64.9	3.0 U	1010
RA-IW-2b	1.1 U	149	4.1 U	228	0.10 U	220000	0.60 U	10.9	7.0	1.3 U	676
RA-IW-3a	1.1 U	848	32.7	387	0.10 U	714000	0.60 U	205	11.4	55.5	2060
RA-IW-3b	1.1 U	193	11.6	209	0.10 U	296000	0.60 U	55.2	31.3	1.3 U	293
RA-IW-4a	1.1 U	395	12.0	152	0.10 U	43800	0.60 U	4.8	41.5	6.6 U	622
RA-IW-4b	1.1 U	171	5.1	70.5	0.10 U	10700	0.60 U	0.86 U	78.9	2.6 U	303
RA-IW-8a	1.1 U	1170	4.1 U	228	0.10 U	76000	0.60 U	4.5 U	5.5	5.2 U	6050
RA-IW-11a	1.7	176	21.4	360	0.10 U	204000	0.60 U	50.1	34.4	6.0 U	4920
RA-IW-11b	1.4	200	41.0	116	0.10 U	339000	0.60 U	48.8	56.3	3.7 U	1150
RA-IW-12a	1.1	2570	22.9	657	0.47	604000	0.60 U	980	11.9	219	6850
RA-IW-12b	1.1 U	179	12.3	162	0.10 U	97900	0.60 U	16.2	107	3.0	427
RA-IW-12c	1.1 U	285	4.2	221	0.10 U	106000	0.60 U	12.2	125	2.7	1170
RA-IW-13a	1.1 U	228	4.1 U	156	0.10 U	212000	0.60 U	0.80 U	100	2.7 U	9610
RA-IW-13b	1.5 U	162	4.1 U	152	0.10 U	129000	0.60 U	1.3 U	101	3.1 U	953
RA-IW-14a	1.1 U	138	4.3	203	0.10 U	337000	0.60 U	0.80 U	51.7	1.5 U	27400
RA-IW-14b	1.1 U	208	4.1 U	169	0.10 U	75500	0.60 U	0.80 U	87.4	2.7 U	1340
RA-IW-15a	1.1 U	167	4.1 U	85.9	0.10 U	78400	0.60 U	4.0 U	19.5	4.4 U	2360
RA-IW-15b	1.1 U	298	4.1 U	51.6	0.10 U	65600	0.60 U	35.8	15.4	12.9	971
RA-IW-16a	1.6 U	266	4.1 U	169	0.10 U	364000	0.60 U	4.9	115	8.7	4600
RA-IW-16b	1.3 U	139	4.1 U	249	0.10 U	151000	0.60 U	7.6	216	12.9	2660
RA-IW-17a	1.1 U	322	4.1 U	129	0.10 U	221000	0.60 U	6.8	57	6.0 U	8600
Avg Treatment Zone	1.2	462	12.8	222	0.12	219000	0.60 U	87.3	57.2	20.0	4050
Primary MCL			10		4		5	100		1300	
Secondary MCL	100	50 to 200								1000	300
Well Number											
	Hg	**K**	**Mg**	**Mn**	**Na**	**Ni**	**Pb**	**Sb**	**Se**	**Tl**	**V**
INJ-1	na	301000	19000	719	151000	10.4	2.8 U	6.2 U	4.2 U	5.3 U	1.0 U
RA-IW-2b	na	217000	30500	1970	118000	32.1	2.8 U	6.2 U	4.2 R	5.3 U	1.0 U
RA-IW-3a	na	161000	12900	300	129000	185	2.8 U	6.3	4.2 R	5.3 U	3.9
RA-IW-3b	na	292000	27100	422	212000	82.1	2.8 U	6.2 U	4.2 R	5.3 U	3.7
RA-IW-4a	na	312000	18200	505	256000	47.1	2.8 U	6.2 U	4.2 U	5.3 U	2.4 U
RA-IW-4b	na	266000	7050	187	156000	6.9	2.8 U	6.2 U	4.2 U	5.3 U	1.0 U
RA-IW-8a	na	47100	28200	9300	29000	3.1	2.9	6.2 U	4.2 U	5.3 U	3.7 U
RA-IW-11a	na	96000	48700	13400	157000	48.4	2.8 U	6.2 U	7.9	5.3 U	2.3
RA-IW-11b	na	117000	27500	1930	91700	71.7	2.8 U	6.5	4.2 U	5.3 U	2.7
RA-IW-12a	na	263000	3390	285	170000	130	2.8 U	6.2 U	4.2 R	5.3 U	5.6
RA-IW-12b	na	342000	25300	1150	188000	26	2.8 U	6.2 U	4.2 R	5.3 U	1.0 U
RA-IW-12c	na	689000	33900	615	236000	23.5	2.8 U	6.2 U	4.2 R	5.3 U	1.0 U
RA-IW-13a	na	778000	59900	5750	480000	44.8	2.8 U	6.2 U	4.2 U	5.3 U	1.0 U
RA-IW-13b	na	394000	32500	2020	276000	22	2.8 U	6.2 U	4.2 U	5.3 U	1.2 U
RA-IW-14a	na	343000	86600	7490	343000	33.7	8.0	6.2 U	4.2 U	5.3 U	1.0 U
RA-IW-14b	na	215000	26900	961	112000	10.7	2.8 U	6.2 U	4.2 U	5.3 U	1.0 U
RA-IW-15a	na	6930	24200	3360	30500	8.4	2.8 U	6.2 U	4.2 U	5.3 U	1.0 U
RA-IW-15b	na	4500	21500	2180	21400	8.9	2.8 U	6.2 U	4.2 U	5.3 U	1.4 U
RA-IW-16a	na	296000	64000	11200	324000	29.7	2.8 U	6.2 U	4.2 U	5.3 U	3.0 U
RA-IW-16b	na	245000	50600	3690	221000	21.9	2.8 U	6.2 U	4.2 U	5.3 U	1.1 U
RA-IW-17a	na	78200	36900	14100	111000	58.8	2.8 U	6.2 U	5.0	5.3 U	1.4 U
Avg Post-Emplace.	na	302000	30500	2940	194000	48.6	3.1	6.2	4.4	5.3 U	2.1
Primary MCL	2						15	6	50	2	
Secondary MCL				50							
na = Not Analyzed; U = Not detected (<MDL); R = Rejected											

that were elevated but did not exceed regulatory limits include aluminum, barium, cobalt, nickel, and zinc. These elevated metals concentrations are not expected to migrate a significant distance downgradient of the reduced zone. This anticipated response will be assessed through long-term performance monitoring of the ISRM barrier emplacement, both within and downgradient of the treatment zone.

All major cations (Ba, Ca, K, Mg, and Na) showed an increase between baseline and post-test monitoring due to injection of the high ionic-strength reagent. The relatively large increase in potassium and sodium was due to the addition of potassium carbonate buffer (K_2CO_3) and the sodium-based reagent ($Na_2S_2O_4$), respectively.

The primary measure of performance for the ISRM permeable reactive barrier is based on comparing Cr(VI) concentrations within and downgradient of the treatment zone after the barrier is emplaced with pre-treatment baseline conditions. These Cr(VI) performance data are included in Table 7.1. As indicated, the preliminary results are promising. Hexavalent chromium concentrations were reduced from as high as 8,500 µg/L in the central portion of the plume (Table 6.3) to below detection limits for all monitoring wells analyzed. Detection limits of the spectrophotometric method used for the Cr(VI) analysis were adversely affected at some locations by strong matrix interference associated with intrusion of source area reagents throughout a small section of the ISRM barrier alignment. This matrix interference may also have impacted trace metals results, as indicated by a comparison of data from affected and unaffected wells. Mean dissolved and total chromium concentrations for wells from the affected area were 59.5 and 225 µg/L, respectively, compared with 3.9 and 4.6 µg/L, respectively, for unaffected wells. As with the other trace metals monitoring results, this response will be assessed through long-term performance monitoring of the ISRM barrier emplacement.

Approximately one month after this initial groundwater sampling event, EPA personnel collected a second round of aqueous samples from selected injection and monitoring wells along the barrier alignment. This second round of post-emplacement performance assessment samples were collected November 10 through 14, 2003, approximately three months after the barrier installation was completed. This sampling date was approximately five months after the first remedial action treatment zone was emplaced and 13 months after the initial pilot-scale test of the ISRM technology. Results from this sampling event are contained in Tables 7.4 through 7.6. Results from the first two post-emplacement sampling events indicates that water quality parameters were little changed during this period. Results from the second sampling event remained consistent with the expected response relative to baseline conditions, including 1) a decrease in the DO concentration associated with the creation of a reducing environment, 2) a decrease in the ORP, 3) a small increase in the pH associated with the pH buffered reagent, 4) an increase in EC associated with treatment residuals, and 5) a decrease in hexavalent chromium concentration within the treatment zone to below detection limits. As with the initial sampling event, some anomalous results were noted for wells experiencing the strong matrix interference effects.

Based on these preliminary results, it appears that the full-scale deployment of an ISRM permeable reactive barrier at the FHC site provides an effective treatment for hexavalent chromium in groundwater and that the remedial objectives are being met. The following section provides a description of the simplified approach used to estimate barrier longevity and a discussion of results.

Table 7.4. Hexavalent Chromium and Field Parameter Results from the Second Performance Assessment Sampling Event

Well Number	Hexavalent Cr (mg/L)	Temp (°C)	EC (mS/cm)	DO (mg/L)	pH	ORP (mV)
INJ-1	0.04U	14.8	2.90	0.07	8.7	-313
RA-IW-2b	0.04U	15.1	2.20	0.08	9.1	-435
RA-IW-3a	U[(a)]	16.3	4.79	0.06	10.2	-484
RA-IW-3b	0.04U	15.0	2.76	0.08	9.5	-447
RA-IW-4a	0.04U	14.9	2.81	0.05	9.5	-163
RA-IW-4b	0.04U	14.6	1.92	0.04	9.7	-272
RA-IW-8a	U[(a)]	14.9	0.80	0.62	8.2	-174
RA-MW-11a	0.04U	15.1	2.03	0.05	9.0	-420
RA-MW-11b	U[(a)]	14.8	2.36	0.40	9.7	-458
RA-MW-12a	U[(a)]	15.1	5.22	0.09	10.0	-478
RA-MW-12b	U[(a)]	14.4	2.73	0.08	9.4	-410
RA-MW-12c	0.04U	14.3	3.80	0.18	9.8	-291
RA-MW-13a	0.04U	14.7	5.08	0.17	7.7	-111
RA-MW-13b	0.04U	14.5	3.60	0.10	8.2	-169
RA-MW-14a	0.04U	14.1	4.86	0.20	7.8	-151
RA-MW-14b	0.04U	14.1	2.41	0.15	8.4	-170
RA-MW-15a	0.04U	14.8	0.62	0.29	7.3	-49
RA-MW-15b	0.04U	14.5	0.56	0.15	7.2	8
RA-MW-16a	0.04U	14.3	3.68	1.03	7.6	-98
RA-MW-16b	0.04U	14.2	2.53	0.10	8.0	-103
RA-MW-17a	0.04U	14.0	1.71	0.25	7.0	-35

(a) Strong matrix interference associated with source area reductant; detection limit not determinable.
U = Not detected (<MDL).

Table 7.5. Post-Emplacement Dissolved (filtered) Trace Metals Results from the Second Performance Assessment Sampling Event

	Dissolved (filtered) Metals (µg/L)											
Well Number	**Ag**	**Al**	**As**	**Ba**	**Be**	**Ca**	**Cd**	**Cr**	**Co**	**Cu**	**Fe**	
RA-IW-2b	0.70 U	122	20.1	194	0.10 U	187000	0.20 U	10.3	17.8	1.0 U	830 J	
RA-IW-3a	0.70 U	18.0 U	111	306	0.10 U	857000	0.20 U	76.0	8.0	1.0	296 J	
RA-IW-3b	0.70 U	11.0 U	22.0	147	0.10 U	255000	0.20 U	15.5	35.0	1.0 U	15.2 UJ	
RA-IW-4a	0.70 U	20.4 U	9.2	164	0.10 U	55700	0.20 U	1.5	29.0	1.0 U	15.2 UJ	
RA-IW-4b	0.70 U	18.3 U	3.6	77.2	0.10 U	14900	0.20 U	0.82	61.9	1.0 U	218 J	
RA-IW-8a	1.2	11.0 U	2.1	208	0.10 U	79400	0.20 U	1.5	3.5	1.0 U	4060 J	
RA-MW-11a	1.5	14.1 U	7.5	285	0.10 U	249000	0.20 U	10.9	24.4	1.0 U	871 J	
RA-MW-11b	0.70 U	11.0 U	37.6	100	0.10 U	336000	0.20 U	3.6	22.5	1.0 U	15.2 UJ	
RA-MW-12a	0.70 U	63.6 U	207	563	0.10 U	931000	0.21	155	7.5	10.2	398 J	
RA-MW-12b	0.70 U	11.0 U	45.7	136	0.10 U	159000	0.20 U	13.5	47.5	1.0 U	15.2 UJ	
RA-MW-12c	0.70 U	11.0 U	10.9	172	0.10 U	162000	0.20 U	1.1	80.0	1.0 U	605 J	
Avg Treat. Zone	0.82	28	43.3	214	0.10 U	298727	0.20	26.3	30.6	1.8	667	
Avg Baseline	0.56 U	18.8	2.6 U	29.2	0.20 U	46175	0.37 U	1274	0.88	1.4	12.0	
Primary MCL			10		4		5	100		1300		
Secondary MCL	100	50–200								1000	300	
	Dissolved (filtered) Metals (µg/L)											
Well Number	**Hg**	**K**	**Mg**	**Mn**	**Na**	**Ni**	**Pb**	**Sb**	**Se**	**Tl**	**V**	**Zn**
RA-IW-2b	na	272000	32700	3350	91000	40.9 J	1.1	5.1	1.8 UJ	1.7 U	1.2	46.5
RA-IW-3a	na	214000	17000	148	119000	180 J	0.90 U	21.5	3.5 J	1.7 U	2.4	356
RA-IW-3b	na	369000	23700	117	127000	59.1 J	0.90 U	3.0	1.8 UJ	1.7 U	1.9	59.4
RA-IW-4a	na	543000	21300	484	228000	35.6 J	0.90 U	2.8 U	1.8 UJ	1.7 U	0.94	3.0
RA-IW-4b	na	436000	8620	454	133000	6.9 J	0.90 U	2.8 U	1.8 UJ	1.7 U	0.60 U	8.3
RA-IW-8a	na	41100	28400	9390	27000	1.3 J	0.93	2.8 U	1.8 UJ	1.7 U	0.70	5.8
RA-MW-11a	na	101000	45300	11700	138000	36.5 J	2.0	2.8 U	1.8 UJ	1.7 U	1.8	34.9
RA-MW-11b	na	132000	28900	2520	88800	57.1 J	0.90 U	6.4	1.8 UJ	1.7 U	1.6	41.1
RA-MW-12a	na	391000	3050	102	148000	241 J	0.90 U	38.4	7.0 J	1.7 U	3.2	264
RA-MW-12b	na	537000	27100	898	143000	36.2 J	0.90 U	4.9	1.8 UJ	1.7 U	2.0	3.6
RA-MW-12c	na	786000	38500	870	206000	23.2 J	1.5	2.8 U	1.8 UJ	1.7 U	0.60 U	2.6 U
Avg Treat. Zone	na	347000	25000	2730	132000	65.3	1.1	8.5	2.4	1.7 U	1.5	75
Avg Baseline	0.49 U	3071	10212	192	9536	1.9	1.1 U	4.0	2.2	2.5 U	3.9	3.1 U
Primary MCL	2						15	6	50	2		
Secondary MCL				50								5000

na = Not analyzed.
U = Not detected (<MDL).
J = Reported value is an estimate. Analyte was detected, but has a large associated error

Table 7.6. Post-Emplacement Total (unfiltered) Trace Metals Results from the Second Performance Assessment Sampling Event

Well Number	Total (Unfiltered) Metals (µg/L)											
	Ag	**Al**	**As**	**Ba**	**Be**	**Ca**	**Cd**	**Cr**	**Co**	**Cu**	**Fe**	
INJ-1	2.0 U	126 U	3.7 U	119 U	0.10 U	55000	0.20 U	1.3	59.4	3.7 U	643	
RA-IW-2b	0.73 U	11.0 U	5.3 U	222	0.10 U	192000	0.20 U	5.1	6.3	1.0 U	15.2 U	
RA-IW-3a	1.3 U	1070	19.9	339	0.10 U	831000	0.20 U	192	8.9	16.5	2070	
RA-IW-3b	1.2 U	191 U	24.3	171	0.10 U	249000	0.20 U	39.2	49.2	3.2 U	357	
RA-IW-4a	0.70 U	191	6.8	177	0.10 U	57900	0.25	0.60 U	31.5	2.4	574	
RA-IW-4b	0.70 U	36.9	3.2	81.7	0.10 U	15800	0.20 U	0.60 U	63.6	1.3	346	
RA-IW-8a	1.8 U	4050	2.0 U	272	0.10 U	81400	0.20 U	19.9	4.9	11.4 U	8020	
RA-IW-11a	1.2	22.1	10.0	269	0.10 U	246000	0.20 U	38.5	29.8	1.9	4340	
RA-IW-11b	1.7 U	154 U	42.8	123 U	0.10 U	312000	0.20 U	69.2	39.7	3.8 U	2480	
RA-IW-12a	0.70 U	296	11.9	573	0.10 U	868000	0.20 U	296	8.3	1.0 U	1550	
RA-IW-12b	0.70 U	17.8	50.4	137	0.10 U	152000	0.20 U	26.0	63.6	1.9	191	
RA-IW-12c	0.70 U	59.1	9.8	166	0.10 U	160000	0.20 U	5.9	80.1	1.0 U	679	
RA-IW-13a	2.3 U	183 U	5.0 U	159	0.10 U	245000	0.20 U	2.1	82.2	3.9 U	14200	
RA-IW-13b	1.7 U	37.4 U	3.3 U	149	0.10 U	135000	0.20 U	0.60 U	96.8	4.0 U	1810	
RA-IW-14a	2.2 U	11.0 U	3.2 U	181	0.10 U	433000	0.20 U	0.60 U	36.8	3.9 U	29400	
RA-IW-14b	1.5 U	85.7 U	2.8 U	229	0.10 U	127000	0.20 U	0.60 U	59.9	3.5 U	1550	
RA-IW-15a	1.7 U	11.0 U	2.8 U	84.9 U	0.10 U	71700	0.20 U	1.5	13.2	4.5 U	1380	
RA-IW-15b	1.2 U	31.0 U	1.5 U	72.4 U	0.10 U	67300	0.20 U	3.2	12.4	12.6 U	619	
RA-IW-16a	3.3 U	94.8 U	4.8 U	110 U	0.10 U	319000	0.20 U	4.7	74.9	29.4	7370	
RA-IW-16b	1.8 U	13.0 U	3.1 U	205	0.10 U	151000	0.20 U	2.5	83.0	4.1 U	786	
RA-IW-17a	3.0 U	72.5 U	1.8 U	130 U	0.10 U	213000	0.20 U	5.7	37.9	4.7 U	8580	
Avg Treat. Zone	1.3	409	12.8	210	0.10 U	260000	0.20	43.6	45.1	4.0	4550	
Primary MCL			10		4		5	100		1300		
Secondary MCL	100	50 to 200								1000	300	

Well Number	Total (Unfiltered) Metals (µg/L)											
	Hg	**K**	**Mg**	**Mn**	**Na**	**Ni**	**Pb**	**Sb**	**Se**	**Tl**	**V**	**Zn**
INJ-1	na	649000	24100	678	169000	8.7	0.90 U	2.8 U	1.8 U	1.7 U	1.0	3.7
RA-IW-2b	na	279000	33200	3360	93100	24.4	0.90 U	2.8 U	1.8 U	1.7 U	0.60 U	4.3
RA-IW-3a	na	218000	17800	206	122000	136	0.90 U	4.4	3.2	1.7 U	5.5	471
RA-IW-3b	na	384000	23300	120	125000	64.5	0.90 U	4.2	2.1	1.7 U	2.5	130
RA-IW-4a	na	557000	21800	587	228000	35.2	0.90 U	2.8 U	1.8 UJ	1.7 U	1.3	15.0 J
RA-IW-4b	na	446000	8660	465	141000	4.9	0.90 U	2.8 U	1.8 UJ	1.7 U	0.60 U	7.7 J
RA-IW-8a	na	41900	28400	9860	25300	4.4	2.1	2.8 U	1.8 U	1.7 U	10.0	164
RA-IW-11a	na	101000	46200	12100	143000	40.2	1.9	2.8 U	1.8 UJ	1.7 U	1.8	192 J
RA-IW-11b	na	125000	30000	3850	85000	64.3	0.91	8.9	1.8 U	1.7 U	2.2	115
RA-IW-12a	na	406000	3420	132	151000	149	0.90 U	2.8 U	3.3 J	1.7 U	5.2	311 J
RA-IW-12b	na	551000	25900	891	144000	40.8	0.90 U	5.4	1.8 UJ	1.7 U	2.4	26.5 J
RA-IW-12c	na	837000	37600	876	220000	23.8	0.90 U	2.8 U	1.8 UJ	1.7 U	0.60 U	3.8 J
RA-IW-13a	na	754000	69600	7180	356000	52.4	0.97	2.8 U	1.8 U	1.7 U	1.5	3.9
RA-IW-13b	na	756000	32600	2040	228000	21.2	0.90 U	2.8 U	1.8 U	1.7 U	0.73	5.0
RA-IW-14a	na	651000	92900	8860	314000	31.8	1.0	2.8 U	2.3	1.7 U	0.60 U	21.2
RA-IW-14b	na	427000	39700	1460	135000	7.1	0.90 U	2.8 U	1.8 U	1.7 U	0.60 U	4.5
RA-IW-15a	na	4680	22300	2800	28600	4.9	0.90 U	2.8 U	2.0	1.7 U	0.60 U	5.6
RA-IW-15b	na	4070	21300	2020	23100	5.9	0.90 U	2.8 U	1.8 U	1.7 U	0.72	3.2
RA-IW-16a	na	440000	55500	12300	244000	25.1	1.1	2.8 U	1.8 U	1.7 U	2.1	4.3
RA-IW-16b	na	437000	38800	2280	147000	9.3	0.90 U	2.8 U	1.8 U	1.7 U	0.60 U	5.4
RA-IW-17a	na	87500	34900	12900	95200	49.5	1.5	2.8 U	1.8 U	1.7 U	0.60 U	4.8
Avg Post-Emplac.	na	449000	33400	3290	167000	44.3	1.0	3.5	2.0	1.7 U	2.3	92.4
Primary MCL	2						15	6	50	2		
Secondary MCL				50								5000

na = Not analyzed; U = Not detected (<MDL).

7.2 Estimated Barrier Longevity

As discussed in Sections 6.2 and 6.3, results obtained from a 2D radial reactive transport model were used to provide a more quantitative estimate of the spatial distribution of reduced iron that was generated during the ISRM treatments. These same iron distributions were used to provide bounding estimates of barrier longevity. The reactive transport model used in this analysis was developed during the injection design effort and was verified with dithionite arrival response data from two separate locations along the barrier alignment. The emplaced Fe(II) distribution was simulated at the 3a/b and 4a/b injection well locations (Figure 6.11). These locations were selected because 1) they are within the central portion of the plume where characterization of barrier effectiveness and longevity is most critical, 2) their adjacent location allowed for the estimation of reductive capacity generated at each well and in the overlap zone between the two wells, and 3) the different injection strategies used at these two wells provided a comparison of the resulting reduced iron distribution from a constant versus staged injection concentration approach.

Barrier longevity was estimated at these three locations by evaluating the distribution of reductive capacity along cross-barrier transects (i.e., perpendicular to the barrier alignment) and determining how long, based on estimated groundwater velocities and bounding estimates of oxidizing species concentrations present in the groundwater, it would take to consume the available reductive capacity. The total quantity of reduced iron at a given location along the barrier was calculated by summing the Fe(II) present in a volume with a unit width (i.e., one grid block wide), a length of 60 ft (the full cross-barrier model domain), and a thickness equal to the depth interval of interest. The resulting total Fe(II) values for this representative aquifer volume are presented in Table 7.4. The rate of groundwater flow through this volume of sediment was estimated based on the average hydraulic conductivity for each unit at the various locations (see discussion of the hydraulic conductivity distribution in Sections 4.1 and 4.2) and an average horizontal hydraulic gradient value based on water level measurements and hydraulic analysis performed by EPA Region 10 personnel and documented in a technical memorandum to the EPA RPM. Table 7.7 provides the resulting gradient and average hydraulic conductivity estimates.

Oxidizing species concentrations used to provide bounding estimates of barrier longevity included 1) values based on baseline concentrations from the pilot test site [DO = 3 mg/L and Cr(VI) = 3 and 0.3 mg/L for the A1 and A2/A3 zones, respectively] and 2) values based on results of source treatment confirmation sampling [DO = 0.1 mg/L and Cr(VI) = 0.02 mg/L]. The source treatment confirmation sampling results indicated nondetectable Cr(VI) concentrations for all locations sampled. However, to provide a conservative estimate, the analytical method's detection limit was used in the longevity calculation. The dissolved oxygen concentration used in the calculation was a conservative estimate based entirely on expected site conditions because no DO analyses were conducted during the confirmation sampling. Although conditions downgradient of the source treatment area are expected to be generally anoxic, a small amount of dissolved oxygen was assumed in the calculation.

Table 7.7. Bounding Estimates of Barrier Longevity

Location and unit	Total Fe(II)[(a)] (moles)	Avg K (ft/d)	Gradient (ft/ft)	Estimated GW velocity (ft/d)	Estimated barrier longevity[(b)] (yr)	Estimated barrier longevity[(c)] (yr)
Adjacent to 3a/b						
A1	403	129	2.8E-05	0.02	1,900	77,000
A2/A3	753	8944	2.8E-05	2.0	45	1,300
Overlap between 3a/b & 4a/b						
A1	218	333	2.8E-05	0.05	400	16,000
A2/A3	744	8,746	2.8E-05	2.0	46	1,300
Adjacent to 4a/b						
A1	294	537	2.8E-05	0.09	340	14,000
A2/A3	688	8,549	2.8E-05	2.0	43	1,200

(a) Calculated for 2 ft wide, 60 ft long domain perpendicular to barrier alignment, with a 5 ft thick A1 zone and the upper 8 ft of the A2/A3 zone.
(b) Calculated time to re-oxidation of all Fe(II) in the barrier segment based on the average K and head gradient shown, and assuming influent oxidizing species concentrations based on average baseline conditions at the pilot test site (DO = 3 mg/L for both units and Cr(VI) = 3 mg/L and 0.3 mg/L for units A1 and A2/A3, respectively).
(c) Calculated time to re-oxidation of all Fe(II) in the barrier segment based on the average K and head gradient shown, and assuming influent oxidizing species concentrations based on results of source treatment confirmation sampling (DO= 0.1 mg/L for both units and Cr(VI) = 0.02 mg/L for both units).

The values used for the lower-bound estimate of barrier longevity, which, as discussed above, are based on baseline conditions at the pilot test site, are not expected to occur along the portion of the barrier where source area treatment was conducted. Instead, these higher concentrations provide a conservative estimate of conditions that could exist where source area treatment was incomplete or in regions of the barrier that extend beyond that impacted by source area treatment.

As indicated by a comparison of longevity estimates for the A2/A3 zone at the three locations, the adopted injection strategy provided an effective means of generating a uniform reduced iron distribution over the targeted aquifer volume (at each well and in the overlap zone between the wells). The relatively large longevity estimate in the A1 zone adjacent to the 3a/b well pair is associated with the different injection strategy used at this well. As discussed in Section 6.3, the 3a/b injection used a higher-concentration, shorter-duration injection strategy that resulted in higher near-well reduced iron concentrations. Of note are the higher longevities predicted for the A1 zone, which should be considered qualitative estimates. As indicated in Section 6.2, in some cases the reactive transport model significantly over-predicted reagent arrivals in the A1 zone, and subsequently the simulated Fe(II) concentrations for this zone would be overestimated. However, these over-predicted arrivals, which were never more than twice the observed arrival concentrations, can at most account for only half of the estimated longevity. It follows that, although there is more uncertainty in the estimates for the A1 zone, the longevity of this unit is still expected to be significantly greater than that of the A2/A3 zone. The primary

factor controlling the longevity of this unit is its relatively low permeability and the resulting low groundwater velocities and oxidizing species flux rates.

Based on the estimated distribution of reduced iron near the 3a/b and 4a/b well pairs, the installed barrier should provide sufficient reductive capacity to meet remedial objectives. Over portions of the barrier located downgradient of the source area treatment where only limited oxidizing species concentrations are expected, the ISRM permeable reactive barrier is estimated to last well over 1,000 years. Over portions of the barrier where source area treatment may have been incomplete or where the barrier extends beyond the area impacted by source area treatment., the barrier is estimated to last more than 40 years.

8.0 Summary and Conclusions

The full-scale ISRM permeable reactive barrier was installed by coalescing individually emplaced treatment zones at eight locations along the barrier alignment to form a continuous linear barrier. Over a two-month period from late May through early August 2003, eight injection operations were conducted that resulted in the successful installation of a 250-ft ISRM permeable reactive barrier at the FHC site. During these operations, a total of 168,000 lb of dithionite and pH buffer, which, when placed in solution, produced 560,000 gallons of reagent, were injected along the full barrier alignment. Initially, the dithionite injection concentration was maintained at 0.08 M throughout the emplacement operation. However, during subsequent injections, a two-stage injection strategy was adopted, with higher dithionite concentrations (0.08 M) used during the first stage and lower concentrations during the second stage (0.04 M) to help mitigate the effects of density sinking of the reagent and allow for more uniform spatial coverage of the reduced iron zone.

Based on the hydrogeologic and contaminant distribution conditions encountered, the depth interval targeted for treatment consisted of the A1 zone and the upper portion of the A2/A3 zone. Because the permeability of the A1 zone is lower than that of the A2/A3 zone, groundwater velocities in the A1 zone are significantly slower than those at greater depth, indicating the need for less treatment in the A1 zone. However, this velocity advantage in the A1 zone is at least partially offset by its higher hexavalent chromium concentrations. To investigate the relative importance of these two competing factors, a simple spreadsheet model was constructed that assumed oxidizing species [i.e., DO and Cr(VI)] concentrations based on average baseline conditions and relative groundwater flux based on hydraulic property estimates. Based on this analysis, it was estimated that the A1 zone should receive approximately 25% as much treatment capacity as the A2/A3 zone to generate uniform treatment zone longevity. This reagent allocation was maintained throughout the emplacement operations.

Approximately 15% of the total injected reagent mass was recovered during the withdrawal phase of the initial remedial action emplacement at the 3a/b well pair. This relatively poor recovery, which is consistent with the recovery response observed during the pilot test (~ 5%), is most likely associated with the heterogeneous nature of the formation materials at FHC and density sinking of the reagent. Following the occurrence of a similar recovery response at the second remedial action emplacement (2a/b well pair) and a consideration of cost relative to the benefits of removing this small percentage of spent reagent, it was decided, with EPA concurrence, that attempts to withdraw the spent reagent would be discontinued.

The dithionite injection BTCs from treatment zone emplacements at the various well pairs provided a qualitative measure of the spatial distribution of treatment. In general, these data indicate that a finite amount of treatment was achieved along the full barrier alignment, although in two cases the iron distribution in the overlap zones between two injection well pairs may have been less than that predicted in the design simulations. These cases include the 2a/b injection,

where very little response was observed at the 11a/b monitoring well pair, and the 5a/b injection, where only limited response was observed in the 13a/b monitoring well pair. These responses are indicative of the formation heterogeneities present at the FHC site and provide an example of the challenges associated with deploying an effective remedial technology at hydrogeologically complex sites. However, it should be noted that in both cases, the monitoring well pair in question did receive substantial treatment during the injection operation on the opposing side of the monitoring well pair (i.e., 3a/b for the 11a/b case and INJ-1/2 for the 13a/b case).

Dithionite arrival response data from injection operations at two of the most highly monitored locations were compared with simulation results from the 2D radial model to determine goodness of fit. Of particular note is the generally good fit in the 'b' wells, which is of primary importance due to the relatively high oxidizing species concentrations and flux rates in this zone. Comparison of predicted and observed responses in the 'a' wells indicates that the 2D radial model has the potential to over-predict reductive capacity in the A1 zone at some locations. The relatively good fit between the predicted and observed arrival responses at these locations indicated that the 2D radial reactive transport model constructed during this effort provided a reasonable representation of actual site conditions, and subsequently was a useful tool for estimating the distribution of reductive capacity generated during emplacement operations at the site. These simulated iron distributions were used to develop bounding estimates of barrier longevity.

Preliminary post-emplacement performance assessment monitoring results are consistent with results from the pilot test and the expected response for an ISRM treatment zone. Observed responses within the reduced iron treatment zone, relative to baseline conditions, included: 1) a decrease in the DO concentration associated with the creation of a reducing environment, 2) a decrease in the ORP, 3) a small increase in the pH associated with the pH buffered reagent, 4) an increase in EC associated with treatment residuals, and 5) a decrease in hexavalent chromium concentration within the treatment zone to below detection limits.

Preliminary performance measures for the ISRM permeable reactive barrier, which is primarily based on comparison of Cr(VI) concentrations within and downgradient of the treatment zone following emplacement of the barrier with pre-treatment baseline conditions, are promising. Hexavalent chromium concentrations were reduced from as high as 8,500 µg/L in the central portion of the plume to below detection limits in all monitoring wells analyzed. It should be noted that detection limits of the spectrophotometric method used for the Cr(VI) analysis were adversely affected at some locations by strong matrix interference associated with intrusion of source area reagents throughout a small section of the ISRM barrier alignment. This matrix interference may also have impacted trace metals results, as indicated by a comparison of data from affected and unaffected wells. Mean dissolved and total chromium concentrations for wells from the affected area were 59.5 and 225 µg/L, respectively, compared with mean values of 3.9 and 4.6 µg/L, respectively, for unaffected wells. As with the other trace metals monitoring

results, this response will be assessed through long-term performance monitoring of the ISRM barrier emplacement.

Based on these preliminary results, it appears that the full-scale deployment of an ISRM permeable reactive barrier at the FHC site provides an effective treatment for hexavalent chromium in groundwater and that the remedial objectives are being met. Over portions of the barrier located downgradient of the source area treatment where only limited oxidizing species concentrations are expected, the ISRM permeable reactive barrier is estimated to last well over 1,000 years. Over portions of the barrier where source area treatment may have been incomplete or in regions of the barrier that extend beyond the area impacted by source area treatment, the barrier is estimated to last more than 40 years.

9.0 References

Deutsch CV and AG Journel. 1998. *GSLIB: Geostatistical Software Library and Users Guide, second edition.* Oxford University Press, New York.

Fruchter JS, FA Spane, JK Fredrickson, CR Cole, JE Amonette, JC Templeton, TO Stevens, DJ Holford, LE Eary, BN Bjornstad, GD Black, JM Zachara, and VR Vermeul. 1994. *Manipulation of Natural Subsurface Processes: Field Research and Validation*. PNL-10123, Pacific Northwest National Laboratory, Richland, WA.

Fruchter JS, JE Amonette, CR Cole, YA Gorby, MD Humphrey, JD Istok, FA Spane, JE Szecsody, SS Teel, VR Vermeul, MD Williams, and SB Yabusaki. 1996. *In Situ Redox Manipulation Field Injection Test Report - Hanford 100H Area.* PNNL-11372, Pacific Northwest National Laboratory, Richland, WA.

Fruchter JS, CR Cole, MD Williams, VR Vermeul, JE Amonette, JE Szecsody, JD Istok, and MD Humphrey. 2000. "Creation of a Subsurface Permeable Treatment Barrier Using In Situ Redox Manipulation." *Groundwater Monitoring and Remediation Review*, Spring, 2000.

Lide DR (ed.). 1996. *Handbook of Chemistry and Physics*. CRC Press, Boca Raton, FL.

Rai D, LE Eary, and JM Zachara. 1989. "Environmental chemistry of chromium." *Sci. Total Environ*. 86, 15-23.

Szecsody JE, MD Williams, JS Fruchter, VR Vermeul, and JC Evans. 2000. "Influence of sediment reduction on TCE degradation, remediation of chlorinated and recalcitrant compounds." *Chemical Oxidation and Reactive Barriers*, p. 369-376.

Vermeul VR, SS Teel, JE Amonette, CR Cole, JS Fruchter, YA Gorby, FA Spane, JE Szecsody, MD Williams, and SB Yabusaki. 1995. *Geologic, Geochemical, Microbiologic, and Hydrologic Characterization at the In Situ Redox Manipulation Test Site*. PNL-10633, Pacific Northwest National Laboratory, Richland, WA.

Vermeul VR, MD Williams, JC Evans, JE Szecsody, BN Bjornstad, and TL Liikala. 2000. *In Situ Redox Manipulation Proof-of-Principle Test at the Fort Lewis Logistics Center.* PNL-13357, Pacific Northwest National Laboratory, Richland, WA.

Vermeul VR, MD Williams, JE Szecsody, JS Fruchter, CR Cole and JE Amonette. 2002(a). "Creation of a Subsurface Permeable Reactive Barrier Using In Situ Redox Manipulation." *Groundwater Remediation of Metals, Radionuclides, and Nutrients with Permeable Reactive Barriers*. Academic Press, San Diego, CA.

Williams MD, SB Yabusaki, CR Cole, and VR Vermeul. 1994. In Situ Redox Manipulation Field Experiment: Design Analysis." *In Situ Remediation: Scientific Basis for Current and Future Technologies*, p. 1131-1152. Battelle Press, Columbus, OH.

Williams MD, VR Vermeul, M Oostrom, JC Evans, JS Fruchter, JD Istok, MD Humphrey, DC Lanigan, JE Szecsody, MD White, TW Wietsma, and CR Cole. 1999. *Anoxic Plume Attenuation in a Fluctuating Water Table System: Impact of 100-D Area In Situ Redox Manipulation on Downgradient Dissolved Oxygen Concentrations*. PNNL-12192, Pacific Northwest National Laboratory, Richland, WA.

Williams MD and M Oostrom. 2000. "Oxygenation of anoxic water in a fluctuating water table system." *Journal of Hydrology*, 230:70-85.

Williams MD, VR Vermeul, JE Szecsody, and JS Fruchter. 2000. *100-D Area In Situ Redox Treatability Test for Chromate-Contaminated Groundwater.* PNNL-13349, Pacific Northwest National Laboratory, Richland, WA.